SOUTHWEST THERMAL MASS STUDY
TESUQUE PUEBLO, NEW MEXICO

The Effect of Envelope Thermal Mass On the Heating Energy Use of Eight Test Buildings in a High Desert Climate

RESEARCH PHASE I
(September 1981 through December 1982)

John Gustinis
David K. Robertson

April 1984

New Mexico Energy Research and Development Institute
Information Center • The University of New Mexico

NOTICE

A variety of organizations have contributed to this study. The U.S. Department of Housing and Urban Development provided funds for the construction of the facility through the Community Development Block Grant Program, Numbers B-78-SR-35-0838 and B-78-SR-35-9203. The U.S. Department of Energy Office of Buildings and Community Systems provided funds for instrumentation, data collection, and analysis, through the Building Thermal Envelope Systems and Insulating Materials program administered by Martin Marietta at Oak Ridge National Laboratory, Subcontract Number 7948. The State of New Mexico Energy Research and Development Institute funded publications under Project Number 2-67-1135. Tesuque Pueblo and Eight Northern Indian Pueblos Council have contributed the use of the land for the test site and the use of the monitor building. The New Mexico Energy Research and Development Institute Information Center at the University of New Mexico administered the project.

SOUTHWEST THERMAL MASS STUDY

THE EFFECT OF ENVELOPE THERMAL MASS ON THE HEATING ENERGY USE OF EIGHT TEST BUILDINGS IN A HIGH DESERT CLIMATE (September, 1981 through December, 1982)

by

John Gustinis
David K. Robertson

NEW MEXICO ENERGY RESEARCH AND DEVELOPMENT INSTITUTE
INFORMATION CENTER, THE UNIVERSITY OF NEW MEXICO
Albuquerque, New Mexico 87131

APRIL 1984

Prepared under subcontract ORNL/Sub/7948 for
Building Thermal Envelope Systems and Materials
OAK RIDGE NATIONAL LABORATORY
Oak Ridge, Tennessee 37830

Operated by

MARTIN MARIETTA CORPORATION
for the
U. S. DEPARTMENT OF ENERGY
Contract No. W-7405-eng-26

Additional support provided by

NEW MEXICO ENERGY RESEARCH AND DEVELOPMENT INSTITUTE
Project No. 2-67-1135

CONTENTS

LIST OF FIGURES

LIST OF TABLES

PREFACE

The Southwest Thermal Mass Study is part of a national effort to characterize the thermal behavior of buildings that incorporate thermal mass in their envelopes. Many traditional building materials, such as brick, concrete, stone, soil, and to some extent logs, are sufficiently massive that their energy storage capability might influence building heating and cooling energy requirements. The study includes test buildings incorporating many such materials, including the traditional Southwestern sun-dried adobe brick.

All the data and analysis in this report are for test buildings of a very simple configuration, to allow careful analysis of the instrumentation and the thermal performance of the buildings. That is, there are neither windows nor doors (to minimize infiltration, and to avoid solar gains through windows), the slab-on-grade floors are insulated above the slab (to reduce complex heat losses and gains to the floor), and there are no internal heat sources other than the heating system itself. These test buildings yielded data that was analyzed to give considerable insight into the effects of building envelope thermal mass. Such insights, and the supporting theory and data, are the core of this report. There is also assessment of data quality: experimental uncertainties have been evaluated, so that current conclusions and future work do not strain beyond the credibility of the data.

The focus of this report is the heating season data collected and analyzed for windowless buildings from December 1981 through December 1982. An earlier published report, entitled "Southwest Thermal Mass Study -- Construction and Instrumentation Phase" (14), covered the initial phase in which the test facility was constructed and instrumented at Tesuque Pueblo, New Mexico, from September 1980 through August 1981. Other measurements, not covered by this report, have been completed as follows. Data was obtained to assess the potential for summer cooling using night ventilation. Winter data with timed internal heat sources explored the radiative and convective coupling of that heat to the building envelope. Windows were installed in all but one of the test buildings, and data was collected for that configuration from January to June, 1983. Analysis of the new data is in process. A report will be issued when that analysis is completed.

John Gustinis
August 5, 1983

ACKNOWLEDGEMENTS

A variety of organizations have contributed to this study. The U.S. Department of Housing and Urban Development provided funds for the construction of the facility through the Community Development Block Grant Program, Numbers B-78-SR-35-0838 and B-78-SR-35-9203. The U.S. Department of Energy Office of Buildings and Community Systems provided funds for instrumentation, data collection, and analysis, through the Building Thermal Envelope Systems and Insulating Materials program administered by Martin Marietta at Oak Ridge National Laboratory, Subcontract Number 7948. The State of New Mexico Energy Research and Development Institute funded publications, Project Number 2-67-1135. Tesuque Pueblo and Eight Northern Indian Pueblos Council have contributed the use of the land for the test site and the use of the monitor building. The New Mexico Energy Research and Development Institute Information Center at the University of New Mexico administered the project.

Among the individuals and institutions that played important direct roles in this project, from its inception to the present, the following are acknowledged:

Barkmann Engineering, Santa Fe, NM
Herman Barkmann

The Bickle Group, Albuquerque, NM
Larry W. Bickle, Robert D. Busch, Charles W. Rouser, Thomas T. Shishman

Eight Northern Indian Pueblos Council, San Juan Pueblo, NM
Walter Dasheno, Joe C. Garcia, Edward W. Smith

McHorse and Donahue, Contractors, Santa Fe, NM
Joel McHorse

Mimbres and Associates, Architects and Planners, Santa Fe, NM
William T. Haney

New Mexico Energy Research and Development Institute Information Center (formerly New Mexico Energy Institute) Albuquerque, NM
Richard W. Cole, James O. Dritt, Oscar V. Hopkins, Paul Shelford, Lisa M. Stratton

New Mexico Solar Energy Association, Santa Fe, NM

Steve Meilleur, Bristol Stickney

Oak Ridge National Laboratory, Building Thermal Envelope Systems and Insulating Materials, Oak Ridge, TN
George E. Courville, Kenneth W. Childs, Jeff Christian, Ted S. Lundy, Howard McLain, James N. Robinson

Tesuque Pueblo
Charlie Dorame, Governor Herman Vigil

United States Department of Energy, Office of Buildings and Community Systems, Washington, DC
Erv L. Bales, Jean Boulin, Ernest C. Freeman

United States Department of Housing and Urban Development, Region 9 Community Block Grants, San Francisco, CA
Astrid Trauth

United States National Bureau of Standards, Gaithersburg, MD
Douglas M. Burch, Frank J. Powell

We thank the Governors of the Eight Northern Indian Pueblos Council for their interest and support, and the members of the Thermal Mass Review Panel for their contributions to this effort. In addition, we thank the Honorable Senator Pete V. Domenici for his support of this project.

ABSTRACT

Eight windowless one-room test buildings, 6.10 m square and 2.29 m high inside, were constructed on a high desert site near Tesuque Pueblo, New Mexico, to study the influence of wall dynamic heat transfer characteristics on building heating energy requirements (such influence is sometimes called the "thermal mass effect"). The buildings are nominally identical except for the walls, and are instrumented to record building component temperatures and heat fluxes; indoor temperature, humidity, globe temperature, and interior surface temperatures; and outdoor weather, solar data, and ground temperatures. This report presents the results from analysis of heating season data for one year.

A simple method of analysis using steady-state methods on time-averaged data is derived from first principles. Energy use data for each building are correlated to weather parameters and building interior conditions, and are compared to predictions of steady-state modeling. Comfort parameters are evaluated for each building, and critically compared. In situ measurements of wall thermal properties and dynamic heat transfer characteristics are presented, including data for adobe walls.

In all cases the measurements were consistent with the steady-state theory using time-averaged data. In particular, the following hypotheses were found to be compatible with experimental results: if a building requires heat continuously, then average heating energy requirements depend only on steady-state thermal resistance, and not on thermal mass; if a building interior temperature floats above the thermostat setpoint for part of each day, then excess energy is required above steady-state predictions using averaged data, and is largest (when normalized to overall building heat transfer coefficient) for buildings exhibiting the least thermal damping in the envelope. The excess energy use results simply from the increased average interior temperature during those hours of the day in fall and spring when heat demand drops to zero. With frequent diurnal air temperature swings of 15 to 20°C and direct normal insolation typically exceeding 1000 W/m^2, the observed annual effect (for the lightest building) was 3.5% ± 2% of total heating energy use.

Chapter 1

INTRODUCTION

1.1 PURPOSE AND GOALS OF THE SOUTHWEST THERMAL MASS STUDY

It is a national goal to understand the energy performance of buildings, in order to assess the long-term national impact of various energy conservation strategies. Although it has long been recognized that mass participating in a building's energy flow influences energy use, a detailed understanding of the role of mass on a building's energy use is only now emerging. Numerous computer simulations indicate that the effects of mass can be significant, but there has been little reliable experimental data obtained with calibrated instrumentation to verify the simulations.

Such information is of vital interest to producers of massive building materials -- such as bricks, logs, concrete, adobe, and stone -- who are concerned that building code requirements reflect the energy-conserving aspects of building thermal mass in a reasonable way.

To increase the fundamental understanding of building mass effects, and to provide the supporting experimental evidence, the United States Department of Energy supports a coordinated Thermal Mass Program, administered through the Building Envelopes Program at Oak Ridge National Laboratory. The primary objective of the Thermal Mass Program is to create a body of knowledge about thermal mass in building envelopes that enables both building owners and the building industry to utilize thermal mass effectively in reducing energy consumption for heating and cooling buildings. The broad program encompasses laboratory and field testing, extensive analysis, diagnostics for energy inefficiencies in existing buildings, and transfer of new information and methods to industry, government, universities, and the public.

A major goal of the national program is to evolve a comprehensive understanding which will include the effects of building envelope mass on energy consumption, occupant comfort, and utility peak load requirements. Currently available field and laboratory data have been insufficient for this task. Lacking such experimental data, existing analysis methods could not be verified with confidence. The role of the Southwest Thermal Mass Study, as part of the national program, is to

contribute an accurate and reliable base of experimental results and analysis.

Toward that end, the Southwest Thermal Mass Study has designed and built a research facility at Tesuque Pueblo, New Mexico, specifically to address the effects of mass on building energy performance in the sunny climate of the American Southwest. The study uses a traditional material, sun-dried adobe brick, as the primary material for study of mass effects, in order to extend the body of reliable engineering information on adobe. In addition to five adobe test buildings, there is a concrete masonry building, another of milled logs, and an eighth of insulated wood frame construction, providing eight fully instrumented test buildings with walls of different thicknesses, densities, and thermal diffusivities.

The goal of the Southwest Thermal Mass Study is to obtain and analyze field data on the performance of adobe and other test buildings, for three main purposes. First, to provide reliable basic information on the performance of adobe and other building materials, the study made extended measurements of the thermal performance and energy consumption of adobe, concrete block, log, and frame test buildings in the climate of northern New Mexico. Second, the study performed scientific studies toward developing a coherent, detailed understanding of the complex interaction of building envelope mass, weather, and heating energy use. Third, that understanding together with the accumulated data will allow others to test the limits of validity of various predictive methods used for thermal design of buildings, and to modify and improve such methods for energy-efficient building design.

1.2 PAST WORK AND THE PRESENT CONTEXT IN THERMAL MASS RESEARCH

Most previous work on the behavior of thermal mass in building envelopes used numerical simulations. Generally, researchers have found that the presence of increased mass results in a small reduction in heating or cooling energy required to condition the space (1, 2, 8, 20, 21). However, one study (13) found 20-30% reduction in heating energy required for a heavyweight building as compared with a lightweight building. Two studies (2, 20) found that this reduction is greater in milder climates and one study (1) obtained the largest effect in climates with a large diurnal temperature variation. Another study found that mass is most beneficial when it is located inside insulation (8), where it is tightly coupled to the interior space. Although most researchers agree that mass usually reduces heating and cooling energy requirements, there is not widespread agreement on the quantitative aspects of these effects, and one study (1) found that in some climates additional mass increases cooling requirements.

There is also little information on how best to utilize the thermal behavior of mass of building envelopes. The literature on "passive" solar techniques stresses large amounts of interior mass to absorb the diurnal solar energy pulse admitted through windows. Another approach (6, 10, 15), useful in office buildings, is to utilize the delay of the peak heat flux in the cooling season, and allow the delayed load to be dissipated in the evening when the building is not occupied.

Only a limited amount of experimental work has been done to assess the effects of envelope thermal mass on building heating or cooling energy use. A 1968 study found that a masonry house used less energy than a frame house in the swing seasons in Arizona, despite greater insulation in the frame house (23). A 1973 study on a concrete block house found that envelope mass located on the inside of insulation produced a smaller interior temperature swing than mass placed on the outside (19). The study also found a small reduction in interior temperature swing when mass was added to the interior. The National Bureau of Standards is conducting a field study of wall mass, using six 37.2 m^2 test buildings in both heating and cooling modes (4). The study found no reductions in heating attributable to wall mass when heating was required continuously, but there were significant though small reductions when heating was required for only part of the day. During the summer cooling season, significant savings in cooling energy due to wall mass were observed.

The effects of envelope mass on building energy use are quite complicated. The delay, attenuation, and energy storage properties of any one envelope component are not sufficient to characterize the energy impact of that component. It is the interaction of all heat sources and the heat flow through the many envelope components interacting with the thermostat setpoint that determines a buiding's energy performance. The thermostat-controlled heating plant introduces a strong nonlinearity in the system at zero heating demand: when there is demand for heat, the heating plant supplies energy as needed; but when there is an excess of heat for part of a day the heating plant cannot reversibly store that excess. Instead, the indoor temperature floats above the thermostat control point, affecting heat flow through all envelope components. It is the curse of nonlinear systems that the effects of component pieces cannot be considered one at a time, and then superimposed. The entire building, with its space conditioning system, must be considered as one inseparable system, except in a few simple cases.

At the DOE-ORNL Thermal Mass meeting in Knoxville, Tennessee in June 1982 (7), over a dozen papers in thermal mass research were discussed. The field is evolving rapidly and published literature lags considerably behind current understanding. However, it is clear that a consensus in thinking about the energy storage effects of thermal mass is emerging. That

consensus was summarized in an overview paper by Oak Ridge National Laboratoty (ORNL) (5). The summary stated that, compared to a light building having similar insulating R-value, the incorporation of thermal mass in a building envelope has the following effects:

- thermal mass in a building envelope component delays and attenuates interior surface thermal flux caused by exterior driving temperature changes
- thermal mass can reduce temperature swings in unconditioned buildings
- thermal mass has little effect on total heating or cooling energy use when heating or cooling is required throughout the day
- thermal mass can result in reductions in heating or cooling load (and consequent reduction of the size of space conditioning equipment) if the building experiences alternating periods of net energy gain and net energy loss
- thermal mass can reduce space conditioning equipment cycling
- thermal mass reduces the effectiveness of thermostat setback

Current research is generally aimed at quantifying thermal mass effects and at developing a sound base of experimental results and analysis which can verify that models used in computer simulations of building envelope thermal performance represent thermal loads accurately.

1.3 CURRENT AND FUTURE WORK AT THE SOUTHWEST THERMAL MASS STUDY

This report covers analysis of the thermal performance of windowless buildings from December, 1981, through December, 1982. Subsequent analysis will include the following for windowless test buildings:

- summer night ventilation tests for a lightweight and a massive test building
- short-term heating season data collection with diurnally cycled internal heat sources coupled radiatively to the north walls; repeated, with the same heat sources coupled convectively to the air
- dynamic simulations of the test buildings by Oak Ridge National Laboratory (ORNL) using DOE-2.1A, with actual site weather data (a separate report will be issued by ORNL)

As part of the planned research, windows were added to all but one of the test buildings, and one of the adobe buildings has been insulated on its exterior. This allows:

- heating season tests with windows installed, and one adobe building insulated with the steady-state R-value of the insulated frame building
- additional test building characterization, as required, for the modified buildings

Possible future work at this facility beyond June, 1983, funding permitting, would include:

- installation of refrigerated cooling equipment for cooling season tests
- late spring and early summer tests with both heating and cooling available to maintain a well-defined range of permitted temperatures
- winter tests with night-time thermostat setback
- winter tests with interior partitions installed, creating two or more zones within the test buildings.

After the fundamental work with thermal mass is finished, the test buildings can be used for simple low-cost measurements to evaluate energy-conserving retrofits (e.g., wall insulation retrofits followed by passive solar retrofits).

The first research phase of the Soutwest Thermal Mass Study has produced data of excellent quality. The analysis of that data has yielded a clearer qualitative and quantitative understanding of thermal mass effects in buildings. That understanding is the subject of this report.

1.4 STRUCTURE OF THIS REPORT

This report is compact, relative to the amount of information it represents in terms of both data and analysis. A variety of analysis techniques are used to present the data, to present a rational interpretation of what the "thermal mass effect" is, and ultimately to estimate the magnitude of the effect. Because of the large amount of material presented, the structure of the report is necessarily complex. For these reasons, the structure of the report is here explained.

This report follows a logical progression: each step follows from the previous step and is a prerequisite to the next step. There are five chapters: Chapters 2 through 6, excluding the

Introduction and Summary. These may easily be divided into two parts: that analysis which can be done by simple observation of the data, without recourse to complex theory, and that which requires theory.

Chapter 2 is a description of the test facility. It contains a brief summary of the information in the Construction and Instrumentation phase report (14) and descriptive characteristics of the test buildings that can be derived from the data (e.g., wall delay and R-value, infiltration characteristics). Appendix B presents the information in greater detail. Also included in Chapter 2 is a brief discussion of data quality, supported by Appendix A which lists experimental uncertainties in detail.

Chapter 3 looks at the data directly, with minimal theory and analysis. The principal objectives here are to get a "feel" for the data, to make sure that everything makes sense, and to show the limits of such approaches.

Chapter 4 presents the theory for the chapters that follow. It establishes the fact that that the "thermal mass effect" only occurs when the system nonlinearity of interior air temperature floating above the thermostat setpoint for part of the day occurs; otherwise, there is no deviation from steady-state theory using time-averaged data. (The reader is referred to Section 4.3, Implications, for a discussion of the "thermal mass effect." The theoretical proof of this chapter may be skipped, but it is a necessary step in the logic for the chapters that follow.) Chapter 4 is supported by Appendix C.

Chapter 5 applies the methods of Chapter 4 by demonstrating agreement with steady-state theory for time-averaged data and showing that floating above the thermostat setpoint produces excess energy use. This involves complex analysis, including: calculation of delayed weather conditions; and normalizations of heating energy use to constant interior air temperature, to constant floor loss, to constant exterior radiative conditions, and to constant (zero) infiltration rates. This method demonstrates that our understanding of heat flows in building components is adequate and lends much credence to the data. Because of the expense of detailed analysis, only short time periods could be analyzed. Other methods must be used to estimate the seasonal effects.

Chapter 6 presents a simpler way of looking at the "thermal mass effect" by simply comparing each building's energy use to that of building 3 (381 mm adobe). The advantages of this method are: all weather parameters are "built in" to building 3 consumption, so that the data is already normalized to a consistent set of weather conditions; only kWh meter readings are used, eliminating extensive data collection; detailed analysis is unnecessary; experimental uncertainties are reduced considerably (to ±2%); and a methodology is provided for estimating the effect.

Chapter 2

SOUTHWEST THERMAL MASS STUDY

The Southwest Thermal Mass Study is a research facility at Tesuque Pueblo, New Mexico, designed to address the effects of envelope thermal mass on building energy performance in the sunny climate of the American Southwest. The study uses a traditional material, sun-dried adobe brick, as the primary material for study of mass effects. In addition to five adobe test buildings, there is a concrete masonry building, another of milled logs, and one of insulated wood-frame construction, providing eight fully instrumented test buildings with walls of different thicknesses, densities, and thermal diffusivities.

This chapter briefly describes the site, test buildings, instrumentation, and building characteristics, with additional information contained in appendices. Descriptions of the instrumentation and buildings, including architectural drawings, are contained in a previous report "Southwest Thermal Mass Study -- Construction and Instrumentation Phase (September, 1980 - August, 1981)" (14).

2.1 THE SITE

The test facility is located in a high desert valley at an altitude of 1930 m, at 35.81 degrees north latitude and 106.97 degrees west longitude, on Tesuque Pueblo land 15 km north of Santa Fe, New Mexico. The winter climate is characterized by 3200 ± 220 heating degree-days (SI, 18.3°C base temperature), estimated from the heating degree-days for sites having similar elevations and latitudes in New Mexico. Insolation is high: over 65% of the extraterrestrial solar radiation flux reaches the test site. This insolation during the day, combined with the clear night skies, produces typical diurnal air temperature swings of 15 to 20°C. Exterior surfaces of insulated walls exposed to the sun can experience diurnal temperature swings over 55°C on windless days. Wind speeds at nearby Santa Fe average 19 km/hr at 10 m height.

2.2 THE TEST BUILDINGS

A brief description of the test buildings and their instrumentation is given below. Instrumentation is discussed at greater length in Appendix A, and test building characterization, including measurement and calculation methods, is in Appendix B.

2.2.1 Construction

The eight windowless test buildings were nearly identical in construction, except for their exterior walls. They are 6.10 m square and 2.29 m high inside, except that test building 7, the insulated frame building, is 6.30 m square with 2.44 m ceilings. The floors are 10 cm concrete slab on grade, with 5.1 cm of aluminum-faced polyisocyanurate or polyurethane foam insulation placed over the concrete to insulate it from the interior. (The two types of foam insulation differ little in R-value.) Concrete stem walls reaching 0.61 m deep are insulated on both sides with 5.1 cm of urethane foam. The stem walls vary in thickness with the walls they support. Flat roofs cover the buildings. They are supported by 3.8 cm by 29.2 cm wood joists on 40.6 cm centers, with spaces filled by glass fiber batt insulation. A polyethylene vapor and infiltration barrier and 2.5 cm gypsum board finish the ceiling. There are neither doors nor windows: a weatherproof roof entrance provides access. The walls, of course, differ from building to building. Their properties are listed in Table 1. Exterior wall surfaces have been stuccoed or painted to match the solar absorptance (α) of the adobe walls, so that $\alpha = 0.78 \pm 0.02$ for all walls.

The heating plant in each building consists of three 1500-watt electrical resistance heaters controlled by a thermostat. Building air is mixed by a 0.14 m^3/s fan blowing downward through a centrally located 0.61 m square destratification plenum. The thermostat is located within the plenum, and heaters are disposed in a triangle around the plenum base, as shown in Fig. 1. The temperature regulation properties of the heating plant are discussed in Appendix B.

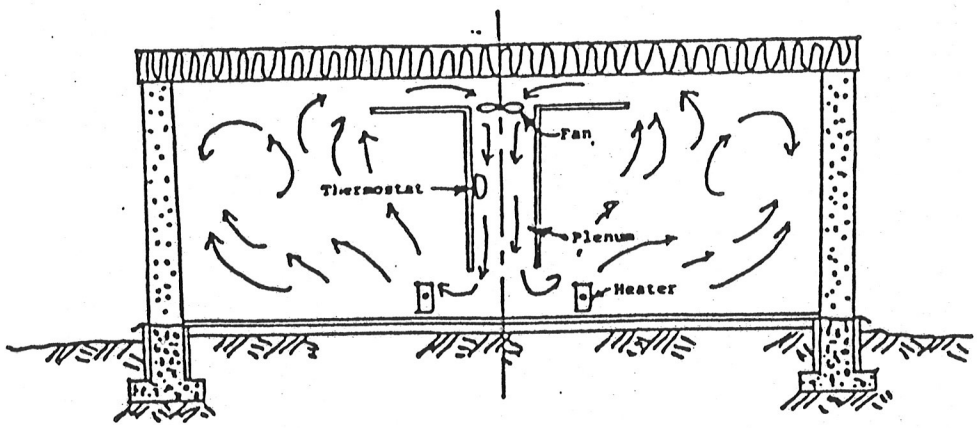

Figure 1: Section Through Test Building, Showing Heating Plant

2.2.2 Instrumentation

Transducer placement was discussed in the construction and instrumentation phase report (14), dated October, 1981. A detailed analysis of the transducers and the uncertainties in the measurements are discussed in Appendix A. A summary of the instrumentation is given below.

The test building instrumentation was simple and straightforward. Each wall of each building was instrumented to measure surface and interior temperatures, and interior surface heat flux. The roofs were of light construction, and identical, so interior and exterior surface temperatures were measured in one building only, to determine roof properties. During most of the year, floor slab temperatures were measured below the 51 mm insulation for one building only, and heat flows were calculated from the insulation R-value and imposed temperature difference. When interior air temperatures floated above the thermostat setpoint for some of the buildings, there was no direct measurement of increased floor losses. To remedy this deficiency, floor instrumentation was extended to all eight test

buildings in the fall of 1982. Inside each test building, air temperatures were measured in the plenum near the thermostat, at mid-height 35 cm from each wall, and 35 cm from the floor and ceiling. A globe temperature was measured at mid-height near the north wall. Humidity sensors inside the buildings proved unreliable, but they were of tangential interest only.

Measurements of outdoor air temperature, wind speed and direction, relative humidity, barometric pressure, solar flux on a horizontal plane and on cardinally-oriented vertical planes, direct-normal solar flux, and long-wave flux on a horizontal surface defined the outdoor conditions. Some ground temperature measurements were also taken.

Measurements of solar absorptance of test building walls, test building infiltration rates, infrared imaging system scans of the buildings to check for inhomogeneities and construction flaws, and other tests were performed as necessary. Results of such measurements are given in Appendix B and summarized below.

Uncertainties in the measurements, including the entire data path, are discussed in Appendix A. Data quality is discussed briefly below.

2.3 DATA QUALITY

The Southwst Thermal Mass Study is designed to look at the sometimes subtle thermal effects of mass in building envelopes. When mass effects are small, it is essential that data integrity be protected from conscious or unconscious biases; and that experimental uncertainties in measured and derived results be quantified, so that inferences are drawn consistent with data quality. The quantification of data quality is critically important to interpretation of this experiment's results.

A top priority was to collect high-quality, irrefutable data. Data collection is the most critical step of an experiment, because it cannot be repeated; analysis, on the other hand, may be repeated if necessary, in whole or in part. Steps to assure high-quality data include documentation, datalogger and sensor calibration, and assessment of experimental uncertainties.

Each step of the experiment has been documented on paper or magnetic media, or both. This includes working drawings of the test buildings, photographs during and after construction, manufacturers' manuals for all critical instrumentation, bound logbooks of all pertinent observations made at the test site, data acquisition software, data analysis software, raw data, and computation results.

Calibration of the datalogger was performed on a periodic basis, and deviations are included in the experimental uncertainty analysis.

Experimental uncertainties of all important measurements were evaluated in some detail, based on manufacturers' data, our measured data, and, in some cases, personal experience. For averaged data and other data calculated from individual measurements, the uncertainties are assigned to the hourly measurements and included in all calculations to assure that the calculated uncertainty is correct. Included with all measured data in this report are estimates of uncertainties. Details of the uncertainties for individual measurements are presented in Appendix A. Generally, for most measurements, they are on the order of ±1-2% (including datalogger uncertainties) at typical operating conditions. (Temperature measurements have an absolute accuracy of 1-2%, but uncertainties in measurements of temperature difference are much smaller.) Notable exceptions are wall flux measurements and some weather measurements, both approximately ±5%; and infiltration measurements, which have uncertainties of ±20-30%. Of these, the wall flux measurements are most important, as infiltration is a small percentage of any test building's heat loss. (See Section 3.3, Component Energy Balances.) The uncertainty in the flux measurements is primarily due to wall inhomogeneities.

The importance of such detailed uncertainty analysis becomes obvious when one puts into perspective the relatively small "thermal mass effect" -- on the order of 5% of total energy use -- compared with, for example, wall energy use based on flux measurements accurate to ±5%, or wall R-values accurate to ±10% or more.

Two additional points need to be made about data quality: first, most problem areas can be addressed in the uncertainty analysis. These include such things as wall inhomogeneities, floor and stem wall loss uncertainties, and variation of infiltration losses as a function of wind direction. Two construction flaws (roof thermal shorts in the insulated frame building - see Section 2.4.1, and indirect infiltration - see Section 2.4.4) were considered effectively impossible to measure or estimate. Second, measurement uncertainty analysis should not be confused with the standard error calculated from linear regression analysis. Where regressions are performed and the results presented, standard errors (± two standard deviations) are also presented.

2.4 TEST BUILDING CHARACTERISTICS

This section summarizes the more important measured characteristics of the test buildings. Measurement methods and other characteristics of the test buildings are discussed in Appendix B.

2.4.1 Roofs

The flat wood-joist insulated roofs are nominally identical, and light enough that thermal mass effects were expected to be small. Roof R-value was determined from measurements on building 1, and roof losses were calculated for each building using that R-value, and the difference between each building's mean interior air temperature and building 1 roof surface temperature (assumed representative of all buildings).

The roofs differ from one another, however. In particular, because the joists extend only to the exterior wall surface, the corner joint between wall and roof structure have different path lengths and conductances. These were neither measured nor estimated: they were ignored, with a potential for large underestimates in building 7 (insulated wood frame building) heat losses, because the wall-ceiling corner has a leakeage path of only 114 mm through wood and gypsum board. In addition, several of the roofs experienced noticeable leaks from puddles sitting on the dead-flat roofs. Others may have had smaller leaks. In any case, water within the roof structure could lower the roof thermal resistance, and there is evidence of this for at least two buildings in the late 1982 data. Roof losses during the coldest weather, neglecting edge effects, were about 150 watts; halving of the thermal resistance due to water would raise the loss to 300 watts, or a third of wall losses for the best-insulated test building. This is a serious deficiency in the data: although it does not threaten quantitative demonstration of important principles, it does increase measurement uncertainties considerably, especially in the late 1982 data.

2.4.2 Walls

The walls differ in construction, and have a range of properties, as listed in Table 1. The listed thermal properties are from measurements through the center of each wall, and so neglect heat flow differences at the base and top, and corners of the walls. For building 7, the measured R-values are for wall sections far from the wood frame members. The wall as a whole exhibits R=2.22 m^2 °C/W, assuming parallel noninteracting heat flow through the wall studs and the wall insulation. The solar

absorptance of all exterior walls was measured as 0.78 ± 0.02 with a pyranometer.

Cores of several adobe walls were taken in March, 1982, for moisture measurements. The moisture content of the 279 mm adobe walls was low, 1 to 2% free moisture by weight, and it varied by less than 1/4 of that value with depth in the walls. The thick 635 mm adobe north wall exhibited a roughly parabolic moisture distribution with depth, reaching 4 to 5% free moisture by weight in the middle of the wall and decreasing to 1% at the interior surface and 2% at the exterior surface. This indicates that the wall was still drying over a year after construction. Thermal resistance measurements using time-averaged data showed no significant differences between any of the adobe walls. What moisture remains in the adobe does not affect the average heat transfer significantly in this experiment.

TABLE 1

Test Building Wall Properties

Bldg.	Thick-ness (mm)	Mass (kg/m^2)	RSI ($m^2°C/W$)	Delay (h)	Impedance Ratio	Wall Description
1	279 ±7	520 ±25	0.35 ±0.04	7.8 ±0.5	2.0 ±0.5	Adobe, mud mortar, adobe plaster.
2	279 ±7	540 ±27	0.37 ±0.04	8.2 ±0.5	2.3 ±0.6	Adobe, cement mortar, adobe plaster.
3	381 ±7	710 ±32	0.48 ±0.05	10.6 ±0.5	3.9 ±1.0	Adobe, mud mortar, adobe plaster.
4	635 ±10	1190 ±60	0.78 ±0.07	18.4 ±0.5	20.3 ±5.1	Adobe, mud mortar, adobe plaster.
5	279 ±7	520 ±26	0.35 ±0.04	8.2 ±0.5	2.5 ±0.6	Adobe, mud mortar, adobe plaster.
6	230 ±4	155 ±5	0.70 ±0.06	5.3 ±0.5	1.5 ±0.4	Gypsum board, vapor barrier, air space, 203 mm CMU.
7	114 ±3	21 ±2 (Bldg. 7 measured	2.70 ±0.09 R-value is between studs)	2.0 ±0.5	1.0 ±0.3	Gypsum board, vapor barrier, wood frame with mineral fiber insul., plywood.
8	178 ±3	77 ±7	1.59 ±0.14	8.9 ±0.5	2.5 ±0.6	Milled logs, butyl caulk.

- - - - - - - - - - -

Notes:

R-values are surface-to-surface, calculated from averaged in situ heat flux, and average temperature difference across each wall.

Delay is between diurnal sinusoidal component of sol-air temperature, and the induced inside surface heat flux, with interior temperature held constant.

Impedance ratio is the amplitude of the diurnal sinewave component of inside surface heat flux, to the amplitude calculated for a massless wall, all with interior air temperature held constant.

2.4.3 Floor Losses

Although stem walls are insulated inside and out to a depth of 0.61 m, and the floor slab is covered by 51 mm of insulation, the floor losses are still considerable. (See Section 3.3, Component Energy Balances.) Floor heat losses are represented by a constant and annual sinusoidal loss to the deep earth, assuming a constant 20.6°C interior air temperature; a steady component that depends on deviation of the thermostat control point from the nominal 20.6°C; and a varying component that depends on floating of interior air temperature above the thermostat control point. In addition, a perimeter loss of 0.2 W/m °C is assumed for all test buildings -- a "reasonable" value which is consistent with the data. (See Section 5.2.1 for details).

2.4.4 Infiltration

This section is a summary of infiltration measurements in the test buildings. The reader is referred to Appendix B.5 for a more complete presentation of these findings.

Natural rates of infiltration for the eight test buildings were measured early in 1982 using a sulfur hexafluoride tracer gas technique. The infiltration rates calculated from the measurements were analyzed using a linear regression model which assumed that the rates depend linearly on the buoyant pressure differences due to inside-outside temperature difference, and on wind-induced pressure differences. The results are summarized in the second column of Table 2. The second column lists the calculated infiltration rates in each building at typical winter weather conditions of windspeed = 4.47 m/s and outside air temperature = 4.4°C. The infiltration rate due to wind-induced pressure differences predominates under typical weather conditions. Because the wind direction was largely from the west and northwest during infiltration measurements, the measured infiltration correlations strictly apply only to the same wind orientation. The buildings are simple and symmetrical, so the correlations are taken to apply, ±20%, to other wind directions through June 1982.

During the summer of 1982, cracks between adobe walls and wood bond-beams were sealed with polyurethane foam to reduce infiltration. Infiltration measurements made in late 1982 proved less reliable than the earlier data, principally because the weather conditions did not include a sufficient variation in outside air temperature. However, correlations with windspeed alone yielded reasonable results, and the calculated infiltration rates at 4.47 m/s windspeed are given in the third column of

Table 2. Note that the rates for the non-adobe buildings were assumed to be the same as in the early 1982 data, as no changes were made to these buildings. The uncertainty in the late 1982 measurements on the adobe buildings are estimated at ±30%. The uncertainty levels in both the early 1982 and late 1982 sets of data are in line with the standard error estimates due to statistical scatter estimated by the regression procedure.

It is important to note that the effects of infiltration on heat loss from a building can differ from the tracer gas loss under the same wind conditions. It is possible that indirect infiltration effects were important in the insulated frame building: infiltration outside the vapor barrier could cause heat losses, but would not affect the tracer gas used to characterize infiltration. This would be a significant factor only in the walls of building 7 (the 114 mm insulated frame). However, it is nearly impossible to measure or calculate and is not included in the analysis or in the uncertainty estimate.

TABLE 2

Infiltration Rates in the Test Buildings

Under Average Conditions *

(Units: Air Changes per Hour)

Building	First Half '82	Second Half '82
1	0.27	0.07
2	0.36	0.23
3	0.33	0.15
4	0.31	0.09
5	0.27	0.08
6	0.06	0.06
7	0.07	0.07
8	0.10	0.10

* wind speed = 4.47 m/s and outside air temperature = 4.4 °C

2.4.5 Comfort in the Test Buildings

The purpose of environmental control of residential buildings is to maintain a reasonable level of human comfort. Comfort is a complex phenomenon, for several reasons. It involves all three sensible transfer mechanisms -- conduction, convection, and radiation -- as well as heat loss due to moisture transfer in respiration and perspiration. It depends on individual metabolic rates, on clothing, and on the thermal environment. Finally, it involves human perception and individual preferences. These subjective factors make comfort difficult to quantify, and invest all standards of comfort with some degree of arbitrariness.

Seven measures are evaluated for two five-day blocks of data: one in midwinter, and one in spring. The measures evaluated are: dry-bulb, wet-bulb, mean radiant, black globe, operative, ASHRAE effective temperature, and the dry-bulb required to satisfy the Fanger comfort criterion. The method of evaluation was to calculate hourly values, print histograms, and calculate means and ranges for each measure.

In this analysis of comfort measures in the test buildings, most of the parameters upon which comfort depends are assumed constant among the test buildings: humidity, relative air velocity, physical activity level, and clothing insulating value. Thus, the analysis reduces to the interaction of air temperature and mean radiant temperature.

The calculations indicated that, if the radiant environment was included in a measure, it was an important consideration for human comfort, and measures which ignore it would not adequately represent comfort levels. The principal finding was that in midwinter, low R-value walls had significantly lower mean radiant temperatures than the higher R-value walls. Since the exterior walls in any of the test buildings are a major part of the radiative environment, those buildings with low R-value walls would have been uncomfortably cold in midwinter. However, in spring, these differences disappeared. Another finding was that massive walls had less variation of inside surface temperatures. Detailed results are presented in Appendix B.6.

Chapter 3

DIRECT EXAMINATION OF THE DATA

The simplest possible data analysis examines the data directly, without recourse to explicit modeling or theory. Such an approach is valuable, despite its simplicity, as an introduction to the data, as a means of estimating data quality, and as justification for more complex methods used in following chapters. This chapter examines raw kilowatt-hour meter readings for the entire calendar year; it examines the variation of time-averaged heating energy use with average outdoor air temperature for 22 data blocks of about 5 days duration each; and it checks the instrumentation by performing an energy balance of heat flow to interior air for the same data blocks.

3.1 RAW KILOWATT-HOUR METER READINGS

Direct examination of the data begins with the kWh meter readings. This immediately gives us an idea of whether the data makes sense or not and how the buildings compare with one another. In addition, it can give us a glimpse of the magnitude of the thermal mass effect.

Figure 2 presents histograms of the total energy used by each building during the entire test period, calendar year 1982. Note that these are raw kWh meter readings and thus can be a basis for only very rough comparisons. This data has not been normalized to consistent thermostat setpoints, consistent infiltration rates, etc.

Note that buildings 1, 2, and 5, the uninsulated 279 mm adobe buildings, have the greatest losses, followed by (in order of decreasing energy use) buildings 3 and 4 (the thicker adobes), building 6 (the CMU), and, finally, buildings 7 and 8 (the insulated frame and log buildings).

Preliminary analysis indicated that the "thermal mass effect" occurs only when the inside temperature floats above the thermostat setpoint for part of each day. For this reason, each bar in the histogram is subdivided into a "control" period and a "float" period. The float period is defined here as that period when any building is floating. (This is always the lightest building, the insulated frame.) The control period is the rest of the heating season; that is, it is the period when all

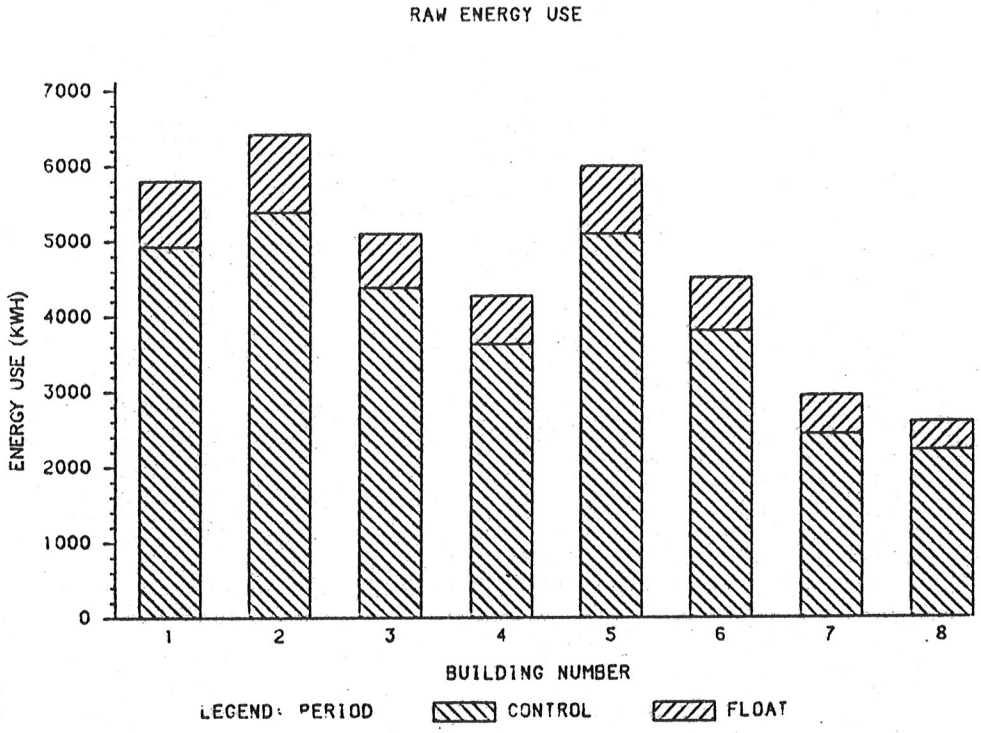

Figure 2: Raw Energy Use - All 1982

buildings are controlled by the thermostat. These periods are determined from interior temperature measurements.

As can be seen from the histogram, again only in a very rough way, the period when any building floats is only a small part of the total annual heating energy use for any of the buildings. In addition, the proportions of energy use between buildings is similar in the float periods to what it is in the control periods. Both of these observations indicate that the mass effect is likely to be small.

3.2 HEATING ENERGY USE VS. OUTDOOR AIR TEMPERATURE

A simple method of estimating heating energy use in small buildings is the degree-day method, which depends only on outdoor air temperature, an interior reference temperature, and a building's overall heat transfer coefficient. The analogous method for data analysis looks at the variation of heating energy use with outdoor air temperature. Figure 3 shows such dependence of heating energy use on outdoor air temperature for a light building (building 7 - 114 mm insulated frame) and a heavy building (building 1 - 279 mm adobe construction). It depicts the average heating energy used for each of 22 blocks of data, covering the time from December, 1981 through December, 1982. Data for those periods when the interior air temperature floated above the thermostat control point is distinguished from data during periods when the thermostat maintained the temperature. The data is scattered much more than could be expected on the basis of measurement uncertainties alone, as explained below. Linear regressions of heating energy as a function of outdoor air temperature reflect such data scatter in the statistical uncertainties (two standard deviations) in regression slopes and intercepts, as given in Table 3.

TABLE 3

Heating Power Regressions vs. Outdoor Temperature

The regression model is:

Heating energy = A + B (Outdoor Temperature)

Bldg.	A (W)	B (W/°C)
1	1477 ± 31	-87.6 ± 4.7
2	1596 ± 32	-90.3 ± 4.2
3	1361 ± 29	-84.1 ± 3.6
4	1118 ±111	-67.1 ± 3.5
5	1529 ± 32	-93.7 ± 4.5
6	1124 ± 21	-63.0 ± 5.2
7	759 ± 18	-41.3 ± 5.2
8	697 ± 21	-39.0 ± 4.4

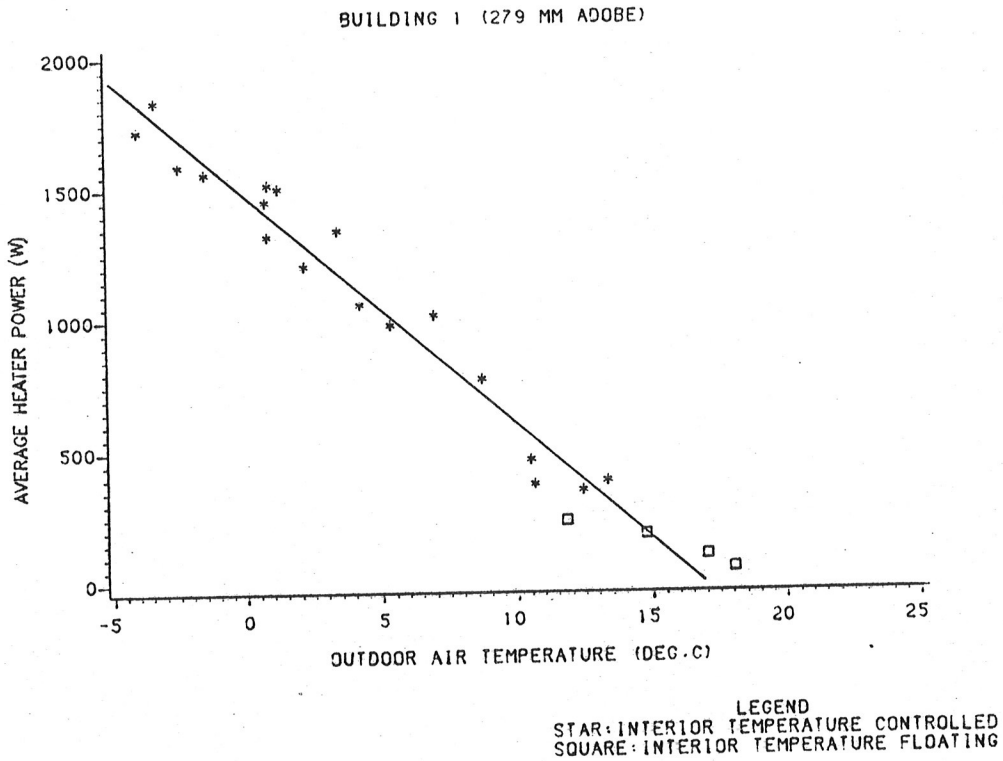

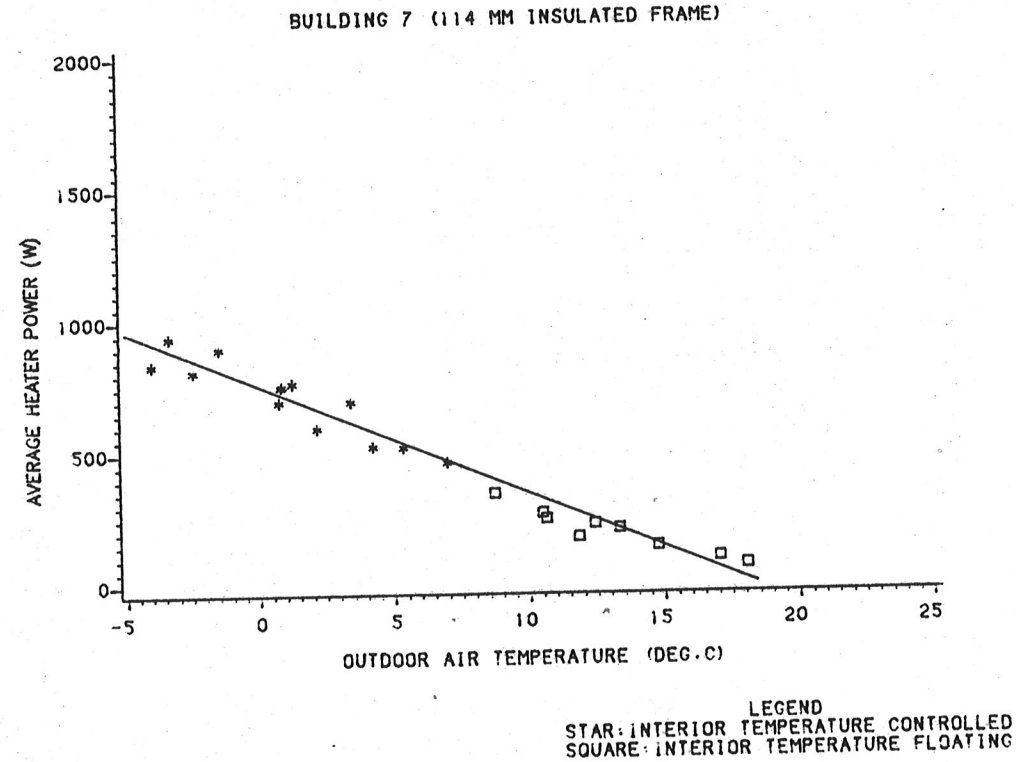

Figure 3: Average Heater Power vs. Temperature for Two Buildings

The scatter in the data is caused by important variables other than outdoor air temperature, and by long heat transmission delay times in thick massive walls. Air infiltration into the building depends on the wind as well as the indoor-outdoor temperature difference; and the degree of solar warming of building components depends on sunlight and wind. These variables are considered in Chapter 5, which models them in a reasonable way, and then applies linear regression to data normalized to windless, dark weather.

Of course, some of the data scatter is due to measurement errors. Such errors are checked by an energy balance method immediately below, and by self-consistency checks in the analysis of Chapter 5.

3.3 COMPONENT ENERGY BALANCES

A component energy balance for each test building under a variety of weather conditions is a sensitive test of the instrumentation: the sum of all measured and calculated energy flows to the interior air should be zero within experimental uncertainties. The results of the component energy balance are presented here to give an early indication of the data quality. Detailed analysis in subsequent chapters will lend even more credence to the data.

Figures 4 and 5 show the energy balance sums for the same two buildings, buildings 1 and 7 (279 mm adobe and 114 mm insulated frame), during each of the 22 time periods chosen for detailed analysis, plotted against average outdoor temperature. The sums consist of the following:

a) The product of measured wall flux and wall area for each wall (uncertainty ±5% ±0.1 W/m^2 calculated from hourly data for each wall before averaging).

b) The product of calculated roof flux and roof area (uncertainty ±5% ±0.1 W/m^2). Roof flux was calculated from measured temperature difference and a calculated R-value of 5.6 m^2 °C/W, taking outdoor roof surface temperature from building 1.

c) The product of calculated floor flux and floor area, plus the product of perimeter, indoor-outdoor temperature difference, and 0.2 W/m °C (±10% estimated uncertainty). The floor flux consisted of a constant term, a sinusoid with annual period, and a term for interior air temperature changes.

d) Infiltration losses, calculated from measured dependence of infiltration on wind and temperature difference (±20% estimated uncertainty until mid-year, then ±30%).

e) The residual, which is the difference between the measured electrical heat inputs (uncertainty ±2% ±6W) and the sum of the other four terms.

The energy balance residuals for all buildings are larger in general than the uncertainty limits of the individual measurements would require. As shown in Figures 4 and 5, they can be systematically correlated to outdoor air temperature. The slopes of the best line through the residuals are small -- well under 10% of the slope B of heater power vs. outdoor air temperature -- except for building 7, which has a heating load 25.7% greater than the heat losses that our measurements account for. Building 7 exhibits this property througout all data analysis. The energy residual points for building 7 are within ±70 W of the best fit line, and the other buildings are within ±100 W. That is a measure of the scatter of individual energy measurement points from general trends. The offset of the energy residual points from zero is not a serious problem for the methods of analysis used later. It must arise from a systematic constant underestimate of heat flow (perhaps the floor), or a systematic error in temperature difference across perimeter, roof, or floor. The effects that we shall seek later manifest themselves as deviations from linearity, so a linear energy balance residual trend against outdoor air temperature is not distressing. (By adjusting individual assumptions about floor losses, roof and perimeter losses, and so on, it is possible to reduce the residuals to small values: this is without benefit, for it hides the true uncertainties in the data.)

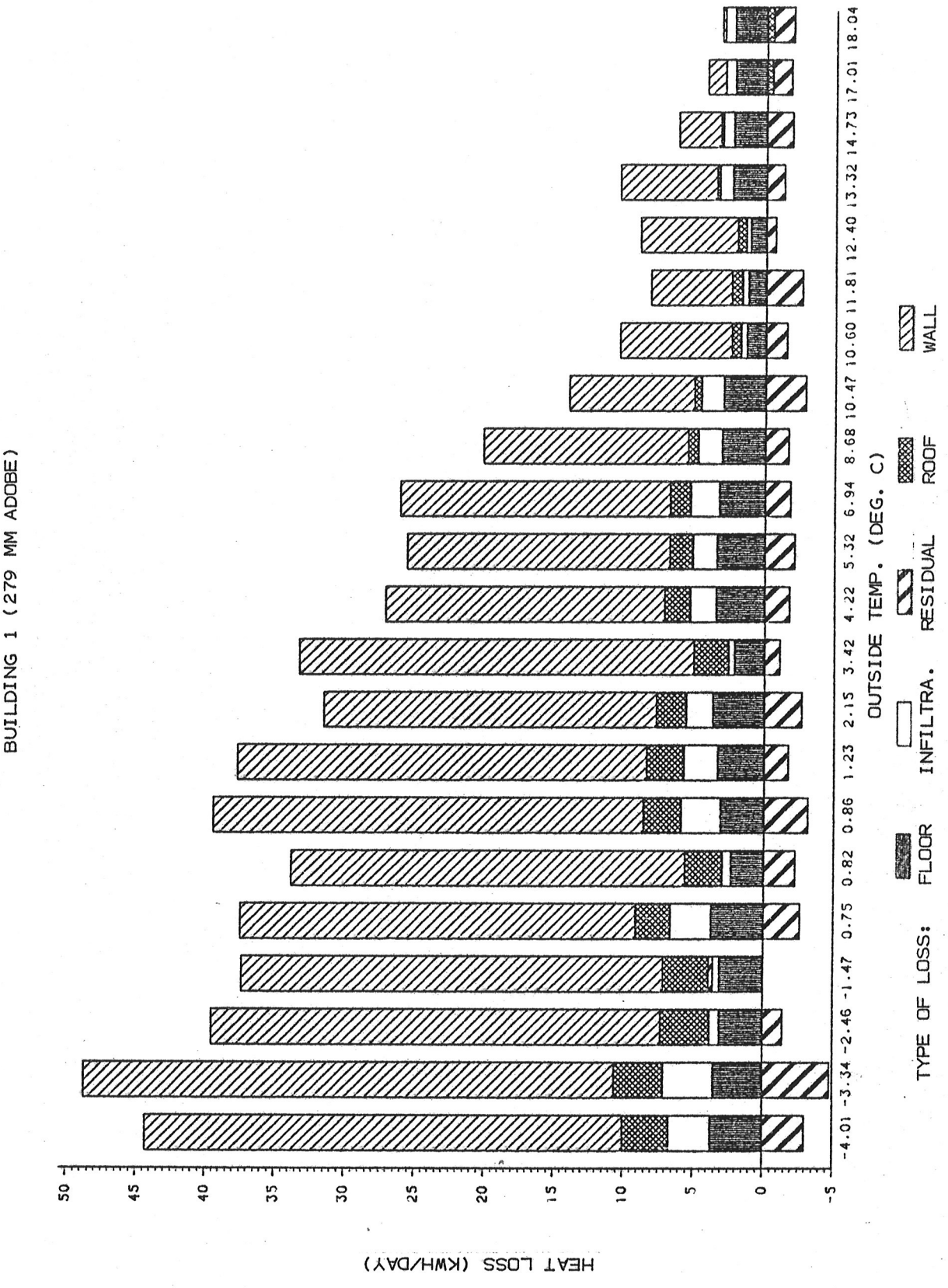

Figure 4: Energy Balance for Building 1

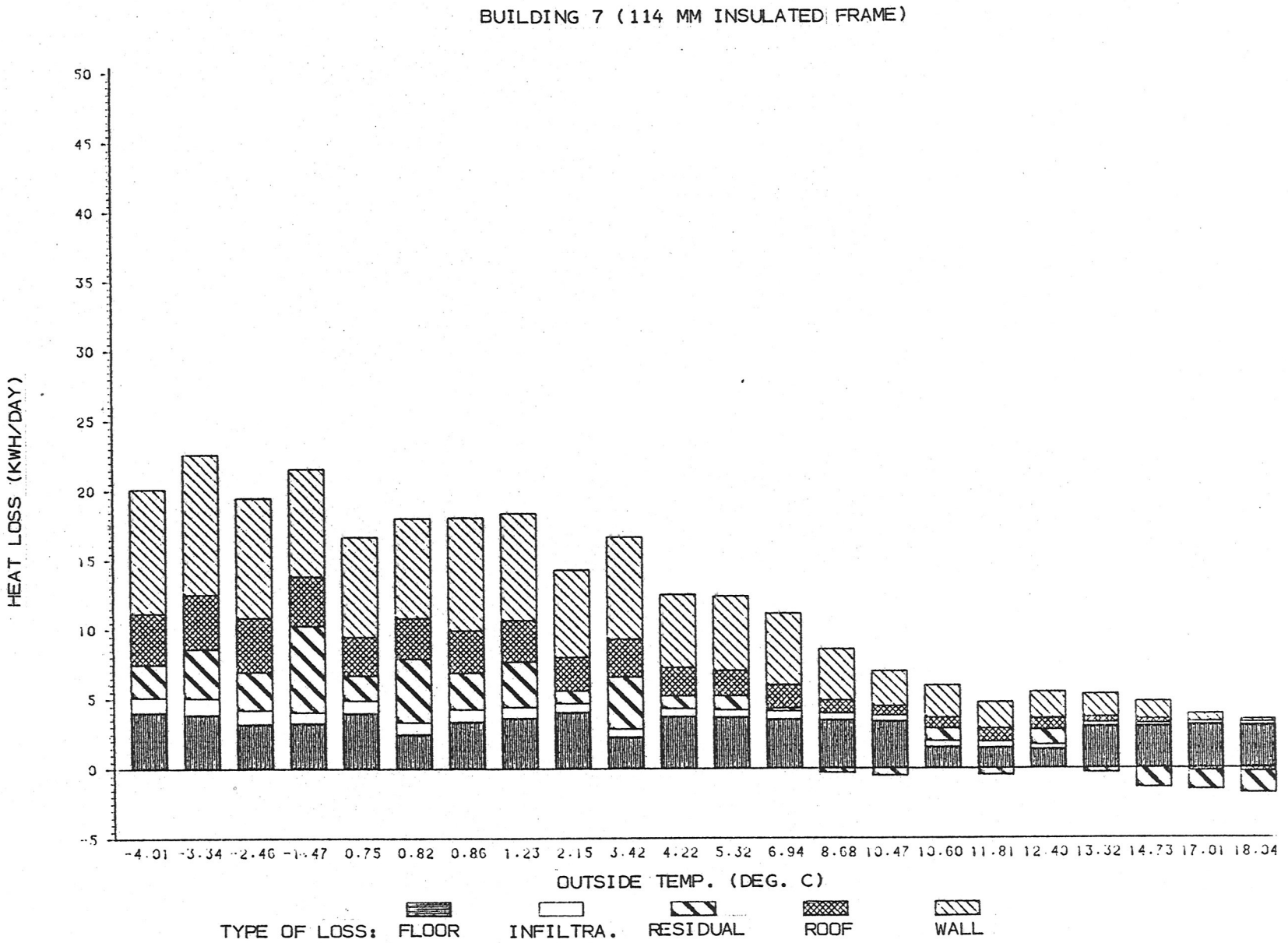

Figure 5: Energy Balance for Building 7

Chapter 4

THEORY FOR TIME-AVERAGED HEAT FLOWS

It is important to develop simple, readily comprehensible models for the effects of thermal mass on heating and cooling energy use in buildings. Simple models, particularly if they are limiting cases for a large class of buildings, serve as valuable tools for testing complex hour-by-hour simulations. Such models also provide a valuable basis for "intuitive" decisions during preliminary design of buildings. In addition, they provide easy methods for testing data against basic concepts, and lend further evidence for data self-consistency. (All experimental data is best regarded as highly suspect until proven otherwise: self-consistency checks are part of that proof.)

This chapter establishes a basis for the analysis techniques used in Chapter 5; for that reason, it is included here in the body of the report. It is a necessary step in the development of the logic of the analysis process (see Section 1.4). However, the reader need not follow the proof, but may instead skip to Section 4.3, Implications.

This chapter is devoted to examining the usefulness and limitations of using steady-state heat transmission methods on time-averaged data -- as simple a model as one could want. The method proves very useful for analysis of Southwest Thermal Mass Study data. It gives a basis for in situ R-value measurements using time-averaged data, it indicates that heating energy use can be predicted easily if weather is sufficiently cold and internal heat gains sufficiently low that heating is required throughout each day, and that the interaction of heat flows with a non-reversible (nonlinear) heating plant is the cause of the "thermal mass effect."

4.1 INTRODUCTION

The heat diffusion equation governing an isotropic but not necessarily homogeneous medium -- a medium like most common construction materials -- is a linear second order partial diffential equation. That is, if a temperature distribution $T(x,y,z,t)$ is a solution to the equation, then $A + B\,(T(x,y,z,t))$ is also a solution, where A and B are arbitrary constants. For linear systems of equations, solutions can be surperimposed; and time-averaging of the equations results in simple steady-state

equations. If the averaging time interval is sufficiently long, and surface boundaries have well-behaved bounded temperatures, then the time-averaged heat flows would be expected to approximate closely the steady-state heat flows that would result if the time-averaged boundary conditions were applied for a long time. Calculations below indicate that such is indeed the case for a slab with simplified linearized boundary conditions. Moreover, the Southwest Thermal Mass Study data presented later in this report is consistent with similar assumptions for much more complex cases.

4.2 THE ISOTROPIC INHOMOGENEOUS WALL

The heat diffusion equation for an isotropic but not necessarily homogeneous medium is

$$\nabla \cdot k \nabla T = \frac{\partial U}{\partial t} \qquad (1)$$

where $k = k(x,y,z)$ is the thermal conductivity,
$T = T(x,y,z,t)$ is the temperature,
t = the time, and
$U = U(x,y,z,t)$ is the internal energy; in the absence of phase changes, U can be linearized to

$$U = \rho(x,y,z)\, c(x,y,z)\, T(x,y,z,t) + U_0(x,y,z),$$

where $\rho = \rho(x,y,z)$ is the density,
$c = c(x,y,z)$ is the specific heat, and
$U_0 = U_0(x,y,z)$ is the internal energy extrapolated to $T(x,y,z,t)=0$.

Buildings usually consist of flat slabs of composite construction forming an envelope that defines the building volume. Consider a slab of thickness L, width M, and height N. Simplify the external and internal boundary conditions by linearizing the radiation terms and including them in the surface heat transfer coefficients h_{in} and h_{out}, and assume that they are constant. If $T_{in}(t)$ and $T_{out}(t)$ are the interior and exterior sol-air temperatures, respectively, then the boundary conditions for a slab insulated at the edges would be

$$h_{in}\,(T_{in}(t) - T(0,y,z,t)) + k(0,y,z)\frac{\partial T}{\partial t}(0,y,z,t) = 0, \qquad (2a)$$

and

$$h_{out}\,(T(L,y,z,t) - T_{out}(t)) + k(L,y,z)\frac{\partial T}{\partial t}(L,y,z,t) = 0, \quad (2b)$$

with the other surfaces having adiabatic boundaries.

The initial condition would be

$$T(x,y,z,0) = T_0(x,y,z) \ . \quad (3)$$

Because all of the above equations are linear in temperature, when they are averaged over the time interval t_0 to t_1, rather simple equations result:

$$\nabla \cdot k \nabla \bar{T} = \rho c \frac{T(x,y,z,t_1) - T_0(x,y,z)}{t_1 - t_0} \quad (4)$$

$$h_{in}\,(\bar{T}_{in} - \bar{T}(0,y,z)) + k(0,y,z)\frac{\partial \bar{T}}{\partial t}(0,y,z) = 0 \quad (5a)$$

$$h_{out}\,(\bar{T}(L,y,z) - \bar{T}_{out}) + k(L,y,z)\frac{\partial \bar{T}}{\partial t}(L,y,z) = 0 \ , \quad (5b)$$

with the other boundaries adiabatic, where

$$\bar{T}(x,y,z) = \frac{1}{t_1 - t_0}\int_{t_0}^{t_1} T(x,y,z,t)\, dt \ ,$$

$$\bar{T}_{in} = \frac{1}{t_1 - t_0}\int_{t_0}^{t_1} T_{in}(t)\, dt \ , \text{ and}$$

$$\bar{T}_{out} = \frac{1}{t_1 - t_0}\int_{t_0}^{t_1} T_{out}(t)\, dt.$$

Equation (4) is now a steady-state equation, with steady-state boundary conditions expressed by equations (5).

If the properties of the slab (k, ρ, and c) as well as the right-hand side of equation (4) were known, the solution for the averaged temperature distribution and heat fluxes could be determined easily. In the special case of steady periodic conditions, if t_0 and t_1 are an integral number of periods apart, then the right-hand side of (4) vanishes, and the solution to the averaged equation is identical to the steady-state solution with the averaged boundary conditions applied. In general, however, building envelope components are subjected to roughly periodic diurnal variations, but with large random variations imposed by variable weather, and the slow annual cycles of the four seasons. That is, the right-hand side of equation (4) is a non-zero heat source or sink term that depends on initial and final temperature distributions, and it is normally not known with any detail.

In all practical instances for buildings, however, the expression for change in wall internal energy represented by the right-hand side of equation (4) is bounded, simply because the internal temperatures in the wall cannot exceed the bounds of recently applied indoor and outdoor sol-air temperatures. That is, there exists $U^* > 0$, such that

$$-U^* < c(x,y,z)\,\rho(x,y,z)\,(T(x,y,z,t_1) - T(x,y,z,t_0)) < +U^* \qquad (6)$$

or

$$-U^* \quad < \quad \frac{\rho\, c\, (T(x,y,z,t_1) - T(x,y,z,t_0))}{t_1 - t_0} \quad < \quad +U^* \qquad (7)$$

If the averaging time interval $(t_1 - t_0)$ is made sufficiently long, then the bounds on equation (7) can be made arbitrarily small, say smaller in absolute value than $\epsilon > 0$. That is, the heat fluxes at the interior and exterior surfaces of the slab will be bounded by the solutions to the steady-state equations

$$\nabla \cdot k(x,y,z)\, \nabla T_-(x,y,z) = -\epsilon \quad , \text{ and}$$

$$\nabla \cdot k(x,y,z)\, \nabla T_+(x,y,z) = +\epsilon \quad ,$$

subject to the boundary conditions of equations (5). These bounding solutions are simply the steady-state solutions with arbitrarily small heat source or sink terms. The heat diffusion equation exhibits no resonance effects, so small causes lead to

small effects. The heat source or sink term of equation (4) can be made arbitrarily small by choosing a sufficiently long averaging time interval. Therefore, for a sufficiently long averaging time, if the sol-air temperatures are bounded and do not change secularly with time, the average heat flux through a wall is arbitrarily near the average heat flux that would be calculated using steady-state methods and time-averaged boundary conditions.

4.3 IMPLICATIONS

This simple result has far-reaching consequences in understanding the effects of envelope thermal mass on building heating and cooling energy use. It is used extensively for Southwest Thermal Mass Study data analysis in later chapters of this report. Its implications are briefly sketched below.

The above exercise is a strong argument that the averaged heat flux through individual building envelope components approaches the steady-state heat flow that would result if the averaged sol-air temperature differences were applied for a long time. This result is important for two reasons. First, it clearly shows that wall thermal mass of itself does not have an influence on seasonal heating or cooling energy use in buildings -- other factors must be involved. Second, it indicates what the nature of these other factors must be. Because linear thermal systems, no matter how complex, have averaged heat flows that are independent of thermal mass when driving temperatures are bounded, it follows that thermal mass can influence average heating energy use only if there are nonlinearities in the system.

The strongest nonlinearity in a simple building is in the behavior of the thermostatically controlled heating plant. Such a plant will normally meet all demands for heating, but it cannot reversibly store excess energy to release it later, when it might be needed. Instead, during periods of excess heat flow to the building interior, the indoor air temperature floats above the thermostat setpoint, increasing the average interior air temperature, and consequently the building heat losses and heating energy use. A light building responds rapidly to external temperature changes, and to changing internal heat loads. Hence, it is much more likely to float above the thermostat setpoint than a massive building that can attenuate heat fluxes induced by outdoor temperature changes, and absorb excess energy introduced into the interior. It is this interaction of the heating demand with the thermostat nonlinearity that is the cause of the so-called "thermal mass effect" on seasonal heating (or cooling) energy use in buildings.

These results are very relevant to understanding the influence of thermal mass on the seasonal heating (or cooling) energy use. If averaged heat flows through the envelope depend only on the average sol-air temperature difference across the envelope components, and on their R-values, and all the equations governing heat flow are linear, then there can be no effect of building thermal mass on the average heating or cooling energy use. Only a system nonlinearity can introduce deviations from steady-state results using averaged data, such as the "thermal mass effect." That non-linearity is caused by the interaction of building heating energy demand required to maintain a given indoor air temperature, and the thermostat setpoint, as follows. If two buildings of identical geometry, color, and steady-state insulating value are exposed to identical weather, and their interior temperatures are maintained at identical thermostat setpoints by reversible heating plants that can absorb excess energy, to return it at a later time when it is needed, then the two buildings will use identical seasonal heating (or cooling) energy regardless of thermal mass differences. After all, the average heat flows through the envelope depend only on the indoor-to-outdoor sol-air temperature differences, which are identical for the two buildings. A real heating plant cannot absorb excess energy to release it when needed. Instead, the indoor air temperature floats up above the thermostat setpoint, resulting in increased building losses due to an elevated average indoor temperature; or, if excessively high temperatures are avoided by ventilation, heat is intentionally dumped and therefore wasted. Thermal mass moderates the variations in heat flow through the envelope, and may absorb excess internal energy as well: both these effects serve to avoid or attenuate interior air temperature excursions above the thermostat setpoint. Therefore a building with little or no thermal mass will encounter the thermostat setpoint non-linearity more often and more severely than a building of similar R-value with thermal mass, and so will use more heating energy.

A real building will use heating energy between the value calculated using steady-state methods applied to hourly data, and the value calculated using steady-state methods on data time-averaged over a time long compared to the building's thermal memory. To place a lower limit on heating energy use for a light building, averaging over a day could be adequate (degree-day method). For heavy buildings, such as the adobe buildings in the Southwest Thermal Mass Study, averaging times of five days or a week are needed. Longer averaging times than the minimum required also produce a correct lower bound on energy use, but it is not the largest easily calculated lower bound.

Building mass that can absorb heat introduced to the interior can be regarded as part of a slightly-reversible heating plant, for it can absorb some excess energy for later release. As far as building seasonal heating energy use is concerned, it matters not at all whether the mass is envelope mass that attenuates

heating load variations, or internal mass that absorbs excess heat. Either positioning of building mass reduces temperature floating, and so decreases energy loss compared to a massless building of the same insulating value.

Chapter 5

DETAILED ANALYSIS OF SELECTED DATA BLOCKS USING STEADY-STATE METHODS

This chapter applies the methods outlined in the previous chapter. Building heating energy use is analyzed by steady-state methods applied to time-averaged data. The first part of the analysis shows that heating energy use can be normalized to depend on outdoor-indoor temperature difference only, with little error. Linear correlation coefficients relating normalized heating energy use and indoor-outdoor temperature differences are obtained, and allow the determination of the outdoor balance point temperature. Using the balance point determined above, the floating of interior air temperature above the thermostat control point becomes an easily measured sensitive indicator of excess energy use that could be eliminated by utilizing thermal mass. The second part of the analysis shows that excess energy losses due to floating can be sufficiently determined by a measurement of mean interior air temperature rise above the thermostat setpoint. This is done by using the overall building heat transfer coefficient, the incremental floor losses due to a rise in indoor temperature, the infiltration losses, the center floor losses, and the effects of solar and long-wave radiation on heat flows.

5.1 INTRODUCTION

Detailed analysis of data using simple but valid methods serves several functions. First, if measured data is self-consistent under the close scrutiny that detailed analysis imposes, then it is likely that the data is as good as our estimates of experimental uncertainties would imply. It is a step beyond the energy balance checks of Chapter 3 in gaining confidence in the data. Second, if the data is consistent with a simple broadly applicable theory, that lends considerable credibility to the theory, and we have a powerful tool for checking the validity of complex dynamic models (DOE-2, BLAST, TARP, and others) for predicting thermal mass effects. One can create artificial weather and buildings that would stress the weaknesses of the dynamic model, knowing what the correct time-averaged response should be.

The methods indicated in the previous chapter easily predict cumulative energy use when a building operates in a linear

heating (or cooling) mode, regardless of building mass. If a system nonlinearity is invoked by interior temperatures that rise above the thermostat control point for heating during part of a day, then the simple theory of the previous chapter predicts that heating energy use will be greater than steady-state methods using time-averaged data would predict.

The method of analysis is based on an energy flow balance to building interior air, neglecting the mass of the air; and on linearized heat transfer through building components. The expressions for heat transfer are manipulated to yield a heating load normalized to standard conditions of wind and sunshine, leaving the indoor-outdoor air-to-air temperature difference as the only significant variable. This procedure eliminates almost all the data scatter seen in the rough preliminary analysis of Chapter 3, so that rather subtle effects are discernible above the data scatter.

5.2 METHOD OF ANALYSIS

Neglecting the mass of the interior air, the energy balance equation for the interior air is

$$Q_{heat} = \Sigma L_{walls} + L_{roof} + L_{floor} + L_{infiltr.}, \quad (1)$$

where Q_{heat} is the auxilliary heat supplied, and
the L's are losses discussed below.

The object now is to define these expressions explicitly, and to manipulate the resulting equations so only terms proportional to indoor-outdoor air temperature difference are left on the right-hand side of the equality sign. The resulting left-hand side of the equation can then be interpreted as a heating load for a building operating in a new, normalized environment. There is an oddity about the operation of this imagined building: it behaves just as the actual building, except that the thermostat is continually adjusted to the actual interior air temperature of the real building, whether the real building temperature floats or not. Also, the heating plant is reversible, swallowing excess energy when it is available, releasing it when needed. (Steady-state theory implicitly assumes a reversible heating plant.) Otherwise, it is the original building. Although one can further normalize to a building with reversible heating plant and interior temperature always controlled to a fixed temperature, we shall be content using the actual measured temperatures, floating or not.

5.2.1 Heat Losses

Infiltration heat losses are not proportional to indoor-outdoor temperature differences alone, so for the present analysis one must normalize to no infiltration at all. The infiltration loss, in watts, is

$$L_{inf} = (A\, WS_{wind}^2 + B\, (1/T_{out} - 1/T_{in}))\, \rho\, c\, V\, (T_{out} - T_{in})\, (1/3600) ,$$

where A,B = infiltration regression coefficients (see Chapter 2),
WS = wind speed (m/s),
T_{out} = outside air temperature (K),
T_{in} = inside air temperature (K),
ρ = density (kg/m^3),
c = specific heat (J/kg °C), and
V = volume of space (m^3).

Wall heat losses include not only indoor-outdoor air temperature differences, but sol-air temperature contributions from solar and long-wave radiation. The heat loss, in watts, for the i-th wall is

$$L_{w,i} = (T_{in} - T_{out})\, U_i\, A_i + \Delta L_{w,i} , \qquad (2)$$

where A_i = the area of the i-th wall (m^2), and

$$U_i = 1 / (R_{in,i} + 1/h_{out,i} + R_{s-s,i}) , \qquad (3)$$

where $R_{in,i}$ = interior surface resistance of the i-th wall (m^2 °C/W),
$R_{s-s,i}$ = surface-to-surface resistance of the i-th wall (m^2 °C/W), and
$h_{out,i}$ = outside surface conductance (W/m^2 °C) .

The outside surface conductance is calculated by the method presented in Appendix C. The remaining quantity is the heat loss increment, in watts, caused by the outdoor radiative temperature differing from outdoor air temperature:

$$\Delta L_{w,i} = - U_i\, A_i\, (I_{sol}\, Q_{cor})/h_{out,i} , \qquad (4)$$

where Q_{cor} = sum of radiative corrections for sky and ground differing from outdoor air temperature (see Appx. C),

and I_{sol} = incident solar radiation (W/m^2) .

The ground surface temperature is represented by earth temperature 25 mm into the ground. Effective sky radiative temperature is calculated from an upward-facing Eppley pyrgeometer, which measures long-wave radiation flux.

The roof losses, L_r, are represented by equations entirely analogous to those for the walls.

Floor losses, in watts, are represented by

$$L_{fl} = P_{fl} \, h_p \, (T_{in} - T_{out}) + L_{ctr,fl} , \qquad (5)$$

where P_{fl} = floor perimeter (m), and
h_p = perimeter heat loss coefficient (W/m °C) .

The perimeter heat loss coefficient is taken as 0.2 W/m °C, about half the value for suspended wood floors with modest amounts of perimeter insulation. (The test buildings have unusually well-insulated floors, with perimeter insulation inside and outside the stem walls, and insulation above the floor slab). The remaining term represents center floor losses in watts. A regression analysis of year-long measurements of building 1 floor losses, plus fall measurements of all test building floors, arrived at the following relationship, including loss increments due to floating of interior air temperatures:

$$L_{ctr,fl} = A_{fl} (L_0 + L_s \sin\theta + L_c \cos\theta) + A_{fl} (T_{in} - T_{std}) / R_{fl} , \qquad (7)$$

where A_{fl} = floor area (m^2) ,
T_{std} = standard interior temperature (20.6°C) ,
R_{fl} = R-value of insulation above floor slab (m^2 °C/W) ,
L_0 = 1.16 W/m^2, L_s = 1.04 W/m^2, and L_c = 0.35 W/m^2.

The L's are coefficients fitted to building 1 floor loss data, after normalizations for interior air temperature differences from standard conditions were applied, and

$$\theta = 2\pi \cdot (J/365)$$

is the time of year expressed in radians, with one year being 2 radians, and J is the Julian day. The above expression, despite its simple assumption for losses due to changes in interior air temperature, fits the measured data quite well.

When the above expressions are combined in such a way that only terms proportional to $(T_{in} - T_{out})$ are on the right-hand side of an equation, then we have a new variable, a normalized building heat loss, in watts, equal to

$$Q_{norm} = Q_{heat} - L_{inf} - \Sigma \Delta L_{w,i} - \Delta L_{r} - L_{ctr,fl}$$

which depend on indoor-outdoor temperature difference only.

All the losses and loss corrections for normalizing to standard conditions are based on processes that can be linearized with good accuracy, and apply to all measured conditions, whether floating or controlled by the thermostat. Even though the interior temperatures are established by a heating system with a strong nonlinearity at zero heating demand, the heat transfer through building components remains linear, and the above equations apply. Of course, as discussed above, the normalized building's interior air temperature behaves as if it were controlled by a reversible heating and cooling plant at precisely the levels observed in the real building, whether the temperature is controlled or floating.

5.3 RESULTS

The above method was applied to 22 blocks of data, each data block about five days in duration, for data acquired from December, 1981 through December, 1982. Figures 6 through 9 show graphs of average heating power for each building plotted against average indoor-outdoor temperature difference. Indoor air temperature is represented by plenum temperature, which has virtue of being well-defined as long as heat is required. The plenum temperature is higher than peripheral zone temperatures near the walls. The time-averaged outdoor conditions used in the equations are averaged over a time period shifted to earlier times by the measured delay of a building's walls. This procedure puts the correct emphasis on slightly earlier weather and sunshine, which is then passed through the walls with its principal diurnal sinusoidal component delayed.

Figures 6 through 9 clearly show that the normalized energy use for each building is proportional to the indoor-outdoor temperature difference. Since floating of the indoor temperature above the thermostat setpoint increases the indoor-outdoor temperature difference, floating must result in increased energy use.

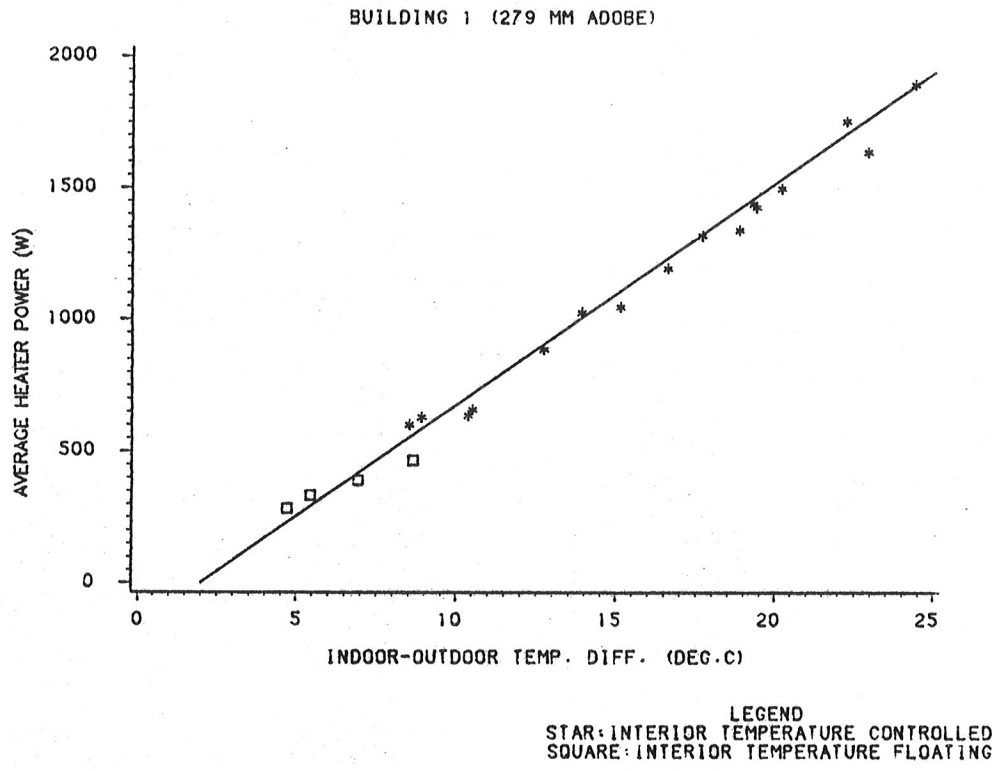

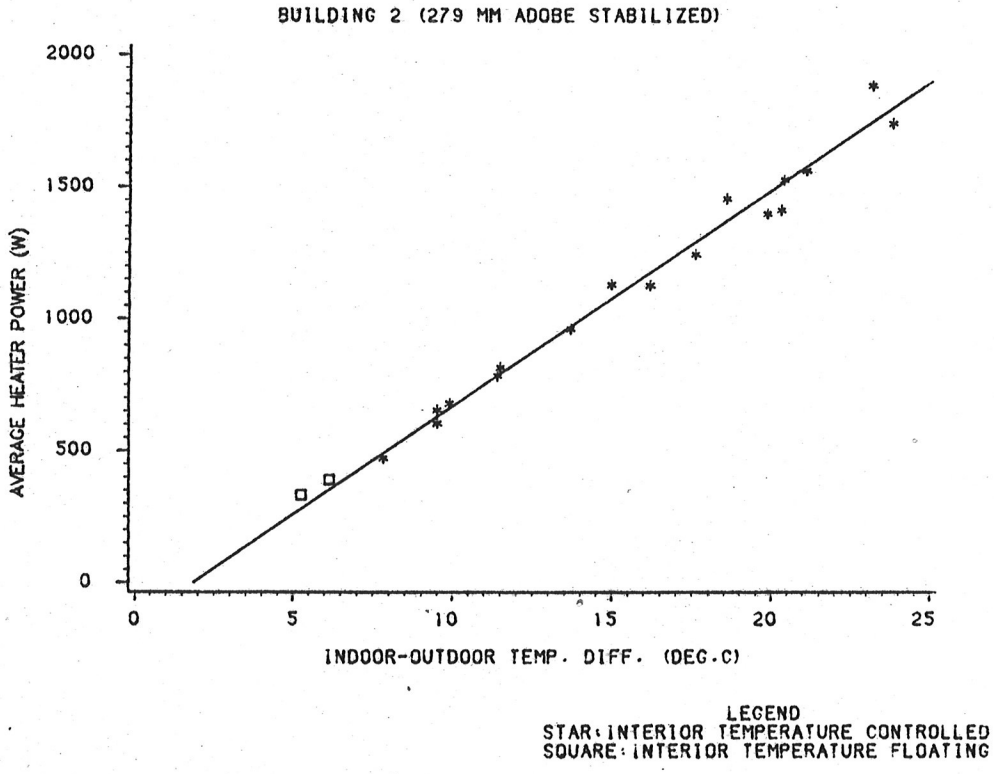

Figure 6: Steady-state Regressions - Buildings 1 and 2

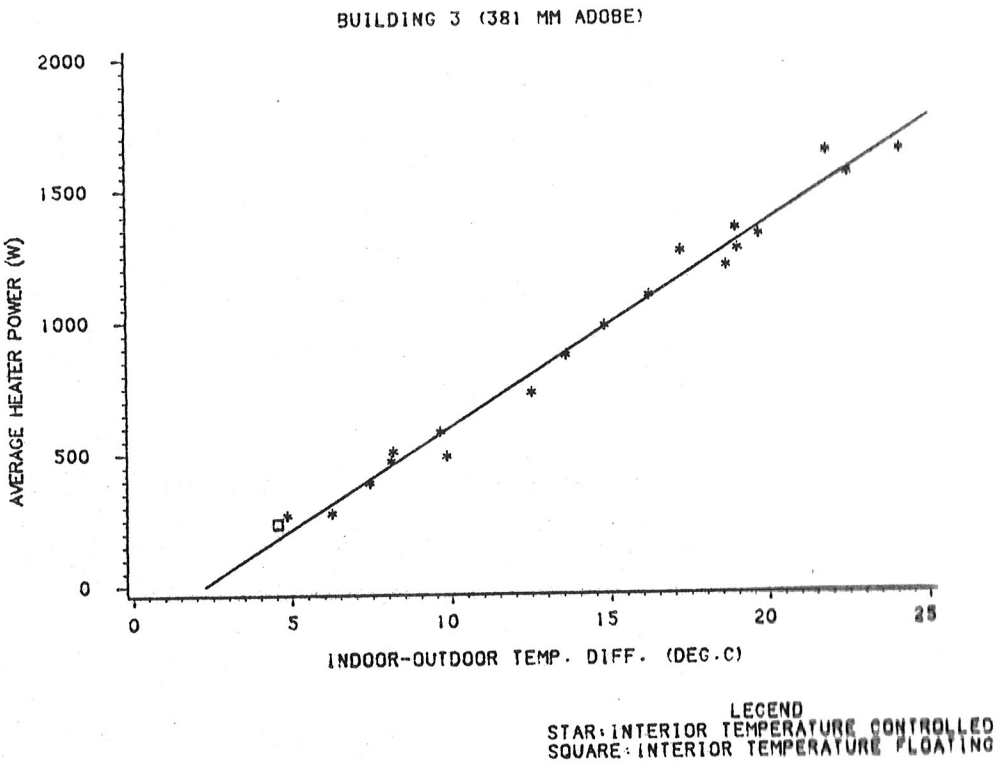

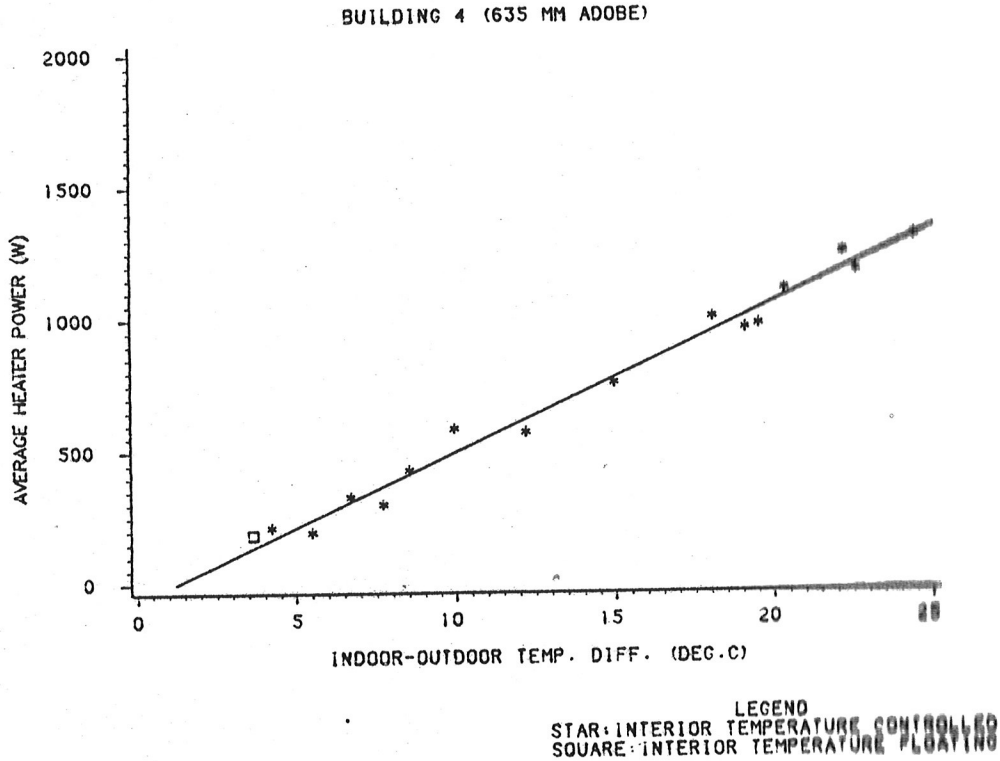

Figure 7: Steady-state Regressions - Buildings 3 and 4

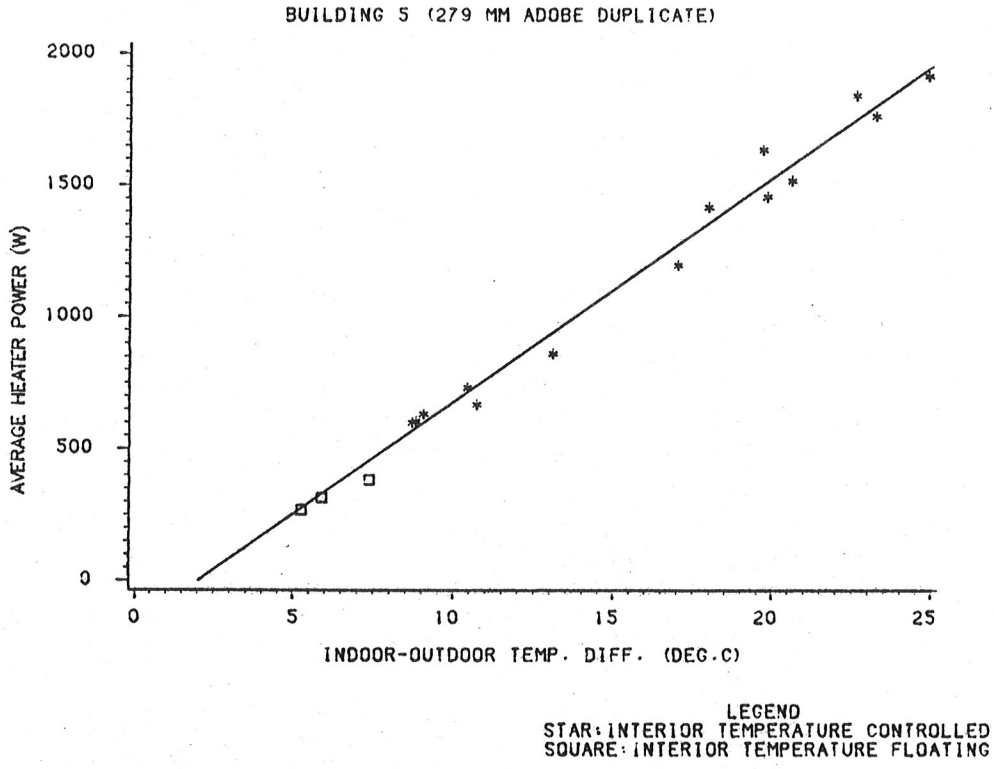

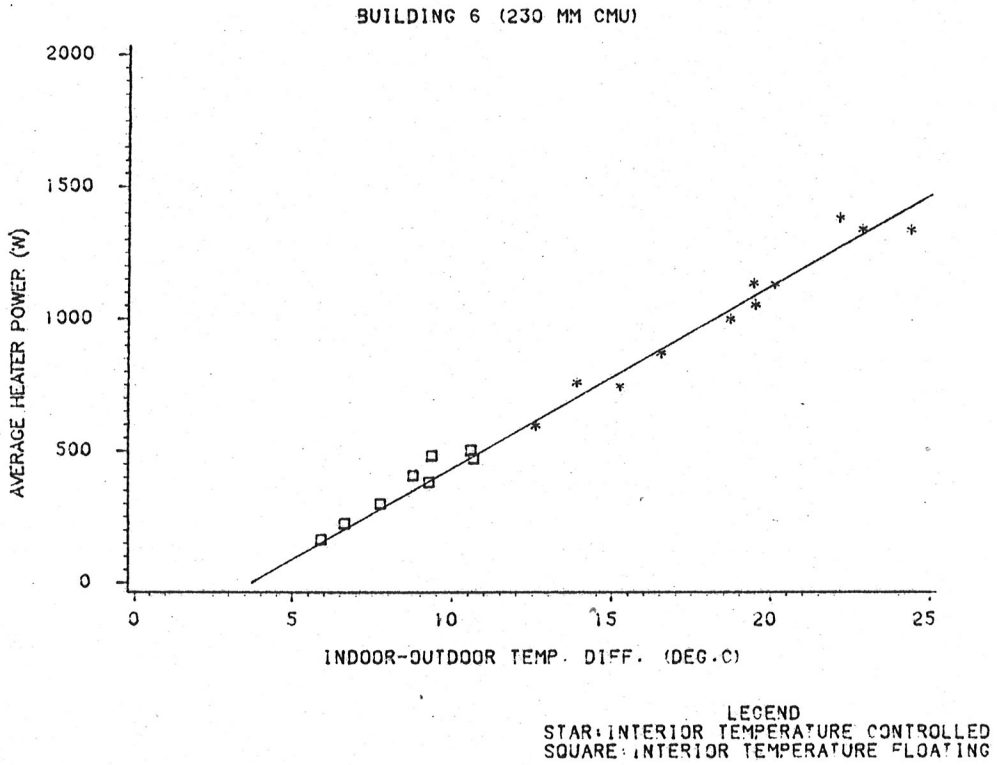

Figure 8: Steady-state Regressions - Buildings 5 and 6

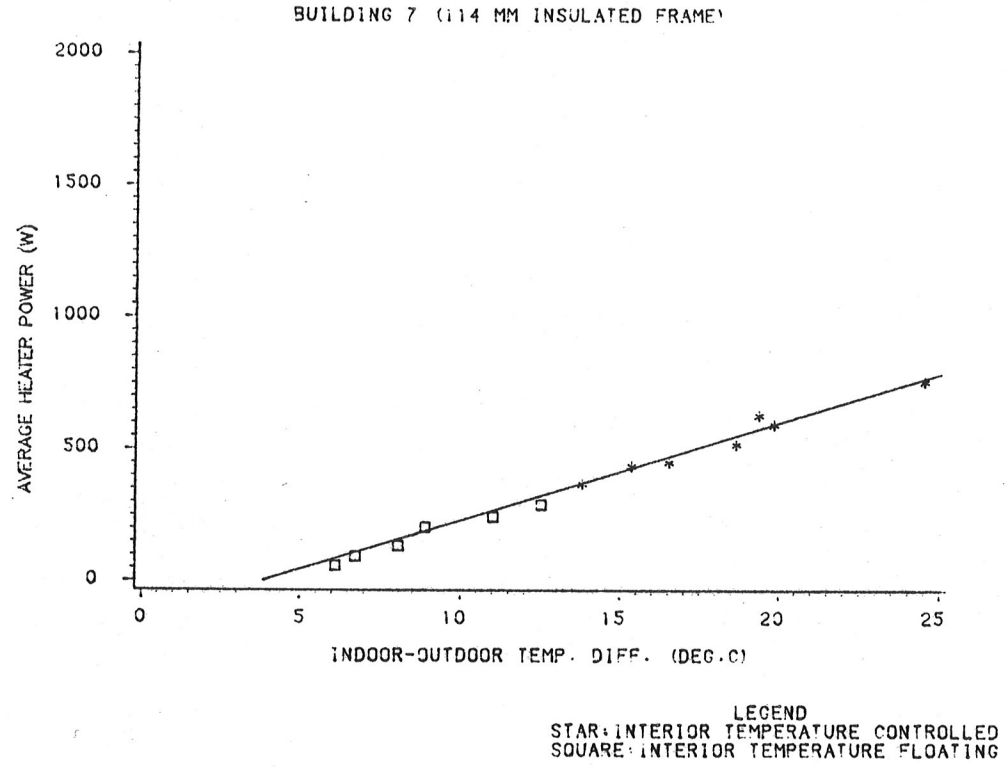

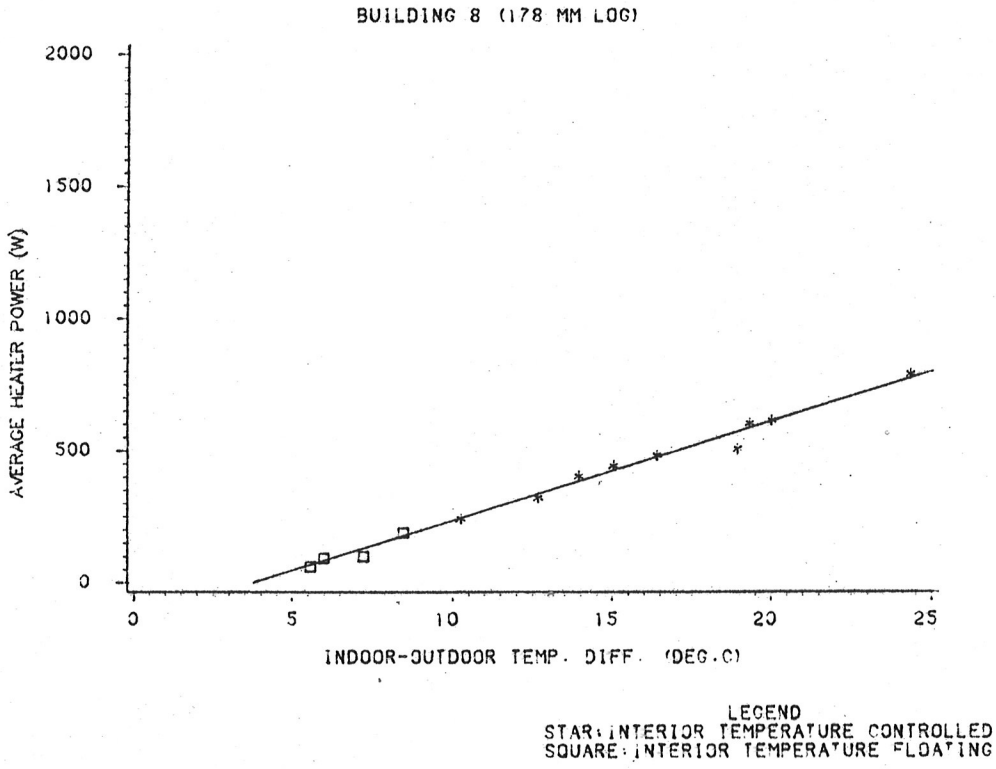

Figure 9: Steady-state Regressions - Buildings 7 and 8

The slope of the best-fit regression line through points corresponding to non-floating data are shown. They should be simply the summed (UA)-products for the building's envelope, including perimeter losses but not infiltration. Table 4 gives the intercepts and slopes of the best-fit lines, and compares the slopes with the summed (UA)-product calculated from envelope heat transfer properties given in Chapter 2.

The normalized regression coefficients have uncertainties as listed in Table 4. These correspond to a 0.90 confidence limit due to the scatter of the points. The summed (UA)-product uncertainties are also listed and correspond to at least two standard deviations. They are mainly from the uncertainties in measured R-values of the walls and roof. The expected agreement between summed (UA) products and normalized regression slopes is somewhat worse than the sum of the two uncertainties would suggest, because the measured R-values used for summed (UA) are also used in the normalizations of heating energy use which decrease the regression slopes. The normalized regression slopes agree with the summed (UA)-products, with some very important exceptions.

Building 7, the insulated frame, exhibits a slope that is 8.1 ± 6.5 W/°C greater than the summed (UA)-products. Construction flaws probably account for this discrepancy: there is a thermal short of solid wood at the wall-ceiling interface; and indirect infiltration (leakage of air under the exterior sheathing, but not through the vapor barrier) occurs where sheathing has pulled away slightly. Such losses do affect the energy use of the building, but are not included in the methodology of calculating summed (UA)-products. The other discrepancies arise from leaking roofs on buildings 7 and 8 in the summer and fall of 1982. The leaks were sufficiently bad that noticeable changes in normalized regression slopes and uncertainties occur in both buildings. The normalized regression coefficients for building 7 in late '82 were A = -225 and B = 47.3; for building 8 they were A = -158 and B = 43.6. Neither building 7 nor building 8 had sufficient late '82 data to analyze separately, so only early '82 data is considered for those two buildings.

What is important about the above procedure is that we have demonstrated a rational normalizing procedure that converts data to standard conditions that depend only on indoor-outdoor temperature difference. The temperature difference corresponding to the building balance point can be easily determined: graphically, it is the intercept with the horizontal axis in Figures 6 through 9; algebraically, it is the ratio A/B of the normalized regression coefficients of Table 4. The balance point sets the stage for accurate estimates of excess energy use due to floating of interior air temperature.

TABLE 4

Summary of Normalized Heating Energy Regressions

The regression equation is:

$$Q_{norm} = A + B\,(T_{plenum} - T_{out})$$

Bldg.	--Raw data-- A (W)	B (W/°C)	-Normalized- A (W)	B (W/°C)	Σ UA (W/°C)
1	-446 ±87	93.6 ±4.9	-169 ±51	84.3 ±3.0	88 ±10
2	-472 ±77	96.6 ±4.3	-151 ±45	81.8 ±2.6	86 ±9
3	-426 ±49	88.7 ±3.0	-174 ±36	77.6 ±2.3	75 ±8
4	-127 ±46	68.2 ±2.8	-67 ±31	56.3 ±2.0	57 ±5
5	-511 ±77	97.4 ±4.3	-173 ±57	85.0 ±3.3	88 ±10
6	-225 ±111	66.6 ±5.7	-256 ±95	69.0 ±5.0	61 ±5
7*	-137 ±110	42.8 ±5.7	-142 ±65	37.1 ±3.5	29 ±3
8*	-182 ±78	44.7 ±4.3	-142 ±40	37.7 ±2.3	36 ±3

- - - - - - - -

* Tabulated regressions for bldgs. 7 and 8 based on early '82 data only. Leaky roofs increased the late '82 regression slopes considerably (see text). See text for explanation of uncertainties.

5.4 THE EXCESS ENERGY USE WHEN A BUILDING INTERIOR TEMPERATURE FLOATS

5.4.1 Theory

Suppose that one knows the balance point T_{bal} of a perfectly sealed building, in an environment without sunshine, with outdoor radiative temperature equal to outdoor air temperature. Then excess energy due to floating of interior air temperature, using data time-averaged over several days, is easy to estimate:

$$Q_{excess} = Q_{heat} \text{ , if } T_{out} > T_{bal} \text{ , and}$$

$$Q_{excess} = (\Sigma UA + A_{fl} / R_{fl}) (T_{in} - T_{ctrl}) \text{ , if } T_{out} < T_{bal} \text{ ,}$$

where T_{ctrl} is the thermostat setpoint.

To estimate the balance point for a building subjected to infiltration heat loss L_{inf}, let the balance point be changed to

$$T_{bal,i} = T_{bal} + (L_{inf} / \Sigma UA) (T_{bal} - T_{in}) / (T_{out} - T_{in}) .$$

On a graph of heater energy use vs: $(T_{in} - T_{out})$, this is a pivoting of the regression line about the y-axis intercept.

To estimate the effect of a heat gain rate R_{rad} due to sunshine and long-wave radiation on the building exterior, as well as floor heat losses L_{fl}, let the balance point be

$$T_{bal,f,r,i} = T_{bal,i} + (L_{fl} - Q_{rad}) / \Sigma UA .$$

With an estimate of the actual balance point for the building in its environment, all that remains is to apply the equations for Q_{excess} above to calculate excess heat use due to floating -- excess heat use that could be eliminated by proper use of thermal mass.

5.4.2 Results

The above procedure was applied to the time-averaged data already used for the regressions earlier in this chapter. The results are presented for two test buildings for several data blocks in Figure 10. The graphs, for a heavy building (279 mm adobe) and a light building (114 mm insulated frame), very clearly show that there is excess heating energy used when a building's interior temperature floats above the thermostat control point for part of a day. (The zero excess energy use line represents a truly reversible system.) The highest outdoor temperature for this data is very near the building balance point. Time periods with slightly warmer outdoor temperatures might produce slightly higher excess energy use, but increasing outdoor temperatures higher yet will reduce excess energy use, until it reaches zero when the building floats the entire day, requiring no heat at all.

This method for estimating excess energy use appears to be qualitatively successful for predicting the onset of excess energy use. Quantitatively, the method suffers from very large experimental uncertainties.

The next chapter will explore another method for estimating excess energy use, in the hope of reducing the uncertainties.

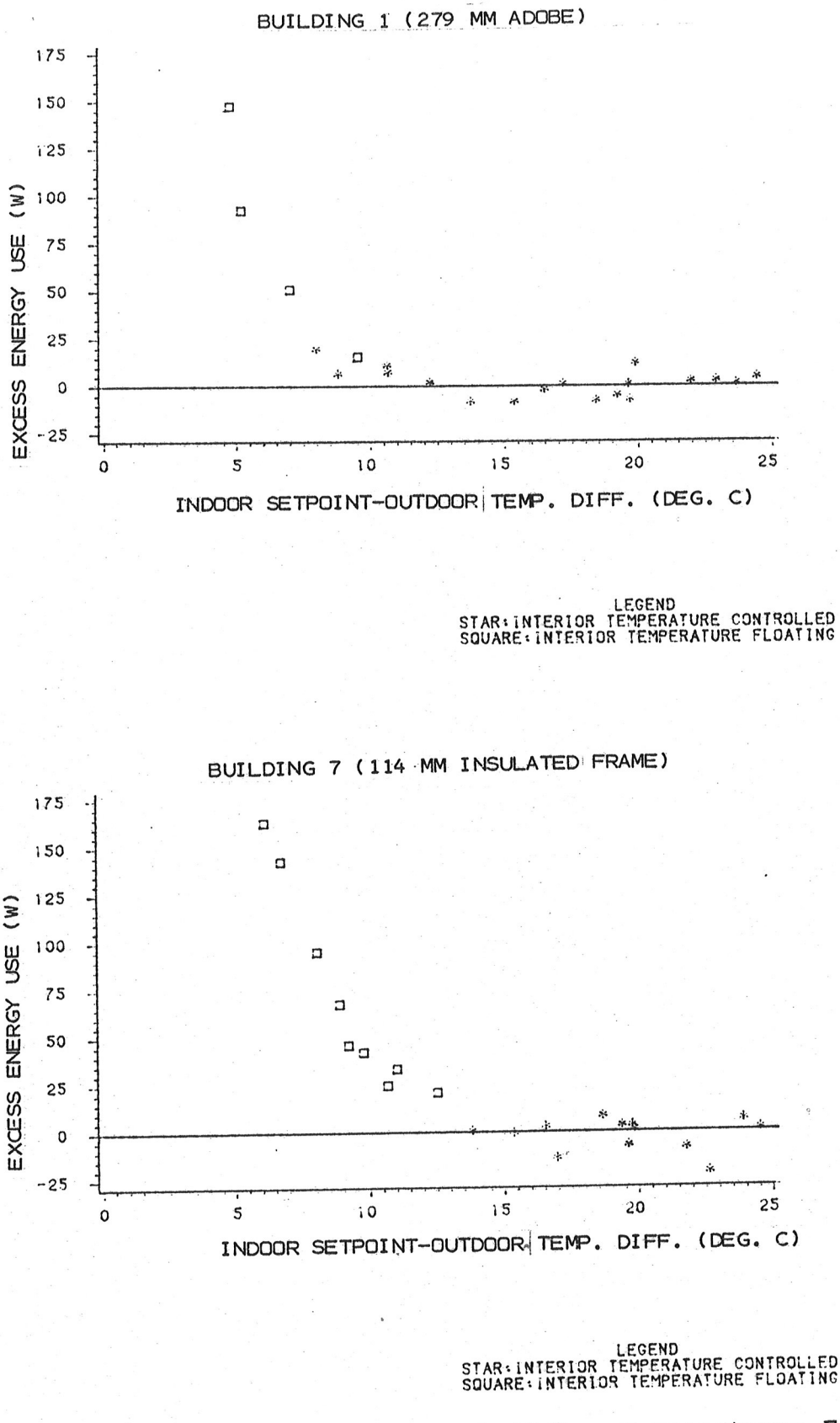

Figure 10: Excess Energy Use When Building Temperatures Float

Chapter 6

DIRECT COMPARISONS OF TEST BUILDING HEATING ENERGY USE

The previous chapter demonstrated that heat flow though the building envelope can be predicted using steady-state calculations with averaged weather data and interior conditions. If the building temperature does not float above the thermostat setpoint, interior conditions are defined by the thermostat setpoint. In the present chapter, a direct comparison of the heating energy required to maintain a thermostatically controlled lower limit on indoor temperature in different test buildings reveals the differences in their seasonal heating energy use patterns.

The methods of this chapter are direct, in the sense that very little calculation is needed, and no complex models are invoked. Uncertainty analysis was applied to each step of the calculations, and conclusions were drawn from the results consistent with the uncertainties in the data.

The results of this chapter indicate that only building 7 (the 114 mm insulated frame) consumes measureable energy in excess of steady-state predictions using averaged weather data. That excess energy consumption is 3.5% ±2% of annual heating energy use. All other buildings incorporate sufficient thermal mass in their envelopes that energy use in excess of steady-state predictions using averaged weather data was less than 2% of annual heating energy use, the uncertainty in the measurements.

6.1 THE DATA

The data used in this analysis was obtained from January 3 to December 22, 1982, and consists of manual readings of kilowatt-hour meters taken and recorded approximately every other day. Figures 11 to 14 show the average daily energy used by each test building, as measured by manual readings of kWh meters, averaged for periods of five or more days, and plotted against the same averaged data for test building 3, which has 381 mm adobe walls. The solid and dashed lines represent two levels of experimental uncertainty and will be discussed in the next section. Building 3 was chosen for a comparison standard because it is the lightest structure which does not exhibit significant floating behavior. (In fact, it did not float significantly more

than building 4, the 635 mm adobe.) In effect, the heating energy required by building 3 serves as an indirect measure of weather severity as 'seen' by the thermostat after the weather information is filtered (in the information theory sense) through the thermal network of a building's envelope. The weather information is not simply outdoor air temperature, but includes all effects: sunshine, wind, long-wave radiation, floor losses, latent heat losses due to rain-wetting of walls, and so on.

From hourly measurements for those blocks of data that were analyzed in great detail, some data points are known to represent energy use when the inside temperature floated above the thermostat setpoint, while others represent energy use when the building temperature did not float at all. In Figures 11 through 14, such points are distinguished from those for which there is no certainty one way or the other.

The energy use is sensitive to thermostat setting, particularly when outdoor temperatures are near a building's float point. For that reason, the energy use data in Figures 11 through 14 has been corrected to a constant 20.6 degrees C thermostat setpoint, as follows. The actual temperature maintained by each thermostat depends on its setting and its sag due to the local heating by the thermostat's anticipator. The sag is a function of the heating demand. From the measured relationship between demand and the thermostat regulating temperature (see Appendix B), and the measured envelope heat transfer characteristics (see Table 4), the kWh meter data can be corrected to represent the energy use for a constant 20.6-degree C interior temperature. The building envelope heat transfer coefficients have the solar component removed, and so represent only envelope transmission of heat due to air-to-air temperature difference, including averaged infiltration.

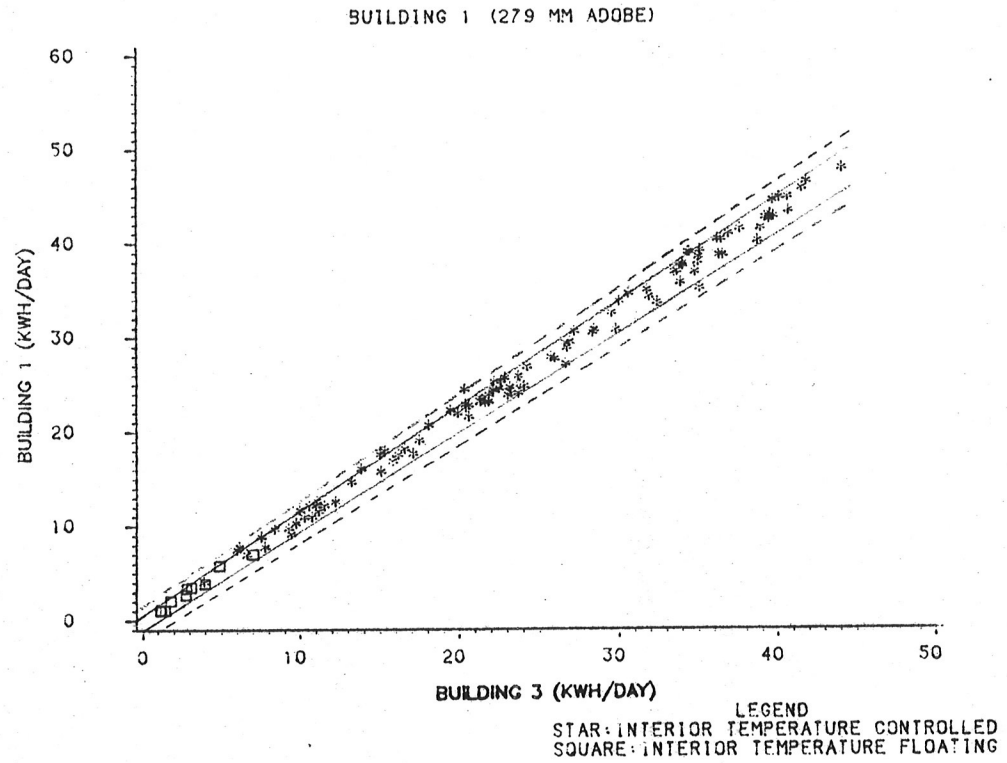

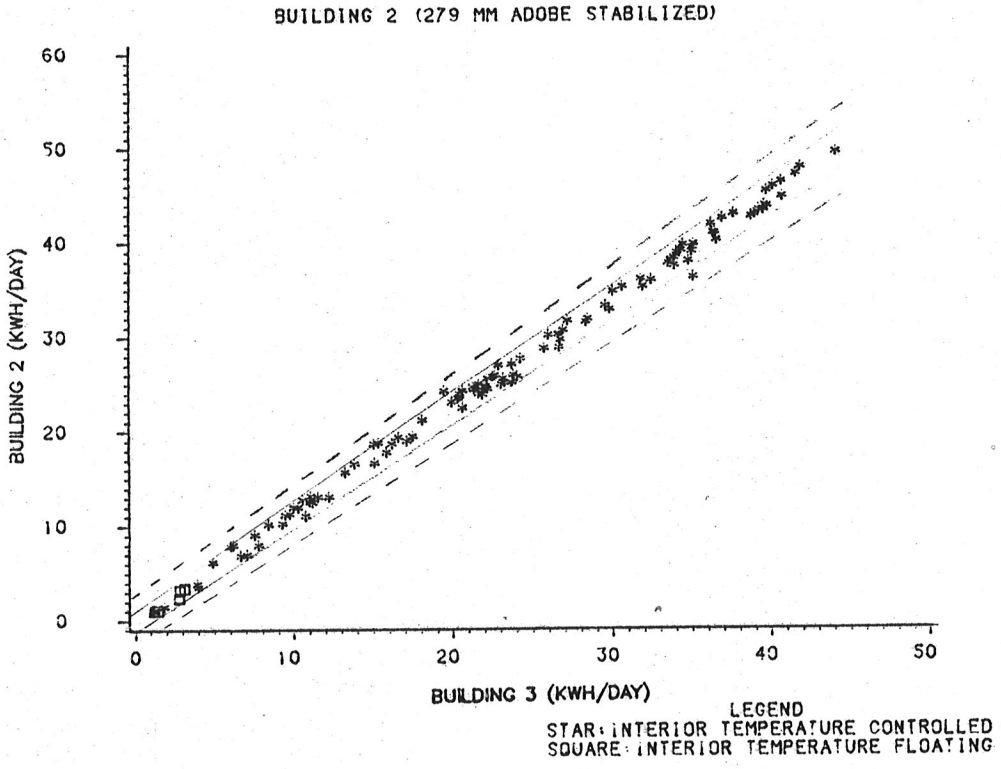

Figure 11: Heating Energy Use Comparisons - Buildings 1 and 2

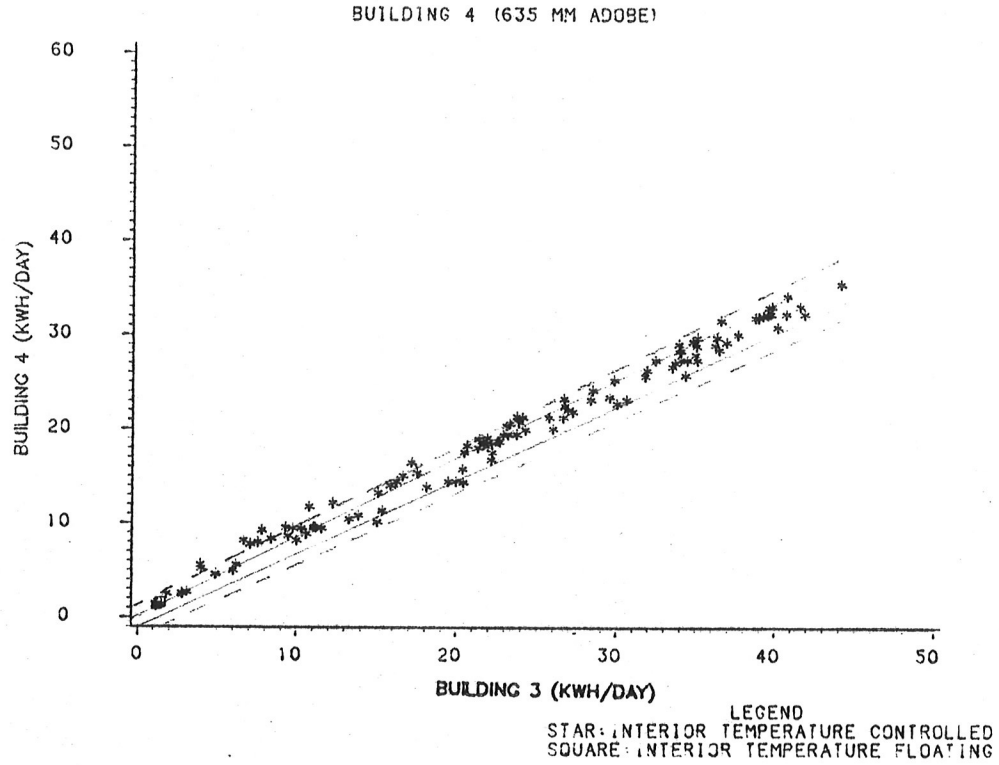

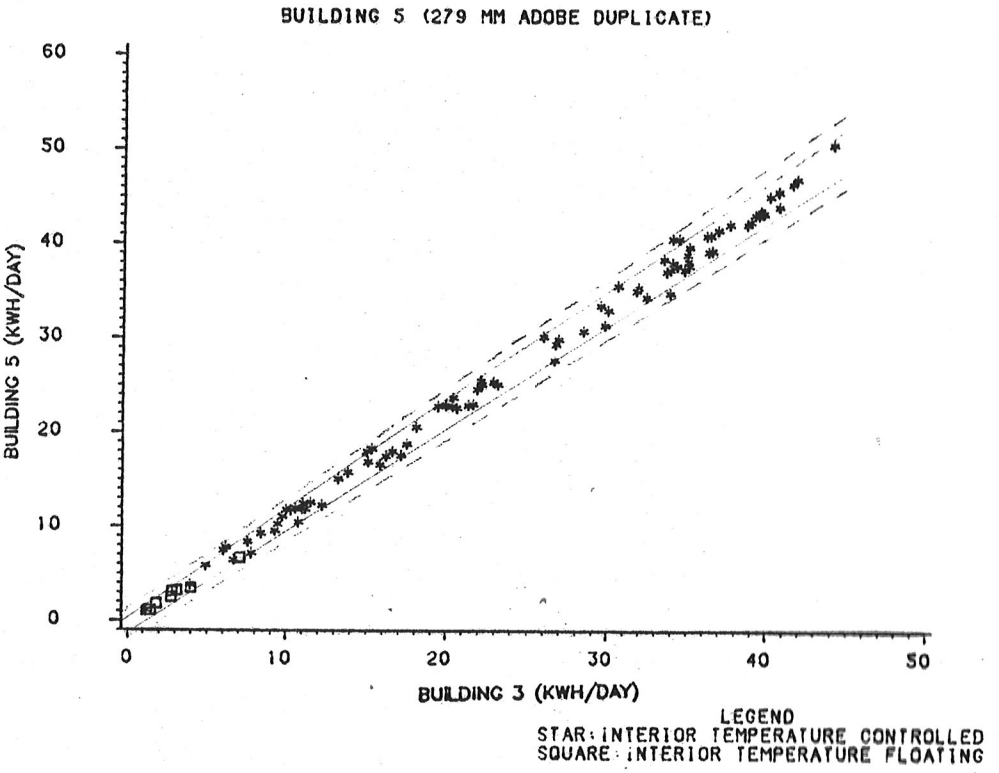

Figure 12: Heating Energy Use Comparisons - Buildings 4 and 5

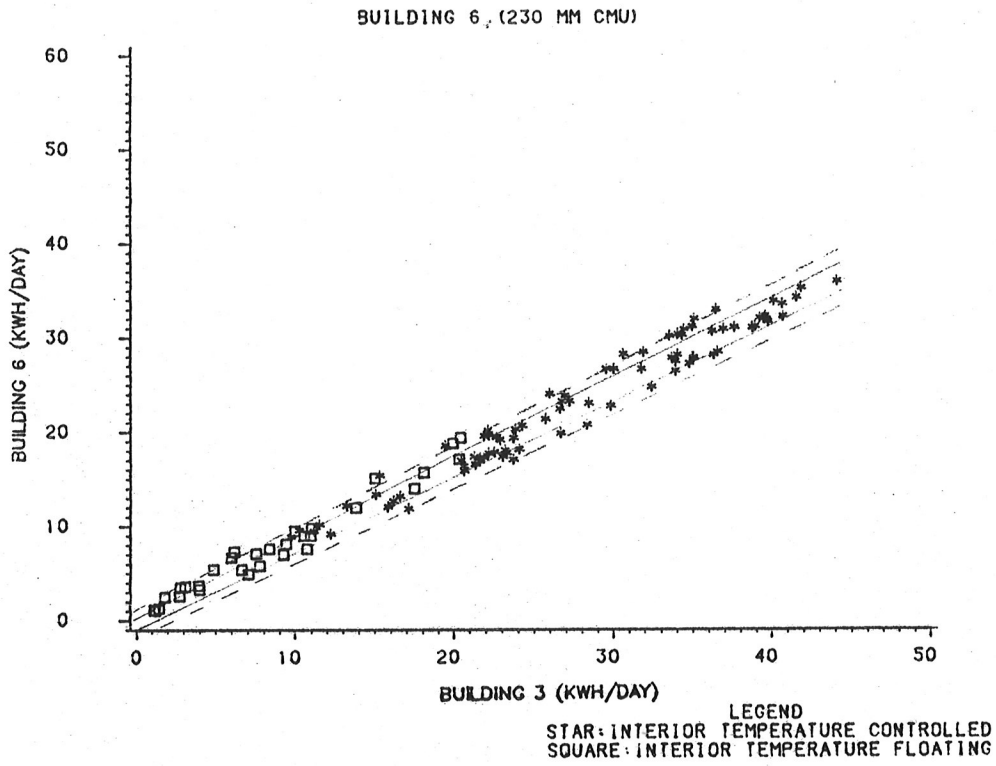

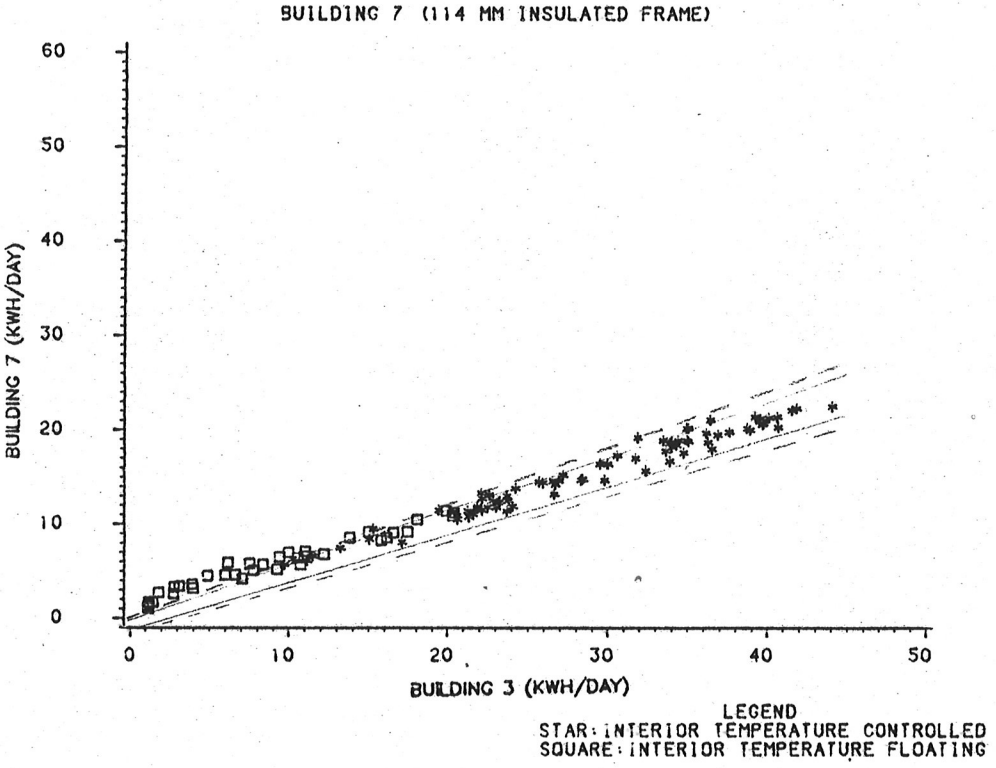

Figure 13: Heating Energy Use Comparisons - Buildings 6 and 7

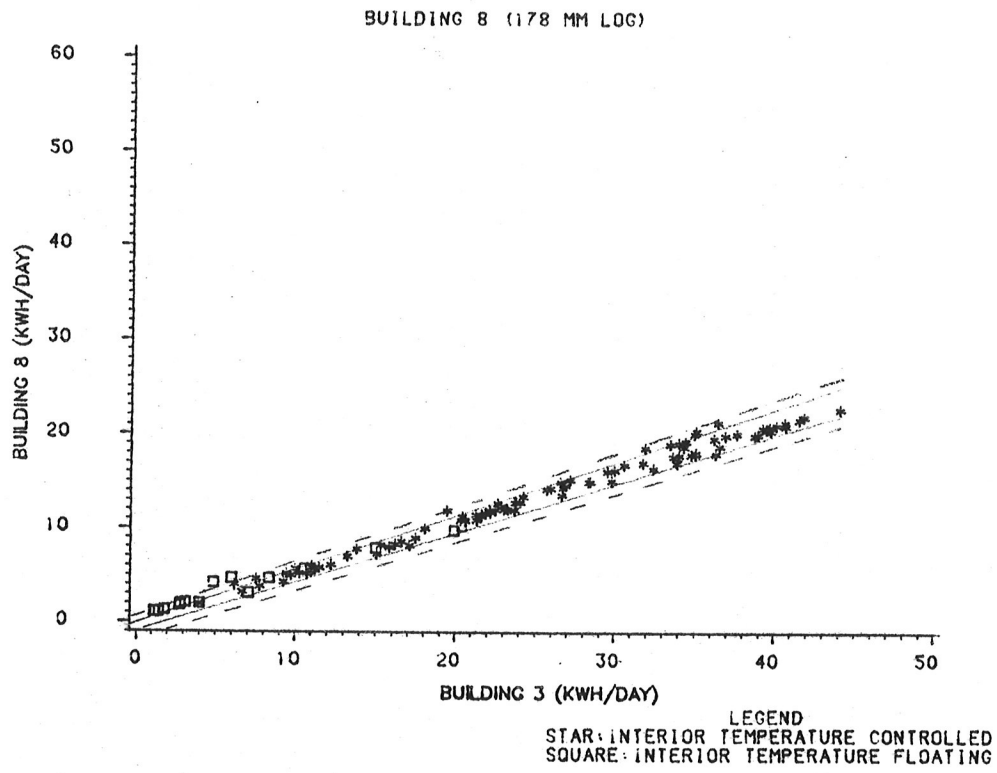

Figure 14: Heating Energy Use Comparisons - Building 8

6.2 EXPERIMENTAL UNCERTAINTIES

The dashed and solid lines in Figures 11 through 14 represent two different levels of experimental uncertainties. The solid lines represent deviations that can be attributed to differences between buildings, not necessarily the walls. The dashed lines are the uncertainty limits for deviations from proportionality that can be attributed to the effects of different wall constructions (rather than unintended differences in floors, for example).

The experimental uncertainties are critical to the evaluation of the results of this chapter, because the "thermal mass effect" we are looking for is small, and it must be established that measurement uncertainty is not mistaken for the effect. Experimental uncertainties are presented in Table 5.

The first uncertainty is measurement uncertainty, which consists of individual point uncertainty and nonlinearity error. The uncertainties in the difference of two kilowatt-hour meter readings, each accurate to ±2% ±0.1 kWh, is ±2% ±0.2 kWh. That

is the uncertainty in individual points, but what is of primary interest here is the shape of the energy use pattern over the year. The shape is influenced by the nonlinearity of the kWh meters, which is estimated at ±0.4% of the maximum power during the experiment, about 50 kWh/day: the nonlinearity error is then ±0.2 kWh. The sum of these is ±2% ±0.4 kWh. This is calculated for each building when building 3 (381 mm adobe) uses 10 kWh/day and 40 kWh/day, and presented in Table 5 under "Measurement Uncertainty." (Building 3 is not included here, because it is not being compared with itself.) Other uncertainties, more difficult to evaluate, are considered below.

The second uncertainty is the random scatter uncertainty, obtained from linear regression analysis of the non-floating data points in Figures 11 through 14. Buildings that have energy storage and delay properties much different from building 3 have a scatter of points because the interior of these buildings "sees" exterior weather from a different time interval than building 3. This scatter is particularly evident for building 4 (635 mm adobe walls). Random short-term variations in the weather (shorter than the averaging time period of 5 or 6 days) produce a random scatter that does not affect the local mean line, but does add considerably to the uncertainty of individual points. This random scatter is shown in Table 5 under "Random Scatter Uncertainty," again calculated for the two levels of energy use. (The thermostat setpoint corrections are generally small, so they introduce negligible uncertainties compared to those above.) The solid lines in Figures 11 through 14 represent the sum of the measurement and random scatter uncertainties. These lines are at least two standard deviations from the mean line, so than fewer than one point in twenty should fall outside them by chance.

Weather variations on time scales of 5 or more days produce systematic shifts of the local mean line, and are discussed under results, below, as the need arises.

The third uncertainty is based on examination of energy balance residuals (see Section 3.3). Looking at all of the 22 data blocks for which the outside temperature was greater than 6°C, the maximum difference between the energy balance residual for each building and that of building 3 was determined. That number is presented for each building in the column labeled "Energy Balance Residual" in Table 5.

The last columns in Table 5 are the sums of the first three uncertainties and are represented by the dashed lines in Figures 11 through 14. These are the uncertainty limits for energy use changes that could be attributed specifically to effects caused by the different wall constructions.

TABLE 5

Energy Use Comparison Experimental Uncertainties

Units: kWh/day

Bldg.	Measurement Uncertainty		Random Scatter Uncertainty		Energy Balance Uncertainty	Total Energy Use Uncertainty	
	10	40	10	40		10	40
1	±0.62	±1.27	±0.03	±0.13	±0.72	±1.37	±2.12
2	±0.63	±1.30	±0.03	±0.11	±1.96	±2.61	±3.37
4	±0.56	±1.06	±0.04	±0.16	±0.60	±1.20	±1.82
5	±0.62	±1.29	±0.03	±0.13	±1.31	±1.97	±2.73
6	±0.57	±1.06	±0.05	±0.21	±0.74	±1.36	±2.02
7	±0.51	±0.83	±0.03	±0.12	±0.98	±1.52	±1.92
8	±0.51	±0.83	±0.02	±0.09	±0.54	±1.07	±1.45

Note: "10" and "40" refer to the uncertainties when building 3 uses 10 kWh/day and 40 kWh/day

6.3 RESULTS

There is now considerable experimental and numerical simulation evidence suggesting that building heating energy consumption is independent of envelope mass, and depends only on steady-state insulating value of the envelope, when building temperatures do not float up above the thermostat setpoint (see Section 1.2 for references, and Chapter 5 for results from the present work). That is, when a building requires heat throughout each day, so that building temperatures do not float, steady-state calculations based on averaged weather data accurately predict heating energy use. (The total heat flow through the walls must be large compared to stored energy changes in the walls, however.) From the results of the previous chapter, building 3 (381 mm adobe) temperature never floats sufficiently to produce a measureable rise in interior air temperature. Hence any building whose energy use deviates from proportionality to building 3 energy use, deviates from energy use calculated using steady-state methods and averaged weather data.

Figures 11 through 14 show that the only unequivocal deviations from proportionality to building 3 energy use occur for buildings 4 (635 mm adobe) and 7 (114 mm insulated frame). Each data point that falls outside the area bounded by the solid lines shows disproportionate energy use with 95% certainty, and several nearby points outside the solid lines represent practical certainty. Those buildings, therefore, at times use more heating energy than steady-state methods using averaged data would predict, but for fundamentally different reasons.

Building 4 (635 mm adobe) uses more than proportional heating energy, compared to building 3 (381 mm adobe), only during a long period of rapid outdoor temperature increase: the daily average outdoor air temperature rises about 22°C in eight days. Because building 4 interior heat demand responds to weather slower than building 3, its heating energy use lags behind the rapid decrease in building 3 energy demand. The effect is illustrated in the upper graph of Figure 15. Several data points, representing 6-day averages with starting times spaced two days apart, are connected in time sequence by arrows. When heating demand is falling, the energy use is higher than proportional; when demand is rising, the energy use is lower than proportional. The few points that lie above the solid line occur during a very exceptional temperature rise. The effect is real, but excess energy used during warming weather is compensated by energy saved during cooling weather. No net annual energy use effect is expected. (During the same period, building 7 also exhibits similar behavior, as shown in the lower graph of Figure 15, except that it has less delay than building 3, and so has the opposite sign for the effect.) Stated another way, the net change in the energy stored in the very thick 635 mm adobe walls was not small, when compared to the total heat flow through the wall during each averaging time period.

Building 7 (114 mm insulated frame) uses more than proportional energy, compared to building 3 (381 mm adobe), but for a different reason than the above. The disproportionate energy use only occurs when the building interior temperature floats above the thermostat setpoint for part of the averaging time period. Even when building 3 requires no heating energy whatsoever, building 7 requires about 1.5 KWh/day, or 62 watts, to maintain a lower limit of 20.6°C for indoor air temperature. This effect is repeated during mild autumn weather, and adds to the spring effect represented in the data.

In summary, for the rather strict 0.95 confidence level uncertainty lines drawn in the figures, one can say that buildings 4 and 7 both use disproportionate heating energy, compared to building 3. Both buildings certainly use heating energy in excess of steady-state predictions using averaged data. They do so at different times, and for different reasons. Building 4 (635 mm adobe) uses excess energy during a time when the weather is warming rapidly, and would recover that energy

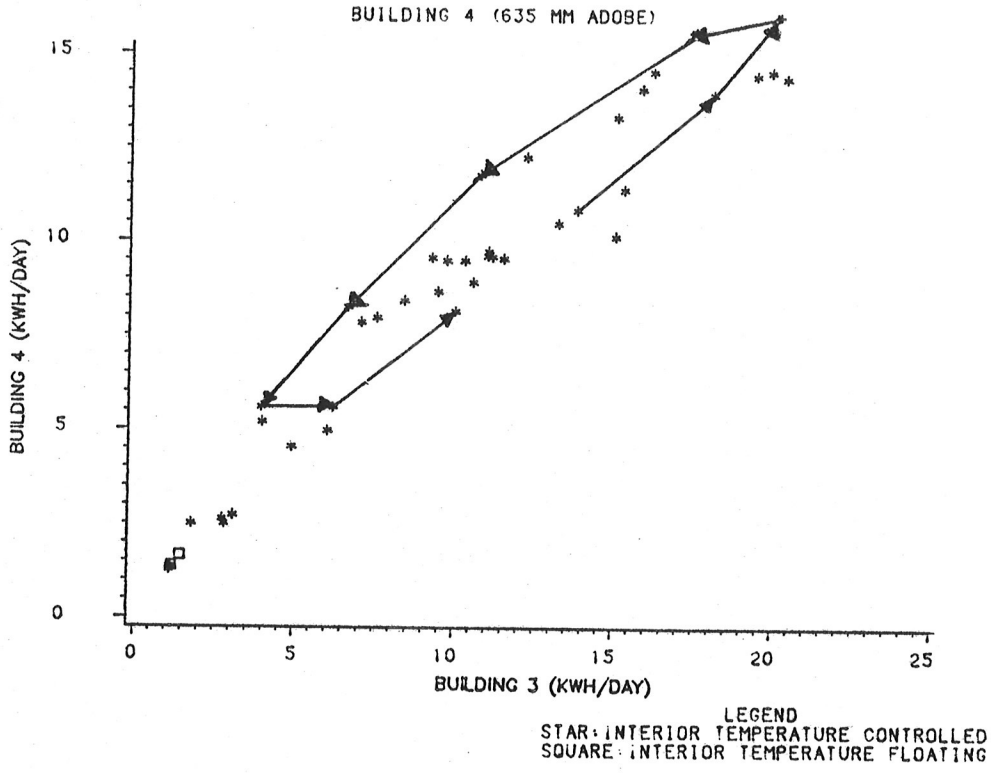

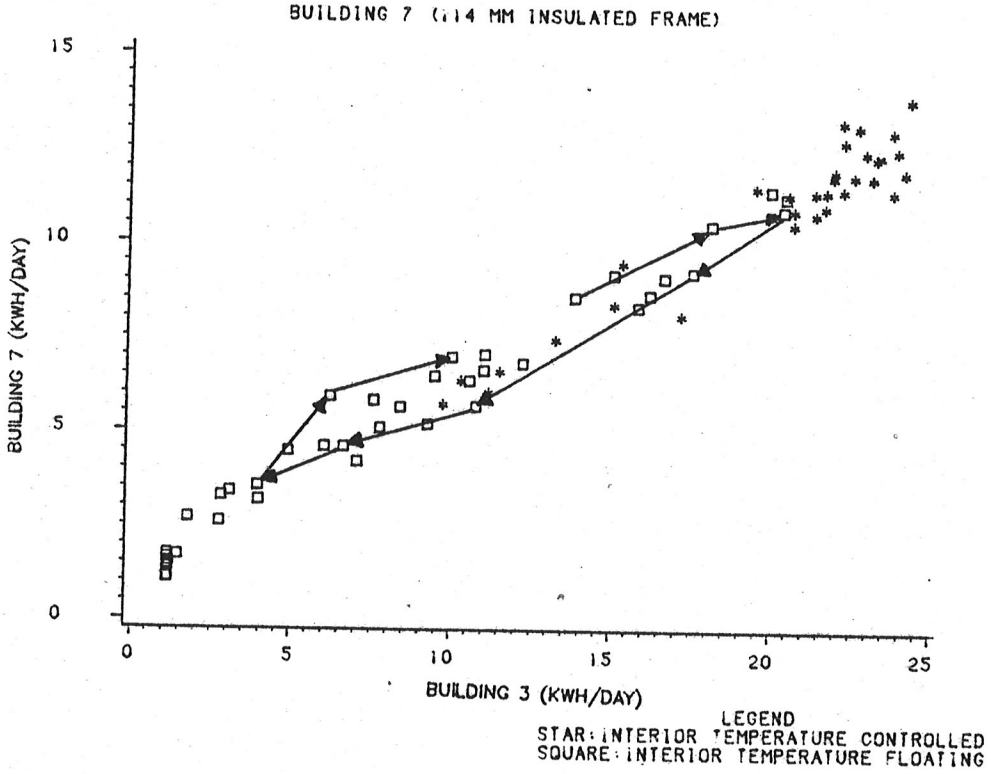

Figure 15: Delay Effects During Rapid Weather Changes

during a period of cooling weather. Building 7 (114 mm insulated frame), however, uses excess energy because interior air temperature floats above the thermostat setpoint, therefore increasing average indoor-outdoor temperature difference and resulting in increased envelope heat losses.

Building 7 is the only building which has a majority of its floating points above the dashed lines. This deviation can be attributed to differences in the walls, because the dashed lines represent uncertainties which include the energy balance residual. For the other buildings, at the 0.95 level of certainty, the observed effect cannot be attributed to the walls, but only to the building as a whole. For example, slight differences in floor losses due to unequal settling of the soils beneath different slabs might be the cause of observed deviations from proportionality. At a reduced confidence level of 0.80 (about 1.3 standard deviations), however, effects in buildings other than building 7 are attributable specifically to differing wall constructions.

The data can be aggregated into two time periods, one during which the weather was sufficiently cold that no building's interior temperature floated above the thermostat setpoint, and another which includes all the data. That aggregated data, corrected to a constant plenum temperature of 20.6°C, is presented in Tables 6 and 7 as "20.6°C Heating Energy." Table 6 represents data for the first half of 1982, and Table 7 represents data for the second half.

These data allow a direct comparison of building energy use deviations from steady-state theory using averaged data, and add to confidence in the data through additional consistency checking. The heating energy use for the time period when no building's interior temperature floated above the thermostat setpoint is equal to the heating energy use predicted by steady-state methods using averaged data, as shown previously. Therefore, the ratio of heating energy used during the entire data period, to the heating energy used when no building floated, gives a direct comparison of energy use patterns for the eight test buildings. That energy use ratio is listed in Tables 6 and 7 as "Ratio."

From the results of the previous chapter, buildings 3 and 4 had no measurable energy use increment due to floating of interior temperatures. Because building 3 is the lightest building which did not float significantly, the building 3 ratio has been subtracted from all other ratios. This difference is shown in the fifth column of Tables 6 and 7, and the relative values indicate the extent of excess energy use. Table 6 shows that, in the first half of 1982, all buildings except 7 have energy use ratios that are within experimental uncertainty of each other. Building 7, the insulated frame structure, has the highest energy ratio -- it is the only one of the eight test

TABLE 6

Comparison of Heating Energy Use Patterns

First Half, 1982

Units : kWh

Bldg.	20.6°C Heating Energy Cold	All	Ratio	Difference From Bldg.3	Uncertainty
1	2967	3585	1.208	±.001	±0.020
2	3076	3710	1.206	-.001	±0.020
3	2741	3308	1.207	--	±0.020
4	2280	2822	1.238	±.031	±0.020
5	2989	3593	1.202	-.005	±0.020
6	2211	2696	1.219	±.012	±0.020
7	1442	1824	1.265	±.058	±0.020
8	1440	1766	1.226	±.019	±0.020

Notes:
"Cold" is heating energy use (kWh) for time period during which no building temperature floated.
"All" is heating energy use (kWh) for all the data.

buildings that uses disproportionate heating energy beyond experimental uncertainties when its interior temperature floats. The effect is 5.8% of the total energy used from January through June, 1982. (For the '81-'82 heating season, about 60% of the heating degree days occur during that time. If the autumn effect were similar, the annual effect would be over 7.5%.)

Table 7 presents the same data for the second half of 1982. The effect is much smaller, about 0.8%. The kWh meter readings begin at the end of September, after 2% of the heating degree days for the '82-'83 heating season had occured. (Cooling season night ventilation tests were being performed during most of September.) Had heating season tests in the fall been started earlier, this small 0.8% effect could have been larger, but the fact remains that most people living in the area near the test site would not have turned on their heating systems for the

TABLE 7

Comparison of Heating Energy Use Patterns

Second Half, 1982

Units : kWh

	20.6°C Heating Energy				
Bldg.	Cold	All	Ratio	Difference From Bldg.3	Uncertainty
1	1799	1965	1.092	±.002	±0.020
2	1852	2027	1.094	±.004	±0.020
3	1622	1768	1.090	--	±0.020
4	1292	1399	1.083	-.007	±0.020
5	1844	2015	1.093	±.003	±0.020
6	1466	1610	1.098	±.008	±0.020
7	917	1007	1.098	±.008	±0.020
8	898	979	1.090	.000	±0.020

Notes:
"Cold" is heating energy use (kWh) for time period during which no building temperature floated.
"All" is heating energy use (kWh) for all the data.

winter until the end of September. It is also possible that there is less variation in the weather in fall, compared to spring (i.e., more late spring storms than early fall storms). Furthermore, the center floor losses, which lag the weather by several months, would be at a minimum during the fall intermediate season, but at a maximum during the spring intermediate season. It is thus possible that the small effect for the late '82 data is real and may be repeatable. The variability of weather, and consequently the variability of the thermal mass effect, during the intermediate seasons is an area that requires further study.

If we add the kWh meter readings from Tables 6 and 7 and calculate the effect for the entire calendar year 1982, it is 3.5% ±2%. It is clear that the deviations from steady-state predictions for windowless test buildings without internal heat

loads are small, even in New Mexico's high desert climate, with diurnal temperature swings often exceeding 15°C, and insolation above 0.7 of the extraterrestial value. The largest observed effect, for building 7, is 5.8% ±2%. No other building shows an effect due to floating larger than the ±2% experimental uncertainty.

Chapter 7

SUMMARY OF RESULTS AND CONCLUSIONS

The Southwest Thermal Mass Study can clearly discern heating energy deviations from the predictions of steady-state theory using averaged data for all test buildings, except the two thickest adobes. The deviations occur only when the interior of a test building floats above the thermostat setpoint for part of each day. The deviations are small -- the largest deviation, for the insulated wood-frame building, would amount to 3.5 ±2% of annual heating energy use, despite the very large diurnal temperature swings and intense insolation typical of the high desert site.

Specifically, the conclusions are as follows:

- if heating is required continuously, the heating plant operates in a linear mode, and the average heating requirement agrees with steady-state theory and is a function of steady-state R-value only
- if the interior temperature floats above the thermostat setpoint for part of each day, the heating plant operates in a non-linear mode and will use energy in excess of that predicted by steady-state theory using averaged data (this is the "thermal mass effect")
- this excess energy use results from increased average inside temperature only
- if heating energy use is normalized to building heat transfer coefficient, this effect is greatest for buildings with least thermal damping in the envelope
- the radiative environment was an important factor for comfort, and those buildings with low R-value walls would have been uncomfortably cold in midwinter
- the observed effect was 3.5% ±2% of total annual heating energy use and occured in the most lightweight structure

Each conclusion, except for the last one, is based on theory and is corroborated by the data. As such, these conclusions are general and apply anywhere. The last conclusion includes specific numerical results and is strictly valid for only those conditions under which the experiment was performed: the

particular materials used in the buildings; the construction and dimensions of those buildings (particularly the fact that they were windowless, thus removing from the experiment the time delay properties of thermal mass); the climate of the test site (high desert, with large diurnal temperature swings and high insolation); and heating season data only (the cooling effect is expected to be much larger).

For most test buildings, the observed effects were too small, compared to experimental uncertainties, to be measured directly by comparing measured energy use to steady-state theory (the analysis methodology of Chapter 5). Rather, by simple recourse to the properties of linear systems, and how they differ from nonlinear systems, a test was devised that compares energy use data against itself, bypassing many of the experimental uncertainty problems (the analysis methodology of Chapter 6).

The observed effect is not a "mass effect" as people have come to use that term. It is not the envelope per se, but its participation in the varying net heat flux to the interior air, and interaction with the thermostat nonlinearity just when heating demand goes to zero, that produces the observed effect. In the present work, attenuation of heat flux variations was the critical property, because there were no variable heat sources or sinks in the buildings. (Future work will address the time-delay property of envelope thermal mass.)

Appendix A

DATA QUALITY

The Southwest Thermal Mass Study is designed to look at the sometimes subtle thermal effects of mass in building envelopes. When mass effects are small, it is essential that data integrity be protected from conscious or unconscious biases; and that experimental uncertainties in measured and derived results be quantified, so that inferences are drawn consistent with data quality. The quantification of data quality is critically important to interpretation of this experiment's results.

A.1 DOCUMENTATION

The following information pertinent to the construction of the test facility, instrumentation of the test buildings, data acquisition, and data analysis has been preserved:

1. Construction data exists in the working drawings for the site. Interior and exterior photographs were taken of the test buildings during and after construction. Critical dimensions were measured after construction for use in data analysis.

2. Manufacturers' manuals for all critical apparatus are available as documentation of equipment performance. Manufacturers' data was used in analysis of experimental uncertainties only when it was consistent with observed performance.

3. Bound logbooks of all hand-recorded observations during construction, instrumentation, and data acquisition were maintained at the experimental facility at Tesuque Pueblo. Any observations that might be of value in data interpretation were recorded in the logbooks.

4. Software used for automated data acquisition and manual on-site data checking was developed specifically for the project. Program listings exist on paper and magnetic media.

5. Listings of software are preserved together with computation results for each step of data analysis.

A.2 CALIBRATION AND EXPERIMENTAL UNCERTAINTIES

Each important measurement's experimental uncertainty is evaluated below. The estimates of uncertainties vary from critical modifications of manufacturers' specifications, to estimates based on our measurements, to little more than guesses based on experience. Even the latter type of estimates of experimental uncertainty are valuable, because they explicitly show what biases might be implicit in interpretation of experimental results.

In all cases, the uncertainty estimates are generous, and include data logger uncertainties. The listed uncertainty corresponds to at least 2 standard deviations, so the probability of measurements falling outside the listed uncertainties is less than one in twenty.

A.2.1 Datalogger

The measurements are converted to digital form by a Doric 220 datalogger controlled by a Radio Shack Model II microcomputer that archives the data on 8-inch floppy disks. Two ranges of the datalogger are used, a ±30.000 millivolt range and a ±3.0000 volt range. Estimates of experimental uncertainty derived from manufacturer's specifications and our experience with periodic calibration of the datalogger are given in Table 8.

TABLE 8

Datalogger Experimental Uncertainties

	Data uncertainty	
	±30.000 mV range	±3.0000 V range
Calibration	±0.01% ±0.005 mV	±0.01% ±0.1 mV
Long-term stability	±0.03% ±0.003 mV	±0.03% ±0.1 mV
Temp. effect for ±10°C	±0.025% ±0.005 mV	±0.025% ± 0.1 mV
Absolute error	±0.065% ±0.013 mV	±0.065% ±0.3 mV
Error if calibration were perfect	±0.055% ±0.008 mV	±0.055% ±0.2 mV
Uncertainty for Southwest Thermal Mass Study when a shorted zero reference channel was supplied for each 20-channel multiplexer board:	±0.10% ±0.004 mV	±0.10% ±0.2 mV

A.2.2 Thermocouples

All temperatures used in data analysis were measured using solid #24 copper-constantan thermocouples. Industry standard specifications for copper-constantan thermocouples are given in Table 9. Any given lot of thermocouple wire can be calibrated to far better accuracy. Unfortunately, three different lots of the thermocouple wire were used in the experiment. In some cases, it is not certain which lot was used. Tests comparing thermocouples from different lots show a maximum difference between wire lots corresponding to 0.56°C measured temperature at 91.1°C, and approximately proportional differences down to the ice point.

Each set of twenty data channel inputs to the data logger is connected to an isothermal input block. A reference junction is connected to one data channel on each isothermal input block, and immersed in an ice bath. In use, the ice reference channel voltage is subtracted from the measurement thermocouple voltage, thus compensating for any data logger zero drifts within ±2 microvolts. Work-hardening of the thermocouple wire at the screw terminals of the data logger can add another ±2 microvolts of error, the largest observed voltage offset seen during

thermocouple calibration testing. Estimates of thermocouple data uncertainties, including data logger uncertainties, are listed in Table 9.

TABLE 9

Thermocouple Measurement Uncertainties

Industry specifications:	
'Standard' copper-constantan	±1°C or ±0.8% whichever is larger
'Special' copper-constantan	±0.5°C or ±0.4% whichever is larger
Southwest Thermal Mass Study estimates of data uncertainties for temperature differences, for -30 to +65°C (including datalogger uncertainties):	
Thermocouples from one lot of 'special' wire	±0.5% ±0.25°C
Thermocouples from one lot of 'standard' wire	±1.0% ±0.25°C
Thermocouples from mixed lots of wire	must be calculated from individual temperature uncertainties

A.2.3 Heat Flux Transducers

Uncalibrated heat flux transducers, Thermonetics Corporation model H11-18-U-G, were calibrated by the National Bureau of Standards using guarded hotbox methods, with the transducers embedded in a flexible neoprene matrix. The Bureau supplied two independent calibrations, in all cases within 2% of one another, and so within 1% of the mean.

The measurement of the heat flux transducer output is used to represent average heat flux through walls, floors, and ceilings -- areas much larger than the transducer, and composed of different materials. Two types of uncertainties are involved: one, due to the disturbance of the local heat flux caused by the

presence of the transducer; and another, due to the mounting of the transducer at a particular place on a randomly inhomogeneous surface, a place that will not normally have the average flux flowing through it. These two types of uncertainty are estimated for different wall types in Table 10. (The estimates are little more than educated guesses here.)

TABLE 10

Heat Flux Measurement Uncertainties

Calibration	±1.0%
Datalogger	±0.055% ±0.004 mV
Imbedded in adobe wall	
inhomogeneity	±3%
flux disturbance	±1%
Total	±5% ±0.004 mV
Mounted on surface of wood or gypsum board	
inhomogeneity	±2%
flux disturbance	±2%
Total	±5% ±0.004 mV

A.2.4 Alternating Current Power Transducers

All electrical power input to each test building is measured by a Hall effect power transducer, Ohio Semitronics, Inc., model PC5-58A. The manufacturer's accuracy specifications give a very wide leeway, to include all effects including power factors near zero at maximum currents. Our resistive heaters have power factors near one. For that reason, the basic percentage of reading error has been left near the manufacturer's specification, but the percentage of full scale error has been reduced drastically.

There is an additional uncertainty, sometimes very large, caused by the method of measurement. The Hall effect transducer is sampled 15 times an hour, and then averaged for the hour. Because the heating plant is either fully on, or fully off, those 15 readings per hour are each either at maximum reading, or at minimum. The resulting hourly uncertainty is described by the binomial distribution, and diminishes when time intervals of several hours or days are involved.

The electrical power input to each test building is also measured by an eddy-disk kilowatt-hour meter that is read manually approximately every other day.

The uncertainty estimates are listed in Table 11.

TABLE 11

Power Measurement Uncertainties

Hall effect transducer manufacturer's specifications:	
Temperature (-10 to +60°C)	±1% ±12 Watts
Accuracy (includes temperature, linearity, power factor, zero, repeatability)	±0.75% of full scale
Southwest Thermal Mass Study estimates for power factor near one:	
Accuracy (as above, but little temperature variation, and power factor near one)	±1.0% ±10 Watts
Kilowatt-hour meter	±2% ±0.1 kWh

A.2.5 Weather Instruments

The weather station consists of a rotating cup anemometer, a wind direction vane, a shielded thermistor thermometer, a relative humidity meter, and a barometer. Table 12 lists the estimated uncertainties in weather station measurements. Only the wind measurements are used for data analysis, to estimate infiltration rates and outside surface convective heat transfer coefficients. The other weather station measurements are of secondary importance. (Outdoor air temperature is measured by thermocouples at several locations which are shaded and radiation-shielded.)

Solar instruments consist of Eppley PSP pyranometers for total horizontal and south-facing total vertical measurements; an Eppley PIN tracking normal incidence pyrheliometer for direct normal measurements; and Eppley PIR pyrgeometer for incoming long-wave measurements facing upward. One Li-Cor pyranometer

faces each of the four cardinal directions to measure incident radiation on their vertical surfaces. Uncertainties for the solar instrumentation are also listed in Table 12.

TABLE 12

Weather Instrument Data Uncertainties

Texas Electronics weather station:	
Windspeed	±5% ±0.5 km/h
Wind direction	±5 degrees
Temperature	
shaded	±0.25°C
direct sun	reads up to 1 °C high
Relative humidity	±10% rel. hum.
Barometer	±0.5 mm Hg
Solar instruments and datalogger:	
Eppley PSP pyranometer	±1% ±10 W/m^2
Eppley PIR pyrgeometer	±1% ±20 W/m^2
Eppley NIP normal incidence pyrheliometer	±1% ±20 W/m^2
Li-Cor pyranometers	±5% ±20 W/m^2

A.3 DATA ACQUISITION, PREPARATION, AND VALIDITY CHECKING

Once the data acquisition software was written and debugged, and the transducers were checked for proper operation, most data acquisition was fully automatic. A Radio Shack Model II microcomputer controlled the operation of the datalogger, and archived the measurements of all 500 data channels hourly. Rapidly changing variables, such as weather measurements, heat fluxes, and heater power were sampled every four minutes and their average value was archived at the end of an hour. Approximately every two days the apparatus was checked to see that it was still operating, to aim the solar tracking mechanism, to tend thermocouple reference ice baths, and to record kilowatt-hour meter readings and other observations in the logbook.

Ten blocks of data, each from 8 to 17 days in duration, were selected for detailed analysis on the basis that logbook entries indicated minimum problems with data acquisition. Those ten blocks of data were then transcribed from a high-density magnetic

disc format to a format that could in turn be transcribed onto 9-track magnetic tape. The magnetic tape served as input to create Statistical Analysis System (SAS) data files for data analysis.

Printed plots of all the critical data for each hour were painstakingly scrutinized for discontinuities, large random errors, ice bath integrity, and equipment malfunction. A few days' data was rejected because of ice bath problems -- the thermocouple reference junction ice bath had either melted or frozen sufficiently to shift temperatures by 0.3°C or more. There were a few malfunctioning thermocouples and flux sensors, and an entire data block with ice bath problems for test building 4. When the suspect data was eliminated, there remained 22 shorter data blocks of high quality, ranging from 4 to 7 days in duration. These data blocks were then subjected to the detailed analysis that is discussed in later chapters of this report.

A.4 SPECIAL MEASUREMENTS

Measurements of solar absorptance of the test building walls, test building infiltration, infrared imaging system scans of the buildings to check for inhomogeneities and construction flaws, and other special tests were performed as necessary. The results of these special tests, and the experimental uncertainties associated with them, are presented in Appendix B, Test Building Characterization.

Appendix B

TEST BUILDING CHARACTERIZATION

This appendix presents measurements that characterize the thermal behavior of the test buildings.

B.1 THE WALLS

B.1.1 R-values of the Walls

Wall and roof R-values were calculated from in situ measurements of surface-to-surface temperature differences, and inside surface heat flux, using the relationship

R = (Mean Temp. Difference) / (Mean Heat Flux) .

This relationship is rigorously true only if initial and final stored energy distributions in the walls are identical. For sufficiently long averaging time periods, the changes in heat energy stored in the walls are small compared to the net transmitted flux, and the relationship is a good approximation.

R-values were calculated for each wall of each building, using data blocks from January to June of 1982, averaged over each 4 to 7 day data block. Data was selected to be sure that net transmitted energy was large compared to changes in stored energy. Only data for which the average flux exceeded 3.15 W/m^2 was used. For adobe walls of 279, 381, and 635 mm thickness, average wall fluxes exceeding 3.47, 4.73, and 7.89 W/m^2 respectively were required. The R-values calculated for each data block were then averaged for each wall, and then for all four walls of each building. The calculated results are presented in Table 13.

The experimental uncertainties arise from the ±5% ±0.004 mv uncertainty applied to the mean fluxes for each test buiding, and the ±1% ± 0.25°C uncertainty applied to the mean tempeature difference across the walls. The mean fluxes were 16.1, 16.1, 14.8, 12.9, 16.1, 13.6, 5.4, and 7.9 W/m^2 respectively for these measurements for the eight test buildings. The mean temperature differences across the walls were 5.56, 5.56, 6.67, 10.00, 5.56, 9.44, 9.44, and 8.33°C respectively.

TABLE 13

In Situ R-values

Bldg.	Description	Min. Flux (W/m^2)	Mean R (m^2 °C/W)	± %
1	279 mm adobe	3.47	0.350	± 11%
2	279 mm stabilized	3.47	0.368	± 11%
3	381 mm adobe	4.73	0.477	± 10%
4	635 mm adobe	7.89	0.782	± 9%
5	279 mm adobe	3.47	0.354	± 11%
6	230 mm CMU	3.15	0.696	± 8%
7	Insulated frame	3.15	2.694	± 9%
8	178 mm milled log	3.15	1.585	± 9%

B.1.2 Dynamic Properties of the Walls for Diurnal Temperature Variations

The thermal mass of walls, storing heat that flows through the thermal resistance of the wall, delays and attenuates wall internal flux variations induced by varying exterior temperatures. This is a rough way of speaking; more precisely, the thermal mass and thermal resistance of the walls form a distributed filter (in the information theory sense). Because linear systems of equations govern the heat transfer through the walls, it is valid to superpose the heat fluxes and the excitations causing them. In particular, the excitation pulses can be Fourier analysed, and each Fourier component can be assigned a delay and an attenuation attributable to a wall.

These effects are clearest for simple excitations applied to the wall exteriors. In the field, the test buildings are subjected to rather complex excitations, with varying sunshine, air temperature, and wind. The delay and attenuation are not easily interpreted or defined, because the peak of the fundamental Fourier component does not coincide with the actual peak excitation.

Some simple information can be extracted from the field data, however. All walls are subjected to outdoor air temperature, wind, sunlight, and long-wave radiation. When the wind is predominantly from the west (as it is in this experiment), then the south and north walls are washed similarly by the wind; they

are subjected to the same air temperature; they receive nearly the same diffuse solar radiation and long-wave radiation. In winter, the only important difference is that south walls receive direct solar radiation, and north walls do not. When north wall fluxes are subtracted from south wall fluxes for each building, what remains is the net flux caused by direct solar radiation on the south wall. On clear days, this is a well-defined symmetrical excitation pulse.

Thirteen days of midwinter data, January 11 through January 23, 1982, were averaged for each hour of the day to produce an average day. Figure 16 characterizes the direct solar radiation excitation pulse for the averaged day: it shows the difference between south and north exterior wall surface temperatures for building 7, the insulated 2-by-4 frame building. Because the building is well insulated, the south-north temperature difference is a fair representation of the driving sol-air temperature pulse applied to all buildings.

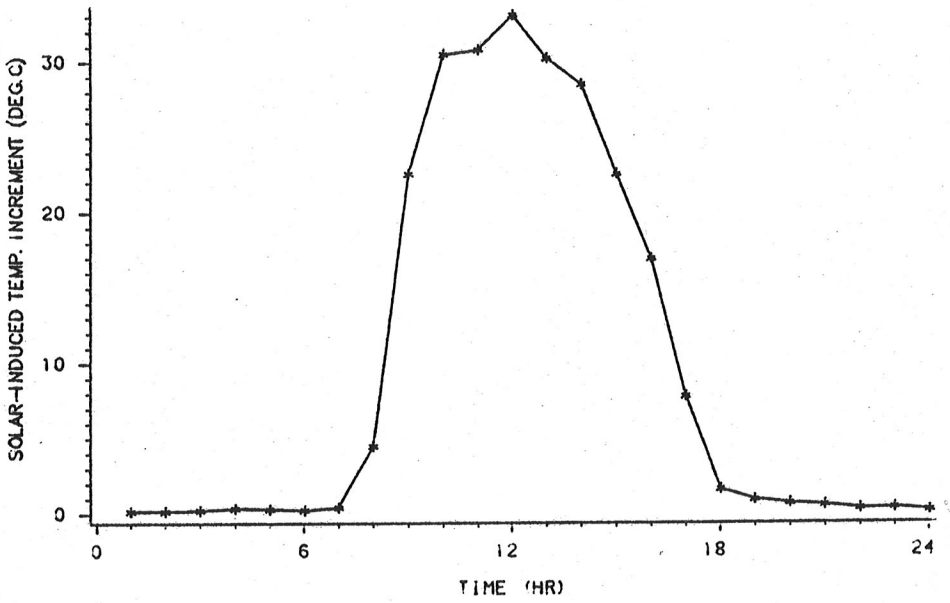

Figure 16: Temperature Pulse for Delay and Attenuation Measurements

Figures 17 through 20 show the interior flux response to the exterior temperature excitation of Figure 16 for all eight test buildings. Table 14 lists the peak-to-peak delays obtained directly from the data, and the delays for the diurnal Fourier sinusoidal component. Minimum, maximum, and mean heat fluxes are also listed.

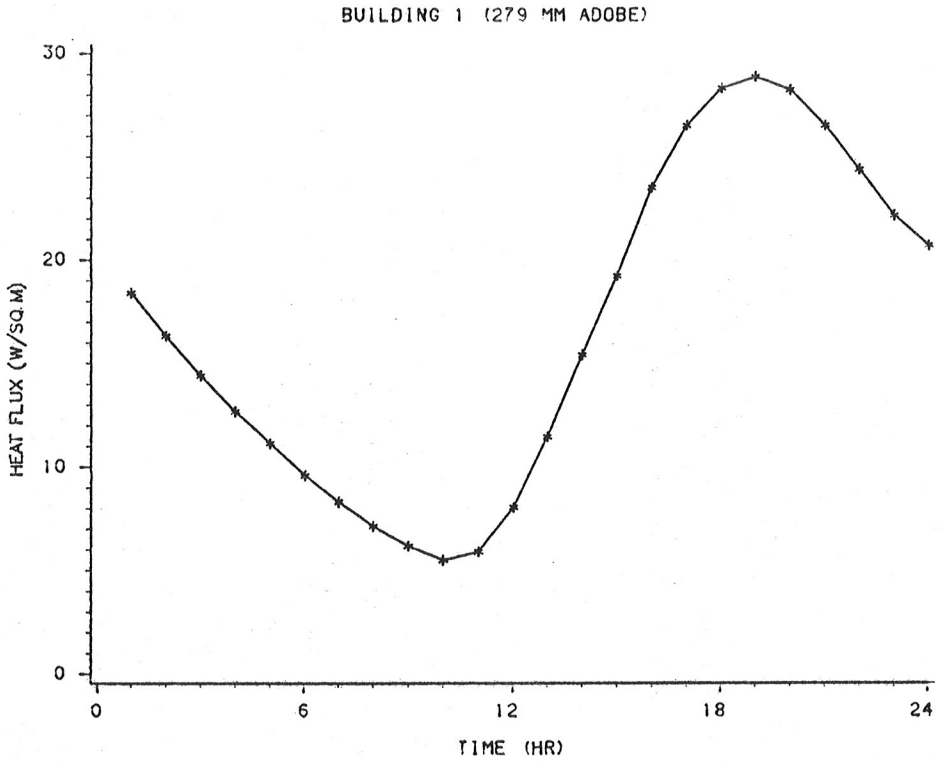

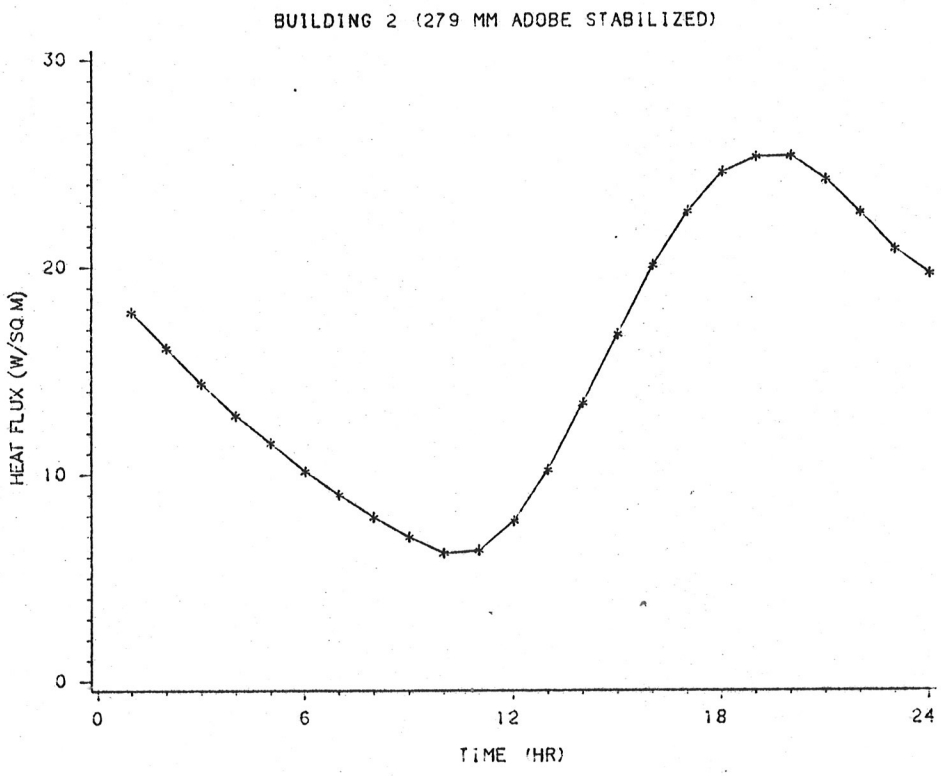

Figure 17: Interior Wall Flux Response for Buildings 1 and 2

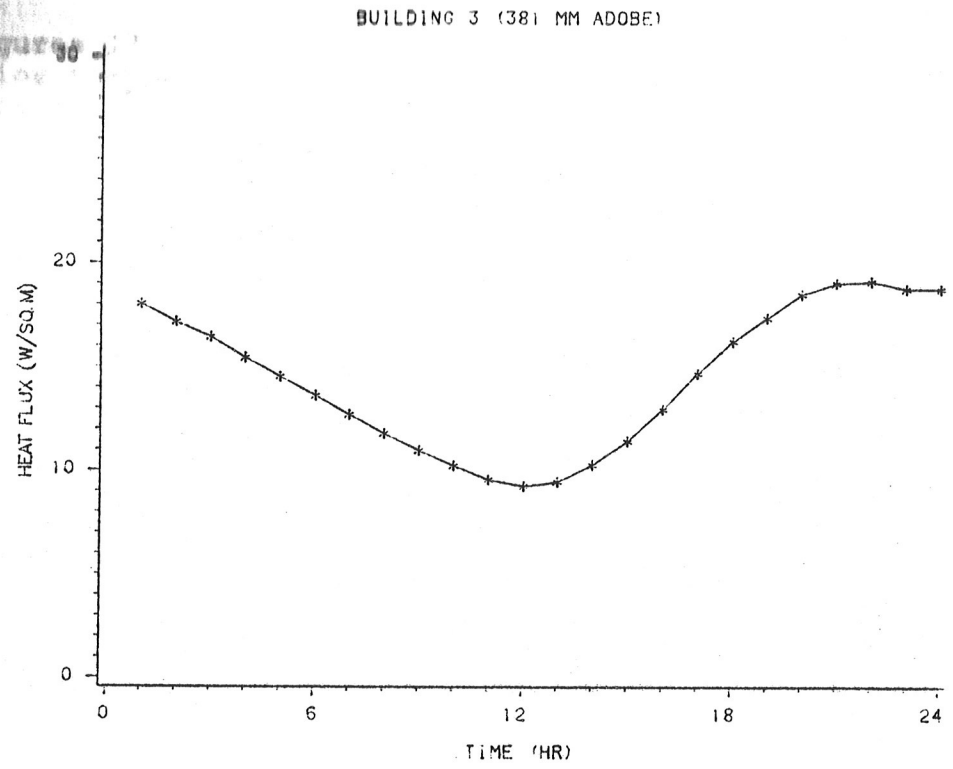

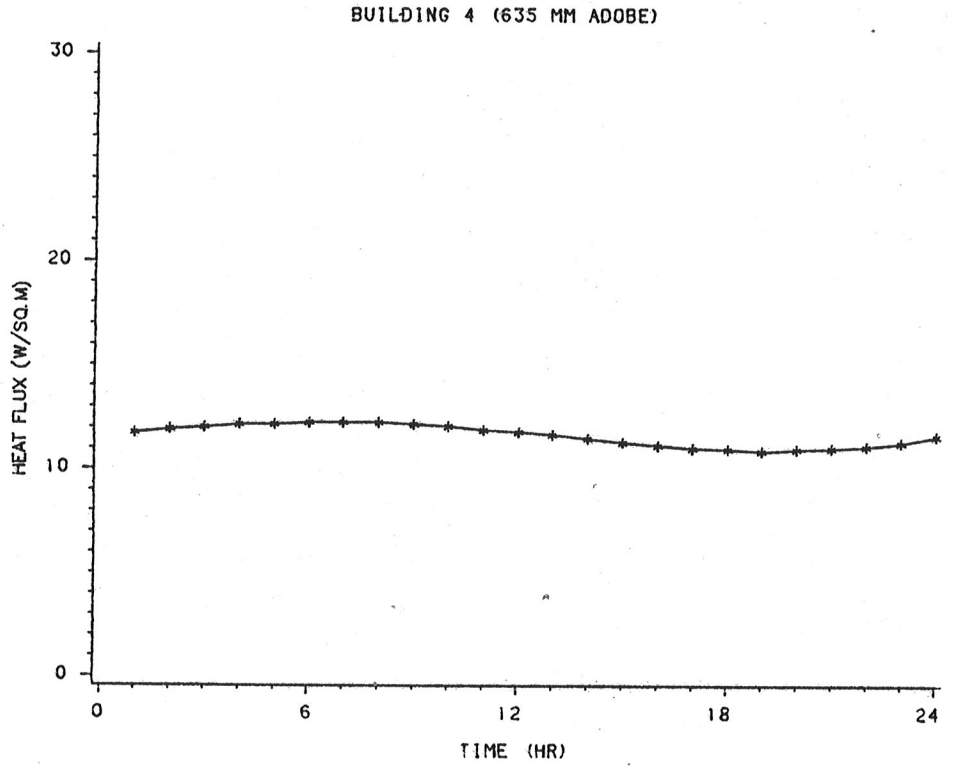

Figure 18: Interior Wall Flux Response for Buildings 3 and 4

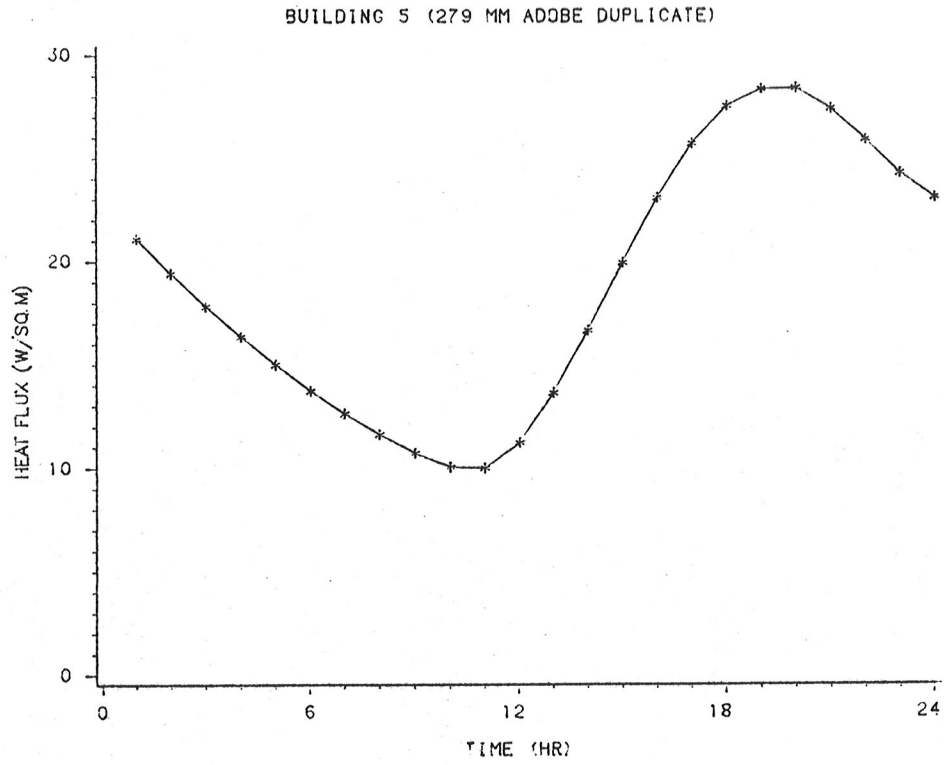

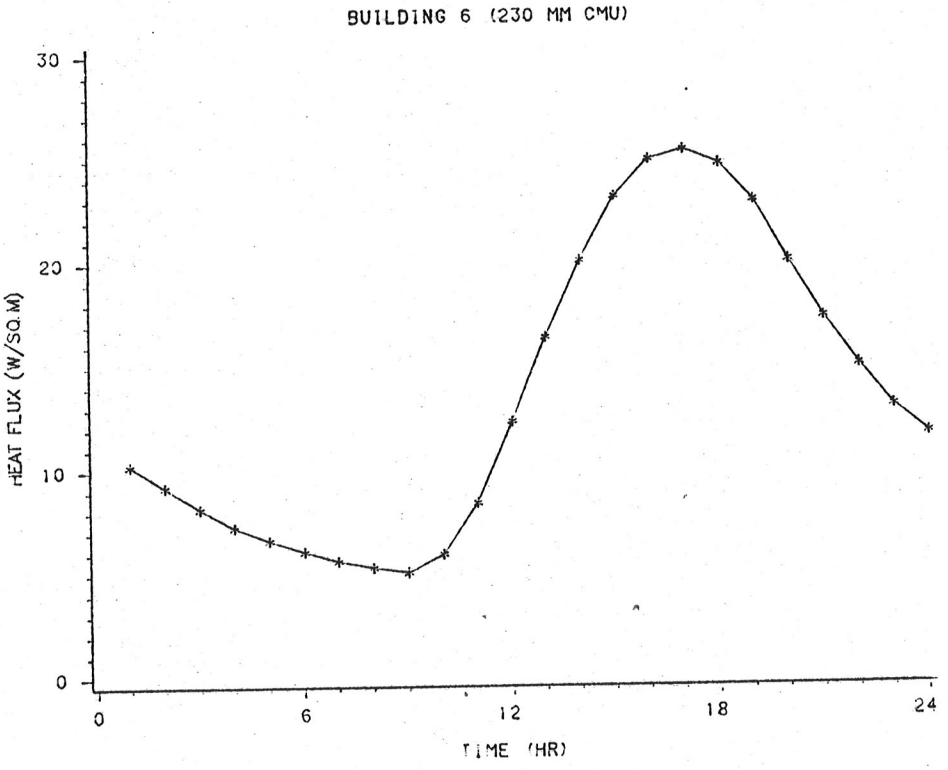

Figure 19: Interior Wall Flux Response for Buildings 5 and 6

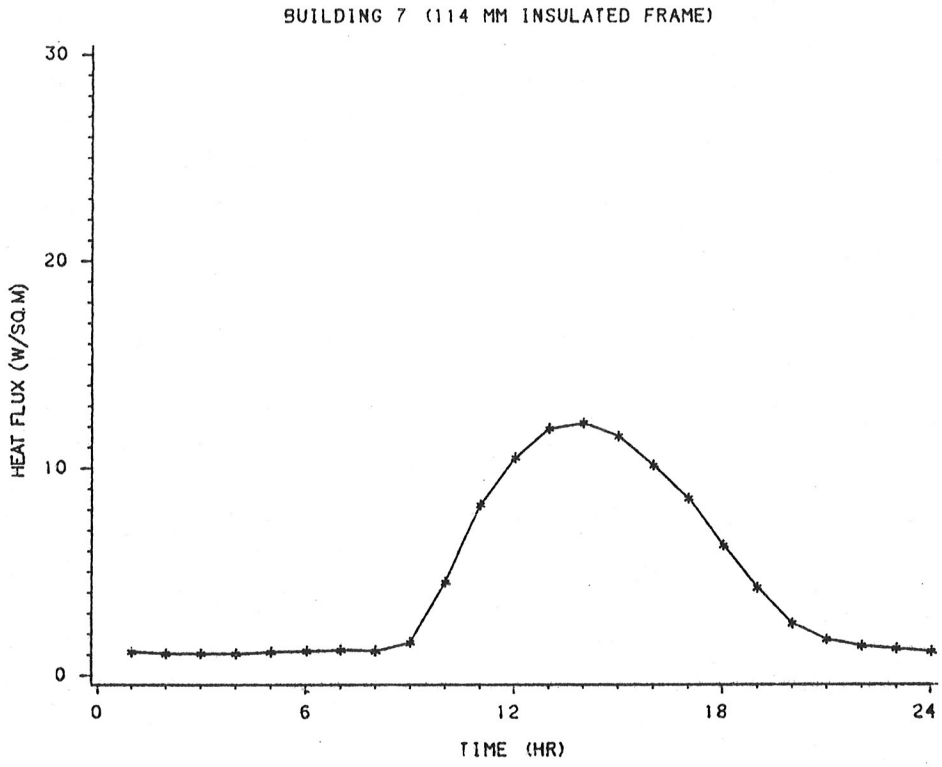

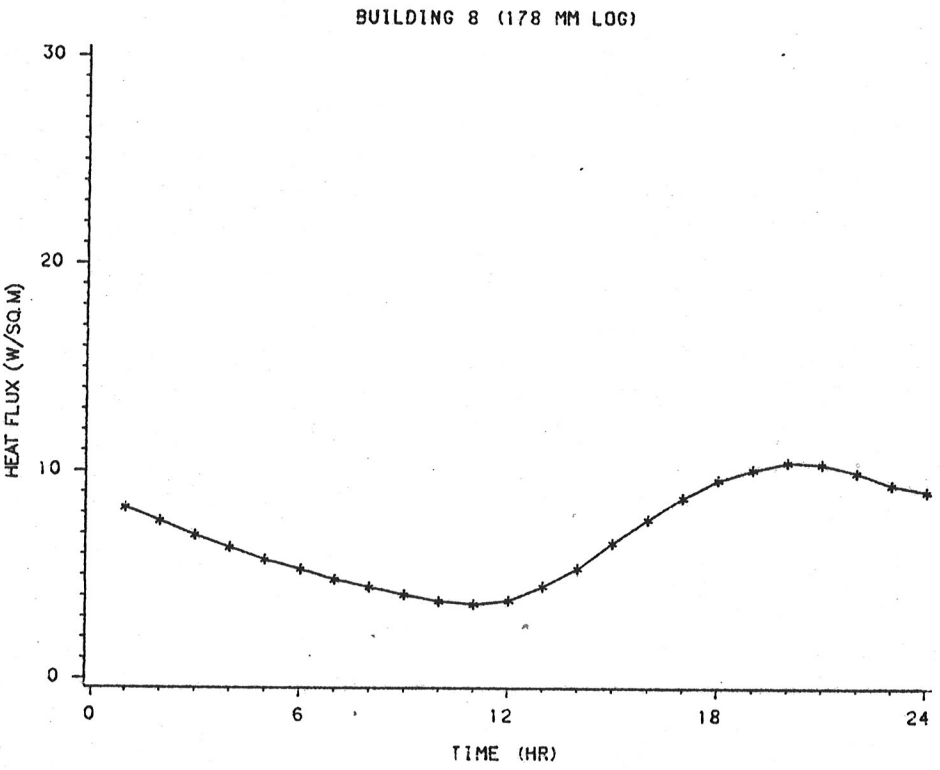

Figure 20: Interior Wall Flux Response for Buildings 7 and 8

TABLE 14

Wall Response to Solar Excitation Pulse

Bldg.	Peak-to-peak Delay (hrs)	Diurnal Sinewave Delay (hrs)	Heat flux (W/m^2) Min.	Max.	Mean
1	6.5 ± 0.5	7.8 ± 0.5	5.36	28.71	16.72
2	7.1 ± 0.6	8.2 ± 0.5	6.31	25.24	15.46
3	9.5 ± 0.9	10.6 ± 0.5	9.15	19.25	14.51
4	18.1 ± 0.7	18.4 ± 0.5	10.73	12.30	11.67
5	7.1 ± 0.6	8.2 ± 0.5	10.10	28.40	18.93
6	4.5 ± 0.6	5.4 ± 0.5	5.05	25.24	14.51
7	1.2 ± 0.5	2.0 ± 0.5	0.95	12.30	4.42
8	8.0 ± 0.7	8.9 ± 0.5	3.47	10.41	6.94

B.1.3 Moisture in the Adobe Walls

Free moisture within porous adobe walls can influence the heat conduction through a wall by providing a better conduction path through the voids in the material, and by increasing the apparent thermal conductivity due to latent heat transfer by water vapor migration. To check for the free moisture content of the walls, in March, 1982, cores were taken through a north and a south 279 mm adobe wall, and through a north 635 mm adobe wall. The cores were subsampled along their length, then weighed, dried for 24 hours at 105 °C, and weighed again. Weight loss was assumed to be moisture.

The measured weight loss for the 279 mm walls was very low: averaging about 1% for the south wall, and 2% for the north, with variation with depth less than 1/4 of this value in the interior. The 635 mm north wall showed an approximately parabolic weight loss distribution, rising from 2% near the wall surfaces to 4.3 ± 0.3% at the center, indicating that drying was still occuring a full year after construction. The surface layer of unstabilized mud mortar in all cases showed a weight loss of only 1%. This was lower than in the adobe brick that incorporates an asphalt emulsion stabilizer.

There was no measurable difference in wall conductivity between the moist and dry walls, and no secular change in thermal conductivity as the thick wall continued drying. That averaged thermal conductivity was calculated from time-averaged data, and

would not reflect changes in dynamic thermal impedance of the moist wall.

B.1.4 Solar Absorptance of the Walls

Solar absorptance is an important determinant of wall surface temperature in the sunny desert climate. A major effort would be required to characterize the the angular dependance of the absorptance, so this was not done. It was simply assumed that the wall is perfectly diffuse, and angular dependencies were ignored. The sunlight incident on the center of a wall was measured, and then the reflected brightness was measured using an aperture that restricted the field of view to the wall. Measurements were made in bright direct sunlight, and in the shade where only diffuse light could reach the walls. Two instruments were used: an Eppley PSP pyranometer, and a silicon photocell light intensity meter. The measured surface absorptance of all walls was 0.78 ±0.02 for all walls with both instruments, using diffuse light. There was a little more scatter in the measurements with direct illumination, and the measured value was lower by 0.02. The value used for all walls was 0.78 ±0.02.

B.2 THE ROOFS

The roofs are well insulated, and receive considerable sunshine on their dark surfaces, so roof heat losses are low. During nearly half the heating season, the roofs gain rather than lose heat. Great accuracy for roof heat flow is therefore not needed.

The surface-to-surface R-value from test building 1 ceiling and roof temperatures and ceiling heat flux between the joists gave an R-value of 5.6 m^2 °C/W ±10%, lower than the R-value of 6.1 m^2 °C/W calculated from ASHRAE values between the joists, but within the experimental uncertainty of that value. The R-value used for calculations was 5.64 m^2 °C/W, which agrees with the ASHRAE calculation when joists and interior surface film are included.

Heat losses and gains through the ceiling were calculated using the above R-value, and assuming steady-state heat flow resulting from the temperature difference between a given test building's plenum temperature, and the roof surface temperature as measured on building 1.

B.3 THE FLOORS

Although the floors are nominally identical, their heat losses differ from one building to another. The floor losses are characterized by an annual sinusoidal loss to the deep earth, by additional losses because actual plenum temperature differs from the nominal 20.6°C, and by a perimeter loss proportional to the difference between plenum temperature and outdoor air temperature.

The above model is based on one year's heating season measurements of building 1 slab temperature at several locations, and the mean air temperature above the 51 mm polyisocyanurate foam lying on the concrete slab. In addition, there are about two months of similar floor data for all eight buildings obtained in late 1982. This data was consistent with the following simple model. Assuming a constant plenum temperature of 20.6°C, the central floor losses can be calculated, in watts, as

$$L_{ctr,fl} = A_{fl} (L_0 + L_s \sin\theta + L_c \cos\theta) ,$$

The additional losses because plenum temperature differs from the nominal can be calculated as

$$L_{cor,fl} = A_{fl} (T_{in} - T_{std}) / R_{fl} ,$$

and the perimeter losses are

$$L_{perim,fl} = P_{fl} h_p (T_{in} - T_{out}) ,$$

with terms defined as in Section 5.2.1, Heat Losses.

B.4 HEATING PLANT AND CONTROLS

The heating plant in each test building consists of three 1500-watt electrical resistance heaters controlled by a thermostat. The physical arrangement was shown in in Figure 1, with arrows indicating approximate airflow in the building. Although the air is mixed by a 1.42 m^3/s fan blowing downward through a 0.186 square meter destratification plenum, there are four distinct convective loops within each building. A central convective loop around the plenum and heaters is surrounded by convective loops near each of the walls. The thermostat is mounted inside the plenum.

The heating system does not maintain a constant temperature. Rather, the maintained temperature depends on the thermostat setting, the anticipator setting, the thermostat transformer, the

fraction of time that the thermostat demands heat, the airflow around the thermostat, and the temperature of the mounting surface. In the present experiment, the plenum wall on which the thermostat is mounted is very near the plenum air temperature, and none of the parameters is varied for a given building, except the time that the thermostat demands heat, which is proportional to the average heating energy consumed. During that time, the anticipator is supplying local heat to the thermostat, and so affects the mean temperature seen by the temperature sensing element.

Using daily average plenum temperature data for days that required heat at all hours, linear regressions of the form

$$T_{thermostat} = A + B\,Q_{heat},$$

where A = a regression coefficient (°C),
B = a regression coefficient (°C/W),
Q_{heat} = the average daily heating load (W), and
$T_{thermostat}$ = the thermostat setpoint (°C),

express the thermostat setpoint in terms of average hourly heating demand. The regression coefficients for each test building are listed in Table 15. The coefficients for building 8 are different for early and late '82, because apparently the thermostat setting in that building was inadvertantly lowered during the summer of 1982. This did not affect the usefulness of the full-year data, because corrections for variations in thermostat setpoint, where necessary, are applied to all buildings. Although the thermostats and heating plants are nominally identical, the regression coefficients differ considerably. These differences may be due to the plenum airflow patterns near the thermostat: the fan wake is narrower than the plenum, and may 'stick' to any one of the walls -- in some cases, washing the thermostat in the direct air blast, in other cases, not. The effect of the anticipator would be least in those buildings with the greatest flow past the thermostat.

TABLE 15

Thermostat Regression Coefficients

Building	A (°C)	B (°C/W)
1	21.3	-0.00055
2	22.5	-0.00069
3	20.6	-0.00035
4	20.4	-0.00009
5	21.4	-0.00035
6	21.2	-0.00057
7	21.0	-0.00064
8a	21.0	-0.00079
8b	17.2	+0.00087

Notes: 8a is for Building 8 during early 1982.
8b is for building 8 during late 1982.

B.5 INFILTRATION CHARACTERISTICS OF THE TEST BUILDINGS

Natural rates of infiltration for the eight test buildings were measured in early 1982 using a sulfur hexafluoride tracer gas technique. Three sets of tests, covering periods up to 16 hours each, were performed under a variety of weather conditions in which outside temperature ranged from about -6.7°C to about 12.8°C, and wind speed ranged from about 1.8 m/s to about 7.2 m/s. It was observed that the adobe buildings had significantly higher rates of infiltration than the other three buildings. It was determined that this was the result of shrinkage of the mud mortar between the top course of adobes and the bond beams, which produced a continuous 6 mm to 13 mm crack along the tops of the adobe walls which occasionally penetrated the mud plaster on one or both sides of the wall. To remedy this situation, in the summer of 1982 these cracks were filled with polyurethane foam sealant. In midwinter 1982-83, one set of infiltration tests was performed on the adobe buildings to evaluate their new infiltration characteristics.

B.5.1 Methodology

In early 1982, infiltration tests were made during one period when the wind speed was low and the outside temperature was low so that the temperature-induced buoyant pressure would predominate, and two periods when the temperature was high and the wind speed was high so that the wind-induced pressure would predominate. In late 1982, one set of tests was done with low outside temperature and high wind speed. Table 16 lists the mean weather conditions for each of the test periods.

TABLE 16

Weather During Infiltration Measurements

Period	Season	Mean Outside Temp. (°C)	Mean Wind Speed (m/s)
1	Spring	10.4	5.8
2	Spring	-2.7	2.5
3	Spring	9.7	7.2
4	Fall	2.5	6.1

Sulphur hexafluoride was used as the tracer gas. It is chemically inert, it mixes well with air, is transported and dispersed as air is, and it can be detected at very low concentrations. tracer gas concentrations were measured using a Systems, Science, and Software Model 215 BGC Bench/Laboratory Tracer Gas Monitor, which is a silica column gas chromatograph with an electron-capture detector.

A mixture of 0.1 cc of sulfur hexafluoride and 0.9 cc of air was injected into the air destratification plenum of each test building, and the roof hatch entryway was closed, so that the buildings were in their normal configuration for data collection. The hatches remained closed for the duration of each test. The tracer gas was then allowed to mix for one hour within the buildings using the existing destratification fan in each building before sampling began.

For each of the four tests, four or five samples were taken, at a rate of one sample every one hour for each of the adobe test buildings and one sample every three hours for each of the other

test buildings. The adobe buildings were sampled more frequently, as preliminary tests showed them to have a much greater rate of infiltration than the others. An inexpensive battery-operated air pump was used to pump air out from the interiors of the buildings through 6.4 mm plastic tubing. For each sample, the pump was allowed to operate for 60 seconds, and a 10cc sample was taken from the tubing with a standard plastic hypodermic syringe. The needles were stopped with a piece of rubber and taken to Albuquerque for analysis. For each hour during which samples were taken, samples of the two calibration gases were also taken as a reference and to assure that storage in the syringes would not affect the sulfur hexafluoride concentrations.

Initial and subsequent concentrations were mesured one or two days later, using the gas chromatograph. The infiltration rate was then calculated for each time interval from

$$I = \ln (C/C_0) / (t - t_0) ,$$

where I = infiltration rate (air changes/hr),
C = concentration at sample time t,
C_0 = concentration at initial time t_0, and
t and t_0 are times (hr) .

B.5.2 Results

For the early 1982 data, the results were analyzed using a linear regression model which assumed that the rates would depend linearly on buoyant pressure differences due to inside-outside temperature differences, and on wind-induced pressure differences. The regression equation and results are listed in Table 17. To give an idea of what these coefficients represent physically, the last column presents the calculated infiltration rate at typical site winter weather conditions of 4.47 m/s wind speed and 4.4°C temperature.

All five adobe buildings have about 0.3 air changes per hour, and the three other buildings have 0.1 air changes per hour or less. The relatively high rate in the adobe buildings is due to differential shrinkage of the mud mortar and plaster away from the wood bond beams and lintels (for future doors and windows). This assumption is supported by qualitative infrared imaging scans performed during the winter. The other three buildings had no materials with such high shrinkage and thus did not have such high rates of infiltration. It should not be inferred from these results that adobe buildings are necessarily, or even commonly, more "leaky" than buildings of other materials. The adobe

buildings were designed to have as homogeneous wall sections as possible, using the traditional construction, with mud plaster on the inside and the outside. Typical adobe construction today would have sheetrock or plaster on the interior surfaces and cement stucco on the exterior surfaces, neither of which shrinks greatly, and each can be sealed with caulk.

TABLE 17

Infiltration Regression Results - Spring

Regression Equation:

$$L_{inf} = A * WS^2 + B * |(1/T_{out} - 1/T_{in})| ,$$

where L_{inf} = infiltration rate (air changes/hr) ,
WS = wind speed (m/s),
T_{out} = outdoor air temperature (K) , and
T_{in} = indoor air temperature (K).

Results:

Bldg.	Regression Coefficients A	B	Infiltration Rate if WS = 4.47 m/s T_{out} = 4.4 °C
1	0.0113	230	0.27
2	0.0146	421	0.36
3	0.0129	406	0.33
4	0.0135	205	0.31
5	0.0116	250	0.27
6	0.00170	128*	0.06
7	0.00214	128	0.07
8	0.00470	63	0.10

---

* Building 6 low wind data was unreasonable. Regression coefficient B from bldg. 7 was used, then coefficient A was calculated.

Note in the last column of Table 17 that the infiltration rate due to the wind-induced pressure difference predominates under typical weather conditions. (Multiply coefficient "A" by 20 to get that portion of the air change rate). For the adobe buildings, the wind-induced pressure difference is about 80-90%, and for the other three buildings, it is about 60-70%. Since the cracks are generally high in the walls in the adobe buildings, the small effective stack height no doubt contributes to the relatively small effect of buoyant pressure.

For the late 1982 data, after sealing the cracks between the bond beams and adobe mortar, only one set of tests was performed. Because there were no conditions of low outside temperature and low wind speed, and because the effect of temperature-induced buoyant pressure in the adobe buildings is small compared with the effect of wind-induced pressure, a regression of infiltration rate with both pressures yielded unreliable results. However, a regression against wind-induced pressure alone produced reasonable results with standard error estimates not much greater than in the early 1982 infiltration analysis. The regression equation and results for the late 1982 analysis are presented in Table 18 . The last column presents the calculated infiltration rate at the typical winter site wind speed of 4.47 m/s.

Note that infiltration rates have been reduced considerably in all five adobe buildings, with the significant exception of building 2, which has cement mortar; this does not bond to the adobe as well as mud mortar and thus presents more opportunity for air leakage paths. The infiltration rates for buildings 1, 4, and 5 are now very comparable to the rates for buildings 6, 7, and 8.

Uncertainty levels for the predicted infiltration rates are estimated to be ±20% for the initial (early '82) tests on all eight buildings, and ±30% for the late '82 tests on the adobe buildings. These estimates are in line with the standard error estimates from the regression analyses.

All the measurements were made with the wind from the west or northwest. The infiltration characteristics of the buildings could be quite different for different wind orientations, if leakage cracks differ from wall to wall. The buildings are largely symmetrical, so the uncertainties of ±20% and 30% in predicted infiltration rates should cover such errors.

TABLE 18

Infiltration Regression Results - Fall

Regression Equation:

$$L_{inf} = A * WS^2 ,$$

where L_{inf} = infiltration rate (air changes/hr) and
WS = wind speed (m/s)

Results:

Bldg.	Regression Coefficient A	Infiltration Rate if WS = 4.47 m/s
1	0.00335	0.07
2	0.01150	0.23
3	0.00767	0.15
4	0.00433	0.09
5	0.00401	0.08

B.6 QUANTITATIVE MEASURES OF COMFORT IN THE TEST BUILDINGS

B.6.1 Introduction to Comfort Indices

The purpose of environmental control of residential buildings is to maintain a reasonable level of human comfort. Comfort is a complex phenomenon, for several reasons. It involves all three sensible heat transfer mechanisms -- conduction, convection, and radiation -- as well as heat loss due to moisture transfer in respiration and perspiration. It depends on individual metabolic rates, on clothing, and on the thermal environment. Finally, it involves human perception and individual preferences. These subjective factors make comfort difficult to quantify, and invest all standards of comfort with some degree of arbitrariness.

Ambient air temperature, commonly accepted as an adequate measure of comfort, is an insufficient index of comfort under many circumstances. Fanger, in introducing his basic comfort equation (11, p. III.4.1), states that human comfort is dependent

on air temperature, humidity, mean radiant temperature, relative air velocity, physical activity level, and the insulating value of clothing. Measures of comfort can be simple or complex, involving only one of these factors, or several of them. For each of the eight test buildings at the Southwest Thermal Mass Study, we have evaluated seven indices of comfort at mid-height at the center of each test building. The seven indices, along with the parameters included in each, are listed in Table 19.

TABLE 19

Measures of Comfort

Measure	PARAMETERS					
	1	2	3	4	5	6
Dry-bulb temperature	X			X		
Wet-bulb temperature	X	X		X		
Mean radiant temperature			X			
Black globe temperature	X		X	X		
Operative temperature	X		X	X		
ASHRAE effective temperature, ET*	X			X		
Dry-bulb temp. required to satisfy the Fanger comfort criterion	X	X	X	X	X	X

Note: The parameters are as follows:

1 - air temperature
2 - humidity
3 - mean radiant temp.
4 - relative air velocity
5 - physical activity level
6 - clothing insulating value

The reader is referred to the ASHRAE Handbook of Fundamentals (3) for precise definitions of these indices.

These measures were evaluated for all eight test buildings for two five-day blocks of data: one in midwinter, when the average outdoor ambient temperature and the average outdoor temperature swing were approximately -1°C and 9°C, respectively; and another

in spring, when those conditions were 10°C and 17°C, respectively. The method of evaluation was to calculate hourly values, print histograms of each comfort index, and calculate means and ranges of each comfort index, for each data block.

B.6.2 Results

The results are presented in Tables 20 and 21, which summarize the histograms for the seven measures of comfort, test buildings, and the two time periods of evaluation.

TABLE 20

Evaluation of Comfort Measures in the Test Buildings

Midwinter (Jan. '82)
(Mean/Range)

Parameter (°C)	Building Number 1	4	6	7	8
Dry Bulb	20.3/1.4	20.2/1.2	20.3/2.0	20.6/1.9	20.3/1.7
Wet Bulb	11.1/1.0	11.0/0.9	11.1/1.5	11.3/1.4	11.1/1.3
Mean Radiant	15.0/3.3	16.4/0.8	16.5/3.6	18.4/2.6	18.3/1.7
Globe	19.1/1.8	19.4/1.0	19.5/2.3	20.1/2.0	19.8/1.5
Operative	17.5/2.3	18.2/0.8	18.4/2.6	19.4/2.2	19.2/1.4
ET*	20.0/1.4	19.9/1.2	20.0/2.0	20.2/1.9	20.0/1.7
Fanger	30.5/3.0	29.2/0.7	29.0/3.4	27.3/2.4	27.4/1.6

Note: The 'Fanger' number is not a comfort index like the others, but is the dry-bulb temperature that would be required to satisfy the Fanger comfort condition for each test building. If 'Fanger' is several degrees higher than the actual dry-bulb, the building would be uncomfortably cold.

Looking first at each parameter for building 1 in midwinter, the first column presents the seven indices for that building. The dry-bulb, at 20.3°C, is typical for all buildings. The range

TABLE 21

Evaluation of Comfort Measures in the Test Buildings

Spring (Apr '82)
(Mean/Range)

Parameter (°C)	Building Number 1	4	6	7	8
Dry Bulb	21.1/1.6	20.4/1.7	21.2/4.3	21.5/5.9	20.9/2.5
Wet Bulb	11.7/1.2	11.1/1.2	11.7/3.1	11.9/4.2	11.5/1.8
Mean Radiant	19.2/3.8	19.2/1.1	19.9/5.7	20.4/5.9	20.0/2.7
Globe	20.7/1.9	20.1/1.5	20.9/4.5	21.3/5.9	20.7/2.6
Operative	20.1/2.6	19.7/1.4	20.5/4.9	20.9/5.9	20.4/2.6
ET*	20.8/1.6	20.1/1.7	20.8/4.2	21.2/5.7	20.5/2.5
Fanger	26.5/3.4	26.6/1.0	26.0/4.6	25.5/4.6	25.8/2.3

Note: The 'Fanger' number is not a comfort index like the others, but is the dry-bulb temperature that would be required to satisfy the Fanger comfort condition for each test building. If 'Fanger' is several degrees higher than the actual dry-bulb, the building would be uncomfortably cold.

of the dry-bulb during this period was 1.4°C. The wet-bulb, at 11.1°C, is also typical, as 30% relative humidity was assumed in each. This assumption is based on portable calibrated humidity sensor readings and the fact that the drying process in the adobe walls is effectively completed (see Section 2.3.2). The range of the wet bulb was 1.0°C.

Mean radiant temperature (MRT), calculated by summing the measured surface temperatures that the point at the center of the building "sees" (not including the plenum itself), weighted by the solid angle, is 15.0°C, 5.3°C lower than dry-bulb. This is common for low R-value walls. The range of MRT is 3.3°C, more than double the range of the dry-bulb.

The globe temperature combines the effects of MRT and dry-bulb temperature, and so at 19.1°C is slightly lower than dry-bulb. Operative temperature, based on a human-sized mannequin and thus having a weaker convective coupling per unit area than the globe,

lies halfway between dry-bulb and MRT, at 17.5°C. The ranges of these two measures are between the ranges of dry-bulb and MRT, as expected from the means.

The effective temperature, ET*, has no real MRT coupling (because MRT is assumed equal to dry-bulb), and is slightly lower, at 20.0°C, than dry-bulb due to the assumed 50% relatave humidity that ET* requires. This index would be more useful in large buildings with interior partition walls, for which MRT is close to dry-bulb, and humidity is controlled.

The last measure of comfort examined is the dry-bulb temperature required to satisfy the Fanger comfort criterion and is evaluated from the generalized Fanger comfort charts. It is denoted as 'Fanger' in the table. For building 1 in midwinter, its value is 30.5°C and is high due to the low MRT. Low relative air velocity (0.1 m/s), sedentary activity level (50 kcal/hr m^2), and medium clothing level (1.0 clo) are assumed. This number indicates what the dry-bulb temperature would have to be to provide optimum comfort if all other conditions remained constant.

The other buildings in mid-winter exhibit the following trends. Dry-bulb and wet-bulb are similar to building 1, since they have very similar thermostat setpoints and identical assumed humidity levels. The ranges of these two measures are small, varying from 1.2°C for building 4 to 2.0°C for building 6. MRT is highest for the buildings with highest R-value walls, buildings 6 and 7. The range of MRT is lowest for the most massive building, building 4, at only 0.8°C. However, the lightest buildings with high R-values have intermediate ranges at 2.6 and 1.7°C, and, interestingly, building 6 has the greatest range of MRT, at 3.6°C. Effective temperature closely follows dry-bulb, and globe and operative temperatures reflect their respective weighted averages of dry-bulb and MRT. The Fanger dry-bulb required for optimum comfort, strongly dependent on MRT, corresponds to variations in MRT since all other parameters are constant from building to building.

For the spring data, the variations among measures and buildings follow similar patterns as in the midwinter data, but with some exceptions. One exception is the slightly elevated mean dry-bulb and the dramatically increased range in dry-bulb for buildings 6 and 7, indicating floating has started to occur in those two buildings. The most obvious exception is that the values of all measures for all buildings are now much closer together. This is primarily due to the increase for all buildings in MRT, which is only slightly below dry-bulb for this period. All the measures which are dependent on MRT are thus much closer to dry-bulb during spring than they are in midwinter. The conclusion is that buildings with high and low R-value walls have very different comfort levels in cold weather but similar comfort levels in warmer weather.

It is apparent from this examination of comfort levels that the radiant environment is an important consideration. Generally, low R-value walls had cold interior surfaces during cold weather and would have been uncomfortable in cold weather. Measures of comfort that fail to consider mean radiant temperature are of limited utility in assessing comfort in small buildings with low R-value walls. It was also found that massive walls had less variation of inside surface temperatures.

Appendix C

OUTDOOR SURFACE HEAT TRANSFER COEFFICIENTS

The simple methods for estimating surface conductances are usually adequate for design calculations, but are quite indadequate for accurate predictions of outdoor surface sol-air temperatures. It is well known that convective surface film conductances for forced convection can be correlated to Reynolds and Prandtl numbers, and to surface roughness. This implies that surface heat transfer coefficients depend on velocity of nearby fluid, on its thermal and mechanical properties, and on size and roughness of the surface. Under conditions of low wind, natural convection predominates, and surface conductance depends on Grashof and Prandtl numbers. In addition, in the climate of the southwestern desert, sunshine is intense, and radiative heat transfer to sky and earth are very significant. All these effects, as well as sunshine reflection from the ground, and variation of local wind speed depending on wall orientation, must be combined in a reasonable way to estimate outdoor surface conductances and sol-air temperatures. A method for making such estimates is given below. This method is used in the analysis presented in the body of the report, particularly in the detailed analysis in Chapter 5.

C.1 FORCED CONVECTION

For the range of Prandtl numbers encountered in gases and light liquids, Kays (17, p. 239.) derives a simple expression relating Stanton, Prandtl, and Reynolds numbers for turbulent flow over a smooth flat plate parallel to the air motion:

$$St_x = 0.0295\, Pr^{-0.4}\, Re_x^{-0.2} \qquad (1)$$

Kays asserts that this expression is in excellent agreement with experimental data. Averaged over a plate of length L this becomes

$$St_L = 0.0368\, Pr^{-0.4}\, Re_L^{-0.2} \qquad (2)$$

This expression must be modified when there is surface roughness and Reynolds number sufficient for local flow separation around roughness protrusions. In such a case, Reynolds' analogy relating momentum and heat diffusion in turbulent flow becomes invalid, and a correction for roughness must be introduced. Kays (17, p. 197) presents results of Nunner, with correction factor for air in roughened tubes given as

$$\frac{Nu}{Nu_{sm}} = \left(\frac{f}{f_{sm}}\right)^{0.5} \qquad (3)$$

There is other evidence that such an expression is reasonable: Dipprey and Sabersky, in a fine article combining theory, experiment, and review of previous work, show data (9, Fig 16) that supports an exponent between 0.5 and 0.7 for simple geometries and Prandtl numbers for gases and light liquids. Combining equations (2) and (3) gives the convective surface film heat transfer coefficient

$$h_{c,f} = St_L \rho c_p u = 0.0368\, Pr^{-0.4}\, Re_L^{-0.2}\, (f/f_{smooth})^{0.5}\, \rho c_p u$$

an expression valid for Prandtl numbers between 0.5 and 10, for rough flat plates with flow parallel to the plate.

For specific applications, such as the exterior walls of the Southwest Thermal Mass Study, this last equation can be simplified by partial evaluation. Using an average surface film temperature of 4.4°C, wall length 6.10 m, equivalent sand roughness of 3 mm, pressure 80.3 kPa at an altitude of 1930 m above mean sea level, and data from Schlichting (22, Fig 21.6) for friction coefficients over roughened flat plates, the roughness multiplier can be represented as

$$\left(\frac{f}{f_{sm}}\right)^{0.5} = \begin{cases} 1.00 \text{ if } u < 0.46 \text{ m/s} \\ 1.00 + 0.204\,(u - 0.46)^{0.295} \text{ if } u > 0.46 \text{ m/s} \end{cases}$$

where u is in meters per second. The entire equation then evaluates to

$$h_{c,f} = 3.34\,(1 + 0.204\,(u - 0.46)^{0.295})\, u^{0.8}$$

when u > 0.46 m/s, and

$$h_{c,f} = 3.34\, u^{0.8}$$

when u < 0.46 m/s, and where the subscript 'c,f' refers to forced convection.
The above expressions are used for evaluating forced convection heat transfer from walls and roof in the Southwest Thermal Mass Study. (Laminar flow need not be considered: the dimensions of the rough walls are such that if there is a significant wind, then flow is turbulent; and if there is little or no wind but a significant temperature diffence, turbulence is induced by natural buoyant convection.)

The wind speed u in the above equations is not the weather station windspeed, but windspeed near the wall surface outside the turbulent boundary layer. Simple checks with a hot-wire anemometer indicated that windspeed at wall mid-height is about 0.8 of weather station windspeed, and windpeed in the lee of buildings is near a fourth of weather station airspeed. Although it is a severe oversimplification, it was assumed that the heat losses behave as if flow parallel to the wall was occuring as calculated above for a flat plate, with wind speed at 0.8 of weather station windspeed, except in the lee of buildings. The airflow was taken to separate when the plane of a wall was 15° or more in the lee of the wind. From the angle for separation, to walls entirely in the lee, a smooth relation between weather station windspeed and wall wind speed was used:

$$v = 0.8\, u \qquad \text{if} \quad \varphi > 75°$$

$$v = 0.258\, u / \cos\varphi \qquad \text{if} \quad \varphi < 75°$$

where v = wind near a wall
u = weather station wind
φ = the angle between the outward normal to a wall, and the weather station wind velocity vector.

The 75° angle was chosen because flat plates "stall" when the angle of incidence exceeds about 15°.

C.2 NATURAL CONVECTION

At low wind speeds natural convection becomes an important heat transfer mechanism for exterior walls. A rational semi-empirical derivation by Kato, Nishiwaki, and Hirata (16) gives the correlation

$$Nu_x = 0.138\, Gr_x^{0.36}\, (Pr^{0.175} - 0.55)$$

for turbulent natural convection from a vertical plate. The correlation is in excellent agreement with experiment for gases near Pr = 1. For air at Pr = 0.71,

$$Nu_x = 0.0541\, Gr_x^{0.36} = h_x\, x / k$$

Evaluating the above for air properties as indicated in the previous section, the natural convection film coefficient averaged over a wall of height L is

$$h_{c,n} = 9.72 \left[\frac{|T_w - T_{air}|}{T_w + T_{air}} \right]^{0.36} L^{0.08}$$

In the present case, L = 2.29 m, giving

$$h_{c,n} = 11.23 \left[\frac{|T_w - T_{air}|}{T_w + T_{air}} \right]^{0.36}$$

for the Southwest Thermal Mass Study, where the temperatures are absolute, and the subscripts are as follows:

c,n - convective,natural, and
w - wall surface .

C.3 LONG-WAVE RADIATION

For a vertical exterior wall, exposed equally to sky and ground, the energy gain due to long-wave radiation can be approximated as

$$Q_{rad} = 0.5\, \sigma\, \epsilon_w\, A\, ((T_s^4 - T_w^4) + (T_g^4 - T_w^4)),$$

where σ = Stefan-boltzmann constant (5.67×10^{-8} W/m^2 K^4) ,
ϵ = emissivity ,
and the subscripts are as follows:

rad - radiative ,
w - wall ,
s - sky , and
g - ground .

(The approximation neglects backscatter from earth and sky, but is a close one if emissivities are near unity, and sky and ground absolute temperatures differ by only a small percentage.) It is convenient to reference outdoor conditions to the outdoor air temperature, which is not very different from ground temperature or effective sky temperature. Algebraic manipulation of the above equation gives

$$Q_{rad} - Q_{s,corr} - Q_{g,corr} = h_{rad} A (T_a - T_w),$$

where

$$h_{rad} = 0.5 \sigma \epsilon_w (T_a + T_w)(T_a^2 + T_w^2),$$

$$Q_{s,corr} = 0.5 \sigma \epsilon_w A (T_s^4 - T_a^4), \text{ and}$$

$$Q_{g,corr} = 0.5 \sigma \epsilon_w A (T_g^4 - T_a^4),$$

where the subscripts are as follows:

s,corr - corrected for sky temperature , and
g,corr - corrected for ground temperature .

In this formulation, when ground and sky temperatures are known, then most of the long-wave radiative heat transfer can be included in the linearized outdoor surface conductance, which includes h_{rad}.

C.4 COMBINED RADIATION AND FORCED AND NATURAL CONVECTION

The radiative and convective contributions to surface conductance are independent, and may simply be added. The convective contribution, however, consists of natural and forced convection, which cannot be combined so simply. A theoretically sound method for combining natural and forced convection, a method based on solutions to the Navier-Stokes equations, does not exist. So we resort to the simplest linear combination, adding the contributions of radiation and forced convection, and then blending the contribution of natural convection in smoothly at low air speeds:

$$h_{tot} = h_{rad} + h_{c,f} + b\, h_{c,n}$$

where

$b = 0$ if $u > 21.3$ m/s,

and

$b = (21.3 - u)/u$ if $u < 21.3$ m/s ,

where u is wind speed.

The above combination of radiation and forced and natural convection is not unreasonable. If the wall is shrunk down to a 0.30 m size, reducing the roughness proportionately to 0.15 mm, then the resulting graph of surface conductance vs. wind velocity matches the "clear pine" and "smooth plaster" graphs in ASHRAE Fundamentals (3, Ch. 22, Fig. 1), for wall-to-air temperature difference of 35 °C. This is excellent agreement for the size and roughness, and is an independent check on the validity of the above methods for estimating surface conductance.

C.5 ROOF SURFACE CONDUCTANCE

The surface conductance for roofs is estimated much as it is for the walls. For forced convection, the equations derived above for walls apply without change. For natural convection with heat flow upward, McAdams (18) recommends

$$Nu_L = 0.14 (Gr_L Pr)^{1/3}$$

for $Gr > 10$. For the air temperatures and pressures listed above, this reduces to

$$h = 12.5 \left[\frac{|T_{roof} - T_{air}|}{T_{roof} + T_{air}} \right]^{1/3} .$$

For natural convection with heat flow downward, the heat losses are much reduced. There is no appropriate correlation in the literature for the turbulent heat flow down to a horizontal plate. Rather than use nothing at all, we use McAdams' correlation for laminar flow:

$$Nu_L = 0.27 (Gr_L Pr)^{1/4}$$

This reduces to

$$h = 0.51 \left[\frac{|T_{roof} - T_{air}|}{T_{roof} + T_{air}} \right]^{1/4}$$

The radiant interchange is treated as for walls, except that the roof surface sees only the sky. The various modes of heat transfer are combined as they were for the walls.

REFERENCES

1. Allen, C. P. and Clark, G. "Structural Thermal Mass and Comfort Cooling Requirements of Residences in Various U. S. Climates," Proceedings of Solar Energy Storage Options. San Antonio, TX, Mar. 19-20, 1979.

2. Arumi, F. N. "Thermal Inertia in Architectural Walls." National Concrete Masonry Association, 1977.

3. American Society of Heating, Refrigerating and Air-Conditioning Engineers, Inc. (ASHRAE) ASHRAE Handbook, 1981 Fundamentals. ASHRAE, Atlanta, GA, 1982.

4. Burch, D. M., Remmert, W. E., Krintz, D. F., and Barnes, C. F. "A Field Study of the Effect of Wall Mass on the Heating and Cooling of Buildings," Proceedings of the Building Thermal Mass Seminar, Knoxville, Tenn., June 2-3, 1982. Oak Ridge National Laboratory Report No. CONF-8206130, August, 1983.

5. Childs, K. W., Courville, G. E., and Bales, E. L. Thermal Mass Assessment. Oak Ridge National Laboratory Report No. ORNL/CON-97, September, 1983.

6. Coffman, C. B., Duffin, R. J., and Knowles, G. P. "Are Adobe Walls Optimal Phase Shift Filters?," Advances in Applied Mathematics. Vol. 1, 1980.

7. Courville, G. and Bales, E. Proceedings of the Building Thermal Mass Seminar, Knoxville, Tenn., June 2-3, 1982. Oak Ridge National Laboratory Report No. CONF-8206130, August, 1983.

8. Curtis, B., Anderson, B., Kammerud, R., Place, W., and Whitley, K. "Thermal Mass: Its Role in Residential Construction," Changing Energy Use Futures: Second International Conference on Energy Use Managment. Vol. 3, Los Angeles, Oct. 22-26, 1979.

9. Dipprey, D. F. and Sabersky, R. H. "Heat and Mass Transfer in Smooth and Rough Tubes at Various Reynolds Numbers," Intern. J. of Heat and Mass Transfer, Vol. 6, pp. 329-353, 1963.

10. Duffin, R. J. and Knowles, G. "Temperature Control of Buildings by Adobe Wall Design," Solar Energy. Vol. 27, No. 3, 1981.

11. Eckert, E. R. G. and Drake, R. M. Jr. Analysis of Heat and Mass Transfer. McGraw-Hill, New York, 1972.

12. Fanger, P. O. "Calculation of Thermal Comfort: Introduction of a Basic Comfort Equation," ASHRAE Transactions, Vol 73, Pt. II, 1967.

13. Goodwin, S. E. and Catani, M. J. "The Effects of Mass on Heating and Cooling Loads and on Insulation Requirements of Buildings in Different Climates," ASHRAE Transactions. Vol. 85, Pt. 1, 1979.

14. Gustinis, J. P. and Robertson, D. K. "Southwest Thermal Mass Study, Tesuque Pueblo, New Mexico, Construction and Instrumentation Phase." New Mexico Research and Development Institute Information Center, University of New Mexico, 1981.

15. Hopkins, V., Gross, G., and Ellifritt, D. "Computing the Thermal Performance of Buildings of High and Low Masses," Paper No. 2, PH-79-11, presented at the ASHRAE Conference, Philadelphia, 1979.

16. Kato, H., Nishiwaki, N., and Hirata, M. "On Turbulent Heat Transfer by Free Convection from Vertical Plates." International Journal of Heat and Mass Transfer. Vol. 11, No. 7, p. 1117 ff, 1968.

17. Kays, W. M. Convective Heat and Mass Transfer. McGraw-Hill, New York, 1966.

18. McAdams, W. H., Heat Transmission, 3rd ed. McGraw-Hill, New York, 1954.

19. Peavy, B. A., Burch, D. M., Powell, F. J., and Hunt, C. M. "Dynamic Thermal Performance of an Experimental Masonry Building," NBS Building Science Series No. 57, April 1975.

20. Peterson, S. R., Barnes, K. A. and Peavy, B. A. "Determining Cost-Effective Insulation Levels for Masonry and Wood-Frame Walls in New Single-Family Housing," NBS Building Science Series No. 134, August, 1981.

21. Rudoy, W. and Dougall, R. S. "Effects of the Thermal Mass on Heating and Cooling Load in Residences," ASHRAE Transactions. Vol. 85, Pt. 1, 1979.

22. Schlichting, Hermann. Boundary Layer Theory. McGraw-Hill, New York, 1960.

23. Yu, H. C. "A Performance Comparison of a Wood-Frame and a Masonry Structure," National Forest Products Association Technical Report No. 8.

CONVERSION FACTORS

1 mm	= 0.03937 in
1 cm	= 0.3937 in
1 m	= 3.281 ft
1 km	= 0.6214 mi
1 m^2	= 10.76 ft^2
1 m^3	= 35.31 ft^3
1 m/s	= 2.237 mi/hr
1 m^3/s	= 2119 ft^3/min
1 °C difference	= 1.8 °F difference *
1 kg/m^2	= 0.2049 lbm/ft^2
1 kg/m^3	= 0.06243 lbm/ft^3
1 kWh	= 3413 Btu
1 W	= 3.413 Btu/hr
1 kWh/day	= 41.67 W
1 kWh/day	= 142.2 Btu/hr
1 W/m^2	= 0.3170 Btu/ft^2 hr
1 W/m °C	= 0.5779 Btu/ft hr °F
1 W/°C	= 1.896 Btu/hr °F
1 m^2 °C/W	= 5.679 ft^2 hr °F/Btu

* convert from °C to °F as follows:

$$t_F = (t_C \times 1.8) \pm 32.0$$